University of Pisa
PhD program in:
Health technologies: evaluation and management of the innovations in the biomedical field

Gaze control modelling and robotic implementation

PhD Candidate: Davide Zambrano

Dean

Prof. Cecilia Laschi

Referees

Prof. Paolo Dario

Prof. Alain Berthoz

Date of the graduation

28.06.2012

Contents

Abstract

Although we have the impression that we can process the entire visual field in a single fixation, in reality we would be unable to fully process the information outside of foveal vision if we were unable to move our eyes. Because of acuity limitations in the retina, eye movements are necessary for processing the details of the array. Our ability to discriminate fine detail drops off markedly outside of the fovea in the parafovea (extending out to about 5 degrees on either side of fixation) and in the periphery (everything beyond the parafovea). While we are reading or searching a visual array for a target or simply looking at a new scene, our eyes move every 200-350 ms. These eye movements serve to move the fovea (the high resolution part of the retina encompassing 2 degrees at the centre of the visual field) to an area of interest in order to process it in greater detail. During the actual eye movement (or saccade), vision is suppressed and new information is acquired only during the fixation (the period of time when the eyes remain relatively still). While it is true that we can move our attention independently of where the eyes are fixated, it does not seem to be the case in everyday viewing. The separation between attention and fixation is often attained in very simple tasks; however, in tasks like reading, visual search, and scene perception, covert attention and overt attention (the exact eye location) are tightly linked. Because eye movements are essentially motor movements, it takes time to plan and execute a saccade. In addition, the end-point is pre-selected before the beginning of the movement. There is considerable evidence that the nature of the task influences eye movements. Depending on the task, there is considerable variability both in terms of fixation durations and saccade lengths.

It is possible to outline five separate movement systems that put the fovea on a target and keep it there. Each of these movement systems shares the same effector pathway—the three bilateral groups of oculomotor neurons in the brain stem. These five systems include three that keep the fovea on a visual target in the environment and two that stabilize the eye during head movement. Saccadic eye movements shift the fovea rapidly to a visual target in the periphery. Smooth pursuit movements keep the image of a moving target on the fovea. Vergence movements move the eyes in opposite directions so that the image is positioned on both foveae. Vestibulo-ocular movements hold images still on the retina during brief head movements and are driven by signals from the vestibular system. Optokinetic movements hold images during sustained head rotation and are driven by visual stimuli. All eye movements but vergence movements are conjugate: each eye moves the same amount in the same direction. Vergence movements are disconjugate: The eyes move in different directions and sometimes by different amounts. Finally, there are times that the eye

must stay still in the orbit so that it can examine a stationary object. Thus, a sixth system, the fixation system, holds the eye still during intent gaze. This requires active suppression of eye movement.

Vision is most accurate when the eyes are still. When we look at an object of interest a neural system of fixation actively prevents the eyes from moving. The fixation system is not as active when we are doing something that does not require vision, for example, mental arithmetic. Our eyes explore the world in a series of active fixations connected by saccades. The purpose of the saccade is to move the eyes as quickly as possible. Saccades are highly stereotyped; they have a standard waveform with a single smooth increase and decrease of eye velocity. Saccades are extremely fast, occurring within a fraction of a second, at speeds up to 900°/s. Only the distance of the target from the fovea determines the velocity of a saccadic eye movement. We can change the amplitude and direction of our saccades voluntarily but we cannot change their velocities. Ordinarily there is no time for visual feedback to modify the course of the saccade; corrections to the direction of movement are made in successive saccades. Only fatigue, drugs, or pathological states can slow saccades. Accurate saccades can be made not only to visual targets but also to sounds, tactile stimuli, memories of locations in space, and even verbal commands ("look left"). The smooth pursuit system keeps the image of a moving target on the fovea by calculating how fast the target is moving and moving the eyes accordingly. The system requires a moving stimulus in order to calculate the proper eye velocity. Thus, a verbal command or an imagined stimulus cannot produce smooth pursuit. Smooth pursuit movements have a maximum velocity of about 100°/s, much slower than saccades. The saccadic and smooth pursuit systems have very different central control systems. A coherent integration of these different eye movements, together with the other movements, essentially corresponds to a gating-like effect on the brain areas controlled. The gaze control can be seen in a system that decides which action should be enabled and which should be inhibited and in another that improves the action performance when it is executed. It follows that the underlying guiding principle of the gaze control is the kind of stimuli that are presented to the system, by linking therefore the task that is going to be executed.

This thesis aims at validating the strong relation between gaze and actions. In the first part a gaze controller has been studied and implemented in a robotic platform in order to understand the specific features of prediction and learning showed by the biological system. In the second part of this work the gaze behaviour has been studied during a locomotion task. The final objective is to show how the different tasks, such as the locomotion task, imply the salience values that drives the gaze. The main pillar of this work is the study of the biological system, in this case the human active vision, by through the mathematical modelling of its expressed behaviour. Moreover the robotic implementation of these models become a double gain factor both for the possibility of the validation of these model in a real context and for the technological improvements in the robotic field Dario et al. 2005.

Organization of the thesis

Part I The gaze control

The control of the eye movements represents the first step in the study of the active gaze in humans. The mathematical modeling and the robotic implementation of the eye movement has been analyzed in terms of the adaptive and predictive behaviours. In particular, the gaze control has been firstly divided in his principal parts, by focusing on the different responses provided by the gaze control respect to different stimulus. These models have been implemented on the robotic head in order to demonstrate how anticipative, predictive and adaptive behaviours strongly imply the eye movements. Afterwards the focus has been moved on the unified oculomotor system that integrates all the eye movements. The final goal of this section is the robotic implementation of the eye movement models based on learning and prediction, in particular the development of a unified oculomotor system that integrates saccades, smooth pursuit and vestibule-ocular reflex (VOR). The results obtained have been used to model a strategy for the control of the entire oculomotor system in different tasks. The unified oculomotor system coordinates the eye movements and controls the position of the eyes and of the head in order to orient the gaze towards a specific point in the space. So the robot has the capability to: shift the gaze from one object of interest to another (*saccades*); keep the gaze on a moving target (*smooth pursuit*); keep the gaze still in space when the head moves (*fixations* using vestibular and opto-kinetic reflexes). The eye movements integration opens the problem of the best action that should be selected when a new stimuli is presented. The action selection problem is solved by the *basal ganglia* brain structures that react to the different salience values of the environment. All these studies have required the investigation of the applicability of oculomotor system models derived from neuroscience research on humanoid robots and consider that the brain uses control strategies based on internal models.

Part II A case study: gaze control during locomotion

The second part of this thesis aim at defining a model of the generation of walking trajectory from gaze. This includes modeling of gaze control in humans and his relationship with trajectory planning for locomotion. Our approach is based on the strong stereotypy observed on the locomotor trajectory as classically observed also for the arm movements. Firstly several known neuroscientific models have been compared in order to explore the different aspects of the human trajectory planning in relation with the gaze. This kind of analysis shedes the light on the different mathematical framework used to describe the human movements. Secondly we used the results obtained from the experiments conducted, to precise the relation between gaze and the variability structure of the trajectory. Based on this study,

a new model is proposed as general framework for the modeling of the locomotor trajectory planning in complex tasks.

Firstly we remarked the gaze as an important factor for the generation of a trajectory, by reporting several aspects: (i) a role for motor prediction, (ii) saccades to important cues (or else), allowing standard prediction, and (iii) fixation on specific elements in the environment, as obstacles or imposed via-points, for steering. In our study we assume that this third component of gaze behaviour is used for internal computation of the future trajectory. And we aim to exploit this information in addition to the motor prediction. We characterized better what are the fixation points, and defined the notion of LFP (Landmark Fixation Point). Secondly, we noted that the generation of locomotor trajectory for animals, in particular for humans, is not simple execution of a fully planed trajectory in advance; in particular some elements along the trajectory seem to be more anticipated than other. Thus we made the hypothesis that these elements correspond to the minimum of variability in the geometry and the kinematic of the trajectory. We determined the points where the geometric trajectory has less variation over repetition (MVPP) and points where velocity has less variation over repetition (MVPV). Third, we analysed the relation between LFPs times and MVPPs times, and fourth, we used this relation to construct a model of generation of trajectory.

Part I.

The gaze control

1. The smooth pursuit model

1.1. Overview

Smooth pursuit is one of the five main eye movements in humans, consisting of tracking a steadily moving visual target. Smooth pursuit is a good example of a sensory-motor task that is deeply based on prediction: tracking a visual target is not possible by correcting the error between the eye and the target position or velocity with a feedback loop, but it is only possible by predicting the trajectory of the target. This chapter presents a model of smooth pursuit based on prediction and learning (Zambrano et al. 2010). It starts from a model of the neurophysiological system proposed by Shibata and Schaal (Shibata et al. 2005). The learning component added here decreases the prediction time, in case of target dynamics already experienced by the system. In the implementation described here, the convergence time is, after the learning phase, 0.8 seconds. The objective of this work was to investigate the applicability of smooth pursuit models derived from neuroscience research on humanoid robots (Dario et al. 2005; BROOKS 1991), in order to achieve a human-like predictive behaviour able to adapt itself to changes of the environment and to learn from experience.

1.2. The smooth pursuit with prediction and learning

One of the most important characteristics of the primate visual system is represented by the space-variant resolution retina with a high resolution fovea that offers considerable advantages for a detailed analysis of visual objects (Thier and Ilg 2005). The space-variant resolution of the retina requires efficient eye movements for correct vision. The purpose of smooth pursuit eye movements is to minimize the retinal slip, i.e. the target velocity projected onto the retina, stabilizing the image of the moving object on the fovea. Retinal slip disappears once eye velocity catches up to target velocity in smooth pursuit eye movements. In primates, with a constant velocity or a sinusoidal target motion, the smooth pursuit gain, i.e. the ratio of tracking velocity to target velocity, is almost 1.0 (Robinson 1965). This cannot be achieved by a simple visual negative feedback controller due to the long delays (around 100 ms in the human brain), most of which are caused by visual information processing. During maintained smooth pursuit, the lag in eye movement can be reduced or even cancelled if the target trajectory can be predicted (Wells and Barnes 1998;

Whittaker and Eaholtz 1982; Fukushima et al. 2002). Infants gradually learn to predict the motion of moving targets and they pass from a strategy that mainly depends on saccades to one that depends on anticipatory control of smooth pursuit. Before an infant can correctly use smooth pursuit, in fact, they use catch-up saccades to correct the delays of their smooth pursuit. As the smooth pursuit system develops, these saccades become less frequent, but they are still used to catch up if the lag becomes too large. Infants, at 1 month of age, can exhibit smooth pursuit, but only at the speed of 10°s^(-1) or less and with a low gain (Roucoux and Culee 1983). The gain of smooth pursuit improves substantially between 2 and 3 months of age (von Hofsten and Rosander 1997). At 5 months of age, this ability approaches that of adults and the relative proportion of saccades is actually quite adult-like. Other studies investigated horizontal and vertical tracking of moving targets and the vertical tracking was found to be inferior to horizontal tracking at all age levels (Grönqvist et al. 2006). These components are mutually dependent during early development of two-dimensional tracking (Gredebäck et al. 2005). These studies demonstrate that the primate smooth pursuit develops with experience.

1.3. Neural basis

Many studies have shown that a separate pathway exists, the dorsal pathway, that processes visual motion information. In the monkey brain, the neural pathways that mediates smooth-pursuit eye movements, described in (Thier and Ilg 2005), starts in the primary visual cortex (V1) and extends to the middle temporal area (MT) that serves as generic visual motion processor. It contributes to smooth pursuit by extracting retinal motion of the target in retinal coordinates (Newsome et al. 1988; Komatsu and Wurtz 1988a;b). By contrast, the middle superior temporal area (MST) seems to contain the explicit representation of object motion in world centred coordinates (Ilg et al. 2004). Recent works (Kawawaki et al. 2006) demonstrate that this area is responsible for target dynamics prediction. Cortical eye fields are also involved in smooth pursuit (Tian and Lynch 1996); in particular the frontal eye field (FEF) can modulate the gain control (Tanaka and Lisberger 2001; 2002; Gottlieb et al. 1994) that determines how strongly pursuit will respond to a given motion stimulus. The gain control works as a link between the visual system and the motor system, therefore the motor learning could concern this stage by altering this link. (Chou and Lisberger 2004). The dorsal pontine nuclei (PN) and the nucleus reticularis tegmenti pontis (NRTP) are the principal recipients of efferent signals originating from the parieto-occipital and frontal areas, that contribute to smooth pursuit (Dicke et al. 2004; Ono et al. 2005). They are considered as intermediary stations that adapt the signal for the extraocular motoneurons. Finally, the cerebellum seems to play a crucial role in supporting the accuracy and adaptation of voluntary eye movements. It uses at least two areas for processing signals relevant to smooth pursuit: the flocculus-paraflocculus complex and the posterior vermis.

These areas might be primarily required for the coordination of the vestibular reflex with pursuit behaviour (Rambold et al. 2002) and for pursuit adaptation (Takagi et al. 2000).

1.4. Schaal and Shibata's model

S. Schaal and T. Shibata (Shibata et al. 2005) presented a biologically motivated smooth pursuit controller that predicts the visual target velocity in head coordinates, based on fast on-line statistical learning of the target dynamics. They proposed a predictive control model that consists of two subsystems: (1) a recurrent neural network mapped onto the MST, which receives the retinal slip, i.e. target velocity projected onto the retina, with delays, and predicts the current target motion; and (2) an inverse dynamics controller (IDC) of the oculomotor system, mapped onto the cerebellum and the brainstem. In the following, x is the target position and $\dot{x}$ the target velocity. The target state vector is expressed as $\mathbf{x}$ in bold, the bar is used to indicate the current estimation of a variable and the hat to indicate the prediction result. Since the brain cannot observe the target state vector $\mathbf{x}$=$[x\dot{x}]^T$ directly, the first part predicts the current target velocity $\hat{\dot{x}}$(t) from the delayed estimated target state $\bar{\mathbf{x}}$(t-Δ). This is calculated from the retinal slip information $\dot{e}$(t) and the eye velocity $\dot{E}$(t) as follows:

$$\bar{\dot{\mathbf{x}}}(t-\Delta) = \dot{E}(t-\Delta) + \dot{e}(t-\Delta) \tag{1.1}$$

The estimated target position $\bar{x}$(t-Δ) is obtained by integrating $\bar{\dot{x}}$(t-Δ). According to neurophysiological studies (Kawawaki et al. 2006), the MST area predicts only the velocity information about the target dynamics. To predict the target velocity the model uses a second order linear system to represent the target dynamics:

$$\hat{\dot{x}}(t) = \mathbf{w^T}\bar{\mathbf{x}}(t-\Delta) \tag{1.2}$$

Where $\mathbf{w}$ represents the vector of regression parameters and $\hat{\dot{x}}$(t) is the predicted target velocity. A recursive least squares algorithm (RLS) (Ljung and Soderstrom 1987) is employed for learning, because it is robust and it guarantees convergence. Originally, RLS requires the presence of a target output in the update rules, but the predictor can only utilize the retinal signals as the prediction error. Thus, the algorithm is modified as follows:

$$P(t) = \frac{1}{\lambda}\left[\mathbf{P}(t-1) - \frac{\mathbf{P}(t-1)\mathbf{x}(t)\mathbf{x}(t)^T\mathbf{P}(t-1)}{\lambda + \mathbf{x}(t)^T\mathbf{P}(t-1)\mathbf{x}(t)}\right] \tag{1.3}$$

$$\mathbf{w}(t) = \mathbf{w}(t-1) + \frac{\mathbf{P}(t)\mathbf{x}(t)}{\lambda + \mathbf{x}(t)^T\mathbf{P}(t-1)\mathbf{x}(t)}\dot{e}(t+1) \tag{1.4}$$

$$\hat{\dot{y}}(t) = \mathbf{w}(t)^T\mathbf{x}(t) \tag{1.5}$$

Where $\mathbf{P}$ is the inverted covariance matrix of the input data, $\mathbf{x}$ is the input state and λ is the forgetting factor which lies in the [0, 1] interval. For $\lambda = 1$, no forgetting takes place, while for smaller values, the oldest values in the matrix $\mathbf{P}$ are exponentially forgotten. Essentially, the forgetting factor ensures that the prediction of RLS is only based on $1/(1\text{-}\lambda)$ data points. This forgetting strategy also enables the predictor to be adaptive to the changes in the target dynamics. Another important element of Equation 1.4 is that it explicitly shows the requirement for the time alignment of the predictor output and the error since the learning module cannot see it at time t. Thus, all variables in Equation 1.4 are delayed by one time step, which requires the storage of some variables for a short time in memory. The RLS algorithm is implemented in a discrete time domain, so the algorithm upgrades the variables with the new values every discrete step. The second part of the Schaal and Shibata's model is based on theory and experiments showing that the cerebellum and brainstem together act as an inverse dynamics controller of the oculomotor plant (Shidara et al. 1993; Kawato 1999). The model assumes that the IDC has the capability to cancel the dynamics of the eye plant making it valid to write:

$$\dot{E}(t) = \hat{\dot{x}}(t) \tag{1.6}$$

In accordance with von Hofsten (von Hofsten and Rosander 1997), the prediction in smooth pursuit movements is about 200 ms, so the entire closed-loop delay must be larger of the single visual delay proposed by Schaal and Shibata. In Robinson's model (Robinson et al. 1986), it has been proposed a closed-loop delay of about 150 ms and it has been added a delay block before the eye plant. In order to simulate a prediction of 200 ms, in this work it has been added a delay block before the eye plant, so that the predictor must adapt its dynamics both to visual delay and eye plant dynamics.

1.5. Proposed model of smooth pursuit with prediction and learning

In this work, the model by Schaal and Shibata has been tested in MATLAB-Simulink by using a sampling frequency of 20 Hz, like in the human visual system. The model

was tested on sinusoidal target motions with angular frequency included between 0.5 rad s^{-1} and 2.5 rad s^{-1} with a 0.1 rad s^{-1} step. The model correctly follows the target dynamics reaching convergence after more than 4 seconds of simulation (Fig. 1.1). Fig. 1.2 shows the learned values of the vector of regression parameters

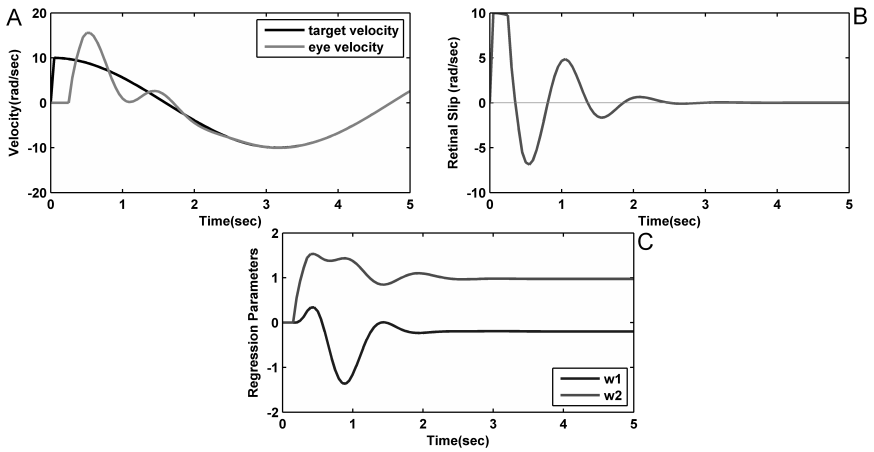

Figure 1.1.: Simulation results in case of a sinusoidal signal with angular frequency of 1 rad s^(-1) and amplitude of 10 rad using Shibata and Schaal's model. Here A and B show the time course of target and eye velocity and the retinal slip, respectively. After about 4 seconds the target velocity and the eye velocity are aligned and the values of the vector of regression parameters w reaches convergence (C) [-0.1987; 0.9751].

w in the angular frequency domain. The converging speed is slower than in humans (Shibata et al. 2005), and if a new target dynamics is presented to the model, it is necessary to wait for the system converging, aside if this dynamics has been already presented or not. With the purpose to obtain a developmental model that can take into account previous experiences, in this work it has been supposed that it is possible to store the previously acquired weights, the regression coefficients. These values are placed in a memory block and then used to improve the converging speed of the model.

Fig. 1.2 shows that there is a direct relationship between the angular frequency of the target dynamics and the final regression coefficients calculated by the RLS algorithm. Such values depend only on the angular frequency of the target dynamics and on the configuration of the system. Instead, they are independent from the amplitude and the phase of the sinusoidal motion. In this work, a module storing the regression coefficients of already seen target motions has been added to Shibata and Schaal's modeladded. Fig. 1.3 shows the proposed model block schema. The velocity information ($\dot{v}$) are processed by the V1 and MT areas in order to extract the target slip on the retina ($\dot{e}$). These operations are made by the Visual Processing module. The Estimator State module generates the target velocity estimation according to Equation 1.1 and it employs the position estimation by integrating the

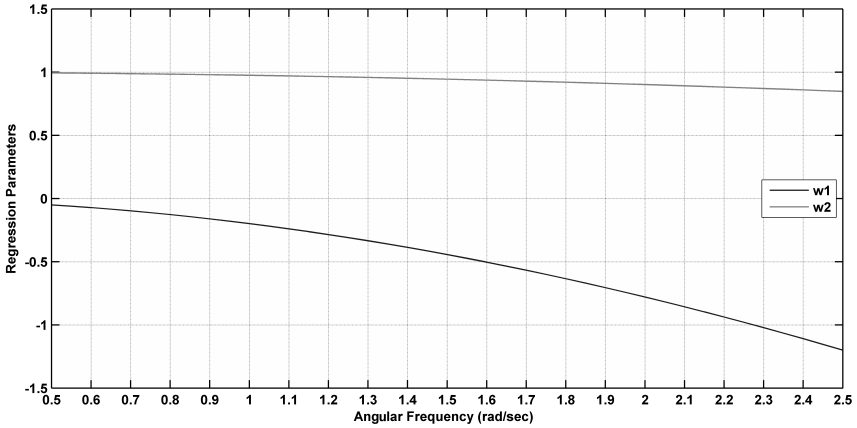

Figure 1.2.: The graph shows the correlation between the values of regression parameters w and the angular frequency of sinusoidal target dynamics.

velocity information. The state vector ($\mathbf{x}$) is sent to the Predictor that provides the next target velocity ($\dot{x}$). The Inverse Dynamics Controller generates the necessary torque that allows the Eye Plant to reach the predicted velocity (Equation 1.6). In general, the system develops an internal representation, i.e. an Internal Model, of the external environment. The Internal Model, namely a memory block, has been added to recognize the target dynamics and to provide the correct weight values before the RLS algorithm. For this purpose, the regression coefficients are stored in a neural network, the Internal Model, for future presentation of learned target dynamics. The Predictor, shown in Fig. 1.3, is the RLS algorithm that minimizes the retinal slip, $\dot{e}$(t), adapting the regression coefficient according the Equation 1.4. The neural network inputs are a sample series of initial velocity values of the target dynamics and the outputs are the correct regression coefficients of the corresponding target dynamics. Such weights are sent to the predictor module in Equation 1.4 to guide the RLS algorithm to final values improving the converging speed. When the new values are ready from the network, it is necessary to wait for another cycle to verify the correctness of this prediction. If the retinal slip given by RLS is greater than the neural network one, the neural network output is used to predict the target velocity. In the other case, the RLS goes on learning the target dynamics, hence it is necessary to train the neural network on the new data. This behaviour is represented by the Selector module in block schema. Notes that the Predictor block in Fig. 1.3 provides a target velocity prediction that overcome the delay in the execution of the movement (Δ_3). The entire close loop delay has been fixed to Δ_2=Δ_1+Δ_3. From a neurophysiological point of view, the visual motion information follows the dorsal pathway and are processed by the primary visual cortex, MT and MST. This area provides the sensory information to guide pursuit movements but may not be able to initiate them. The FEF, in the pre-motor cortex, is more important for initiating pursuit and it is also related with associative memory (Chou and Lisberger

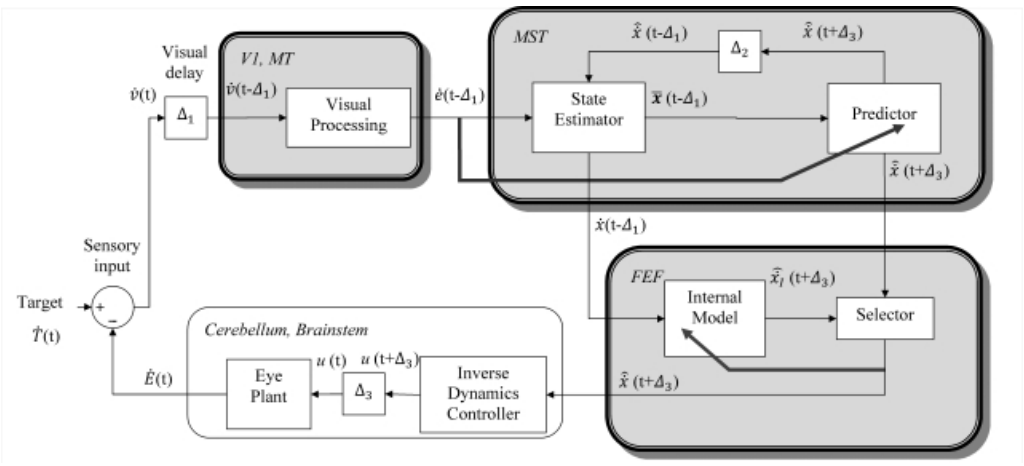

Figure 1.3.: The figure shows a block schema of the proposed model of the smooth pursuit eye movement. An internal model is added to Shibata and Schaal's model to learn the target dynamics and a selector allows to recognize the best prediction between the internal model and the RLS predictor. The internal model is online trained by the values of the regression parameter vector when the RLS reaches convergence.

2004). Then, it is possible to suppose that the brain keeps motion information and use them to obtain a correct smooth pursuit eye movement based on own previous experience.

1.6. Implementation of the proposed model of smooth pursuit

In the proposed model, a neural network has been added to associate a specific sequence of velocity values with the correct regression parameters. For this purpose, it has been used a simple multilayer perceptron (MLP) that maps half second of sampled target velocity (with sampling frequency of 20 Hz) onto corresponding weight values. This network has been developed with Neural Network Fitting Tool on MATLAB with 10 neurons in the input layer, 25 neurons in the hidden layer and 2 neurons in output layer that correspond with the two regression parameters of RLS algorithm. It uses the non linear activation sigmoid function with backpropagation learning rule. In accordance with neurophysiological studies, the model recognizes motion sequences and so it takes only half a second to provide the correct values. Moreover, when the learning is complete, it is possible to obtain correct values also with unknown angular frequency target motions. The model follows a developmental approach, therefore initially the neural network needs to learn by experience. The RLS algorithm learns the target dynamics and reaches convergence. The regression coefficients are used to train the neural network. When the neural network gives as

output a new predicted velocity value, the selector module has to compare this value with the real state of the target to verify the correctness of the prediction. So it has to wait one closed-loop delay for the new values of the target state. If the internal model prediction is better than the actual RLS output, the selector module changes the regression parameters in Equation 1.4 with the neural network output, otherwise it has to wait for the convergence of RLS and to use the regression parameter obtained for the learning of the neural network. The dimension of the input layer has been chosen from experimental trials. The velocity sample number needs to be a trade-off between the motion recognition accuracy (that needs large number of samples) and the system response velocity. Considering the specific system configuration it has been observed that 10 samples (0.5 sec at 20 Hz) are a good solution.

1.7. Experimental Results

The model represents the signal prediction of one axis because it has been proven that the horizontal axis is separate from the vertical axis (Grönqvist et al. 2006). To represent the other axis it is necessary to add another model like this one for the other component of the target dynamics. Moreover, the model predicts only the target velocity, so the position error reaches a constant value after the convergence of the system. In this work, all the learning experiments start from scratch, i.e. with all initial states including the weights of the learning system set to zero. The model was tested on sinusoidal target motions with the following dynamics:

$$x(t) = A * sin(\omega t + \varphi) \tag{1.7}$$

Where x(t) is the target position (expressed in radians) at the time t and A is the amplitude of the dynamics. The angular frequency (ω) has been tested between 0.5 rad s^{-1} and 2.5 rad s^{-1} with 0.1 rad s^{-1} step. Moreover the model has been tested with angular phase between 0 rad and 2π rad with a π/4-rad step and with amplitude between 4 and 20 rad with a 1-rad step. Fig. 1.4 shows the results of an example of simulation with a sinusoidal motion target with angular frequency of 1 rad s^{-1}: the final values of the vector w are -0.1987 and 0.9751. These values are independent from amplitude or phase of the sinusoidal trajectory. The vector of regression parameters is dependent only on the angular frequency of the sinusoidal motion and on the configuration of the system, like the entire closed loop delay. If the angular frequency changes, it will be necessary to wait that the model reaches the new steady state. With these configuration properties, the Schaal and Shibata's model takes more than 4 seconds to perfectly cancel the retinal slip. In all experiments it has been taken into account, as converging speed, the time necessary for the vector of regression parameters to reach the stable state. For this purpose it

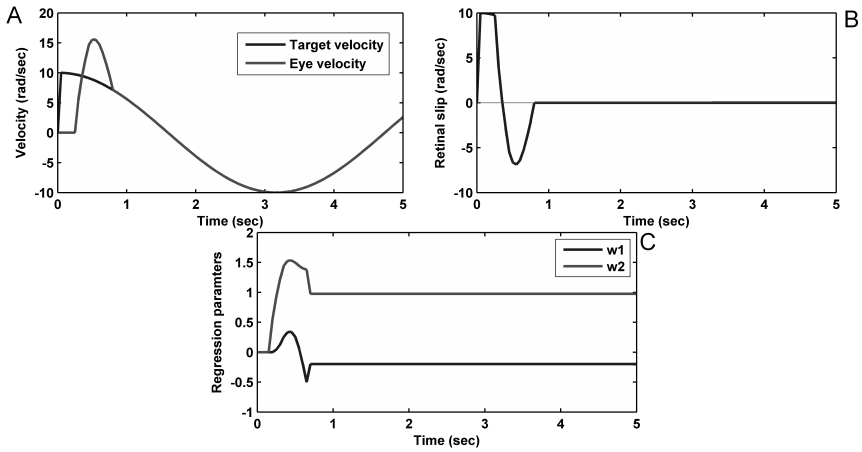

Figure 1.4.: Simulation results in case of a sinusoidal target dynamics with angular frequency of 1 rad s^(-1) and amplitude of 10 rad using the proposed model. Here A and B show the time course of target and eye velocity and the retinal slip respectively. After 0.8 second the values of the vector of regression parameters w are set to the final values (C) [-0.1987 0.9751] and the retinal slip reach zero just after this time.

has been chosen that the difference between elements of the vector of regression parameters and previous values of itself , **e**(k), must be less of 10^(-6).

$$\mathbf{e}(k) = \mathbf{w}(k) - \mathbf{w}(k-1) \tag{1.8}$$

For example, for ω=1 rad s^{-1}, A=10 rad; φ=0 the converging time is 6.75 sec. These values are strictly dependent on the initial conditions of the system and on the target dynamics. Fig. 1.5 shows the results of all simulation tests changing the amplitude in a range from 4 to 20 rad with a 1-rad step and the angular frequency in a range from 0.5 and 2.5 rad s^{-1} with fixed phase. Fig. 1.6 shows the results of all simulation tests changing the phase in a range from 0 rad and 2π rad with a π/4-rad step and angular frequency in a range from 0.5 and 2.5 rad s^{-1} with fixed amplitude. The converging speed increases as frequency and amplitude increase, moreover there is a periodic trend with the phase change. In the improved model it has been assumed that 10 steps are necessary (half a second with sampling frequency of 20 Hz) to recognize precisely the motion. The network outputs the vector of regression parameters and it is placed in Equation 1.4 for at least 5 seconds. The model corrects the prediction and the absolute value of retinal slip reaches steady state after 0.8 sec. When the new values are ready from the network, it is necessary to wait for another cycle to verify the correctness of this prediction so the final converging time is the sum of the time necessary to get 10 samples of target velocity (500 ms at 20 Hz), plus the time to verify that the prediction of neural network is better than the prediction coming from RLS (one closed loop delay, 200 ms) and

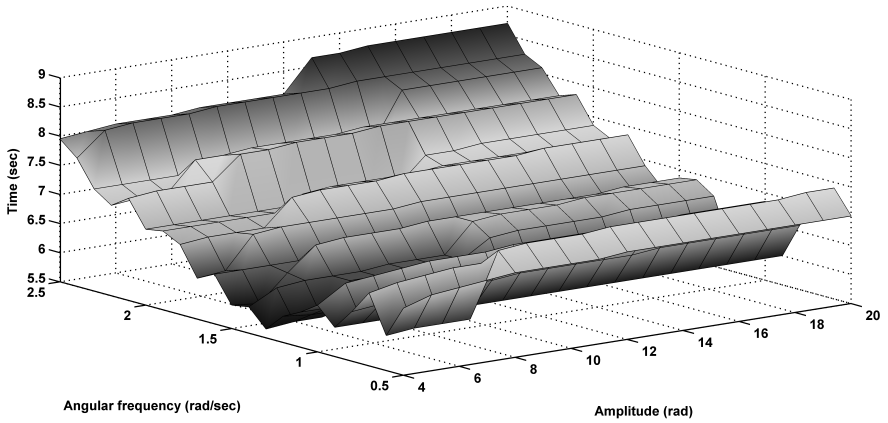

Figure 1.5.: Simulation results in case of a sinusoidal target velocity at several amplitude and angular frequency using Shibata and Schaal's model. The converging time is between 5 and 10 seconds.

the time to move the eye to the correct predicted velocity (100 ms). In order to test the hypothesis that the model can recognise the initial value of the target dynamics, the neural network has been trained on a large training data set. It has been taken into account a sinusoidal target dynamics with the angular frequency included in a range from 0.5 and 2.5 rad s^{-1} with a 0.1-rad s^{-1} step. The neural network must give the correct value of the regression parameter vector aside from differences in the values of the amplitude and the phase of the sinusoidal target dynamics. So, for each angular frequency, 10 values have been taken (with sampling frequency of 20 Hz) of the target velocity (the derivative of the target position), considering the amplitude of the target position included between 5 and 15 rad with a 2.5-rad step, thus the maximum velocity considered is about 40 rad s^{-1}. Moreover, it has been taken into account a different initial phase of the target dynamics in a range included between $\pi/2$ and π rad with $\pi/16$ rad step. It has been taken into account 945 (all combination of angular frequency, phase and amplitude) simulation results and the training set for the neural network is the 70% of this matrix. The 15% is used for the validation set and another 15% is used for the test set. The input matrices have dimension 10x945 and the output target has 2x945 elements. These values have been shuffled to increase the variability of the training set. The results of the learning are shown in Fig. 1.7. The best Mean Squared Error is 9.1844 exp^{-10}. Fig. 1.8 shows the results of the model after the learning of the neural network in two different sinusoidal target dynamics. The figure shows that after 0.8 sec the model recognises the dynamics and gets out the correct values of the regression parameter vector aside the different condition in phase or in amplitude.

This work demonstrates that the smooth pursuit eye movement in humanoid robots can be modeled as a sensory-motor loop where the visual sensory input can be predicted, and where the prediction can be improved by internal models that encode

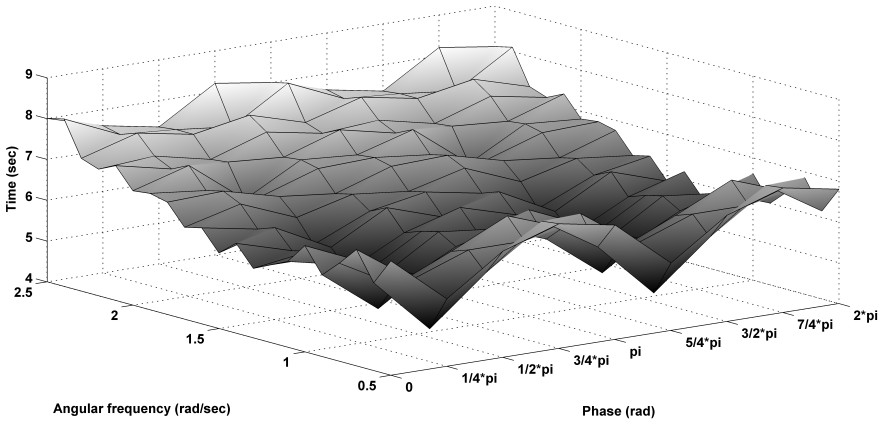

Figure 1.6.: Simulation results in case of a sinusoidal target velocity at several phase and angular frequency using Shibata and Schaal's model. The converging time is between 5 and 9 seconds. The graph shows a periodic trend of the converging time with the phase change.

target trajectories already experienced by the system and that are built by learning. The proposed model includes a learning component that decreases the prediction time for a robotic implementation. The internal model is a feedforward artificial neural network that recognizes the initial sequence of target velocity and gives as output the correct values of the regression parameter vector. The neural network chosen for the internal model provides an improvement for the converging speed of the model but it leads to some considerations. First of all, the dimension of the hidden layer has been chosen a priori so it might be not optimal for another type of data. Secondly, the neural network requires more computational burden than the original model. Thirdly, it needs much memory for storing the training set of data. In the implementation described in the paper the convergence time reaches as low values as 0.8 seconds. As a reference, in the same implementation conditions, the convergence time of Schaal and Shibata's model is more than 4 seconds. This system with this configuration is unable to predict complex dynamics like a sinusoidal sum. Shibata et al. 2001 considered in their work these RLS limitations, but an improvement of the system like they suggested would not change the possibility presented here to take into account the converging results. Such results demonstrate that a memory based approach can improve the performance of the system. So it is possible to suggest that initially the smooth pursuit system needs to learn the target dynamics. During this phase it requires to use a large number of saccades to correct position errors. When the system has built its own Internal Model of the external environment, it uses its experience to rapidly obtain a zero-phase lag smooth pursuit.

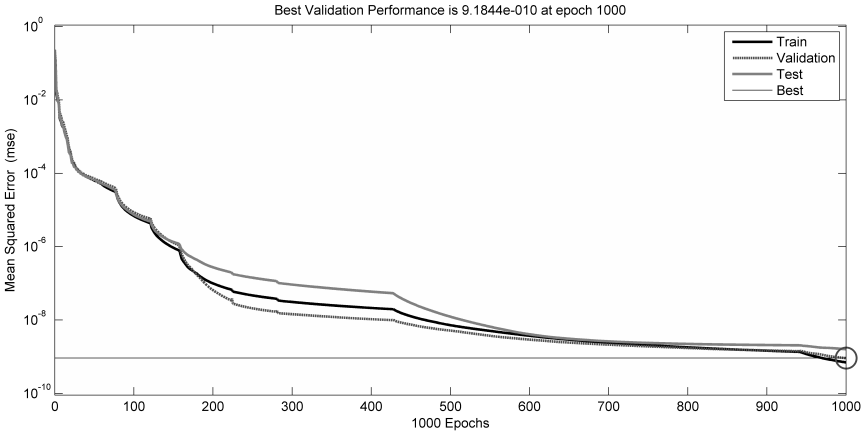

Figure 1.7.: The graph shows the learning phase of the neural network. The Mean Squared Error is less than 10^(-9) after 1000 epochs and is plotted for training set, validation set and test set of data.

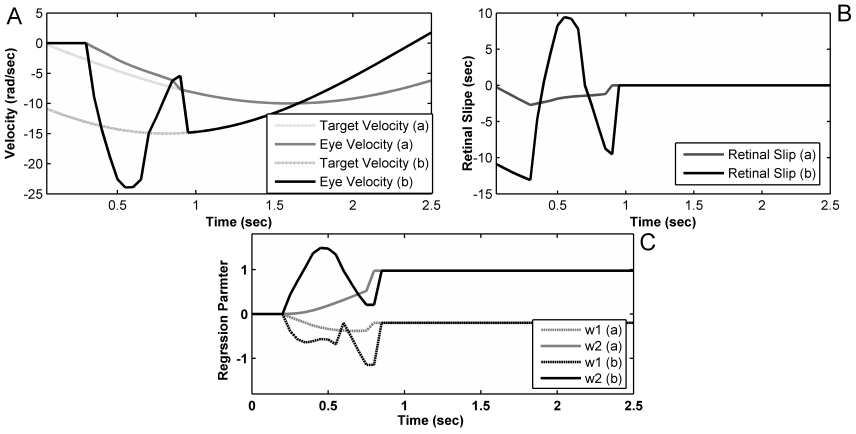

Figure 1.8.: Simulation results in case of two sinusoidal target dynamics with angular frequency of 1 rad s^(-1) and an amplitude of 10 rad and phase of π/2 (a, the grey line) and amplitude of 15 rad and phase of ¾ π (b, the black line) using the proposed model . Here A and B show the time course of target and eye velocity and the retinal slip respectively. After 0.8 second the values of the vector of regression parameters w are set to the final values (C) [-0.1987 0.9751] and the retinal slip reach zero just after this time independently from the differences of the amplitude and the phase of the target dynamics.

2. Smooth pursuit and saccades

2.1. Overview

The space-variant resolution of the retina requires efficient eye movements for correct vision. Two forms of eye movements — saccades and smooth pursuit — enable us to fixate the object on the fovea. Saccades are high-velocity gaze shifts that bring the image of an object of interest onto the fovea. Saccades are fast eye movements (maximum eye velocity > 1000 deg/sec) that allow primates to shift the orientation of the gaze using the position error (difference between the target position and the eye position) (Leigh and Kennard 2004). The duration of the saccadic movement is very short (30-80ms), so they cannot be executed with continuous visual feedback. Smooth pursuit occurs when the eyes track a moving target with a continuous motion, in order to minimize the image slip in the retina and make it perceptually stable (as described in chapter 1). Smooth pursuit movements cannot normally be generated without a moving stimulus although they can start a short moment before the target is expected to appear (Wells and Barnes 1998). The purpose of the work presented in this chapter is to investigate the applicability of a visual tracking model on humanoid robots in order to achieve a human-like predictive behavior. Rather than analyse the saccadic system as a separate module, the present work focuses on the predictive relationship between the smooth pursuit and the saccadic systems. Firstly, it has been analyzed the case of smooth pursuit tracking across occlusions (Falotico et al. 2009) where the tracking stops when the object is occluded an one or two saccades are made to the other side of the occluder to anticipate when and where the object reappears. Another critical case is called "*catch-up*" saccade, a particular combination of smooth pursuit and saccades that occurs when the tracking error in position increases too much (Falotico et al. 2010). Both cases strictly depend on the predictive behaviours expressed by the smooth pursuit system. The described models have been implemented on the iCub robotic platform. Due to the fact that this platform has been taken into account for the robotic implementation of this and the other works, the session sec. 2.2 introduces the mentioned robot.

2.2. The iCub Robot

The RobotCub project has the twin goals of creating an open and freely-available humanoid platform, iCub, for research in embodied cognition, and advancing our

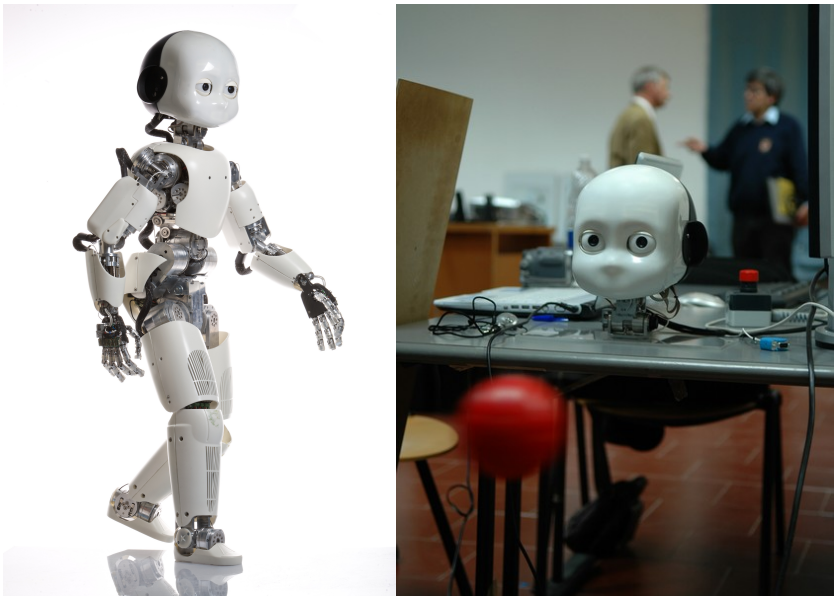

Figure 2.1.: The iCub robot has a physical size and shape similar to that of an about three year-old child. The iCub head contains a total of 6 DOFs: neck pan, tilt and swing and eye pan (independent) and tilt (common).

understanding of cognitive systems by exploiting this platform in the study of cognitive development (Metta et al. 2010; Tsagarakis et al. 2007). To achieve this goal it has been planned to construct an embodied system able to learn: i) how to interact with the environment by complex manipulation and through gesture production & interpretation; and ii) how to develop its perceptual, motor and communication capabilities for the purpose of performing goal-directed manipulation tasks. The iCub robot has a physical size and shape similar to that of an about three year-old child, and will achieve its cognitive capabilities through artificial ontogenic co-development with its environment (Fig. 2.1). The iCub has a total of 53 degrees of freedom organized as follows: 7 for each arm, 8 for each hand, 6 for the head, 3 for the torso/spine and 7 for each leg. In order to guarantee a good representation of the human movements, the iCub head contains a total of 6 DOFs: neck pan, tilt and swing and eye pan (independent) and tilt (common) (Beira et al. 2006). The eyes cyclotorsion was ignored because it is not useful for control, and similar image rotations are easily produced by software. The elevation/depression from both eyes is always the same in humans, in spite of the existence of independent muscles. Similarly, a single actuator is used for the robot eyes elevation (tilt). Eye vergence is ensured by independent motors. Data regarding accelerations, velocities and joint range of the oculomotor system of human babies are not available, and very few studies exist in the literature of psychology or physiology. Overall, the iCub dimensions are those of about three-year old human child, and it is supposed to perform tasks similar to those performed by human children. First, it has been used the smallest range of saccadic speeds as a reference and it has been used the ratio between

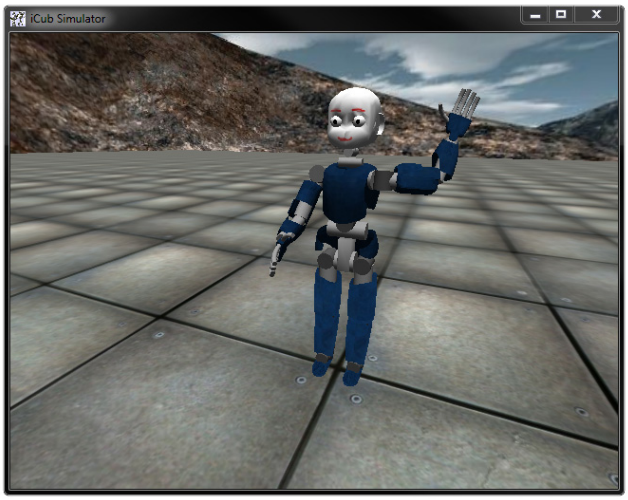

Figure 2.2.: The iCub simulator has been designed to reproduce, as accurately as possible, the physics and the dynamics of the robot and its environment.

neck/eye velocity ($14\% - 41\%$) and acceleration ($2\% - 4\%$) as an important design parameter. The eyes mechanism has three degrees of freedom. Both eyes can pan (independently) and tilt (simultaneously). The pan movement is driven by a belt system, with the motor behind the eye ball. The eyes (common) tilt movement is actuated by a belt system placed in the middle of the two eyes. Each belt system has a tension adjustment mechanism. For the necessary acceleration and speed, the iCub has Faulhaber DC micromotors, equipped with optical encoders and planetary gearheads. In order to guarantee easy assembly and maintenance procedures, the mechanical system architecture is also completely modular, in such a way that it is possible to remove and replace a certain module, without having to disassemble the entire structure. For vision, the main sensory modality, two DragonFly cameras with VGA resolution and 30 fps are integrated in the head. These cameras are very easy to integrate because the CCD sensor is mounted on a remote head, connected to the electronics with a flexible cable. In this way, the sensor head is mounted in the ocular globe, while the electronics are fixed to a non-moving part of the eye-system. All motor control boards are specially designed to fit in the size constraints of the robot. They are all integrated in the head and connect to the remote computer with a CAN bus. To measure the head position (kinesthetic information), the motors have magnetic encoders, for calibration purposes and noting that the protection system drift in case of overload condition, absolute position sensors were applied to each neck joint. The simulator (Fig. 2.2) as stated has been designed to reproduce, as accurately as possible, the physics and the dynamics of the robot and its environment (Tikhanoff et al. 2008b;a). It has been constructed collecting data directly from the robot design specifications in order to achieve an exact replication of the iCub. This means same height, mass and d.o.f.. The iCub simulator was created using open source libraries. It uses ODE (Open Dynamics Engine) for sim-

ulating rigid bodies and the collision detection algorithms to compute the physical interaction with objects. ODE consists of a high performance library for simulating rigid body dynamics using a simple C/C++ API. The iCub Simulator allows controlling iCub robot in the position and in the velocity space, and it provides the encoder value of each motor. The iCub simulator uses YARP as its software architecture. YARP (Yet Another Robot Platform) software (described in (Metta and Fitzpatrick 2006; Fitzpatrick et al. 2008)) is the middleware software used by the iCub humanoid robot. It is worth mentioning that the iCub simulator is one of the few that attempts to create 3D dynamic robot environment capable of recreating complex worlds and fully based on non-proprietary open source libraries.

2.3. Predictive tracking across occlusions

The smooth pursuit is complicated by the fact that the initial visual processing in the human brain delays the stimulus by approximately 100 ms before it reaches the visual cortex (Wells and Barnes 1998; Fukushima et al. 2002). When the pursued object is occluded, the smooth eye movements get effectively interrupted. Subjects switch gaze across the occluder, with saccades, to continue tracking (von Hofsten et al. 2007). This is valid for visual tracking in adults (Lisberger et al. 1987; Kowler 1990) and in infants (Rosander and von Hofsten 2004). Infants react differently from adults to occlusions of the object. Adults always predict the reappearance and their gaze arrives at the opposite side of the occluder slightly before the object. Infants can simply maintain a representation of the object motion while the object is occluded and shift gaze to the other side of the occluder when the conceived object is about to arrive there. In support of this alternative are the findings that object velocity is represented in the frontal eye field (FEF) of rhesus monkeys during the occlusion of a moving object (Barborica and Ferrera 2003). An interesting paper about occlusions and eye movements is proposed by Zhang and colleagues (Zhang et al. 2005). They describe a real-time head tracking system, formulated as an active visual servo problem based on the integration of a saccade and a smooth pursuit process.

2.4. The proposed model for occlusions

This work proposes the integration of different systems in order to obtain a human like behavior of a predictive smooth pursuit of a dynamic target, with saccadic shift of gaze in case of occlusions. The presented model is able to predict target trajectories that present a second order dynamics also in presence of temporary occlusion. It is possible to extend this model to cope with more complex target motions with nonlinear dynamics as suggested in (Shibata and Schaal 2001). (Fig. 2.3) shows the entire system model. The model is basically an extension of the model presented

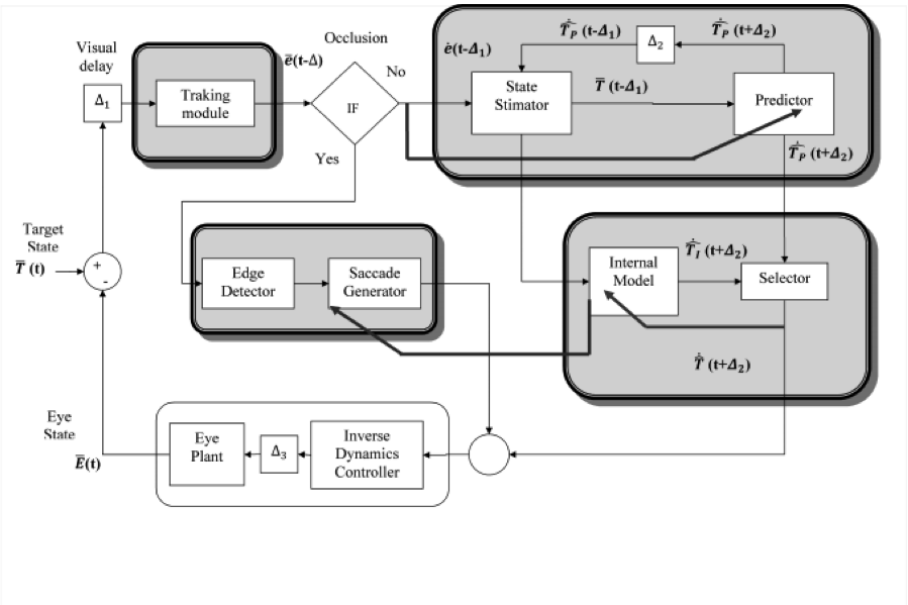

Figure 2.3.: If the object disappears behind the occluder a event of occlusion is notice and another module starts to detect the edges in the image to find where the object will reappear. At this point the saccade generator module repeats the prediction of the target dynamics until the predicted position is equal to the edge detected from the previous module.

by the author in Zambrano et al. 2010 and described in sec. 1.5. The first module is the visual tracker that allows rapid recognition of the object and provides its position in eye coordinates to the next modules. If the object is visible the information about target is processed and the smooth pursuit is executed. The smooth pursuit system requires only measurements of the retinal slip (the target velocity on the retina) to estimate the next target velocity. This information is obtained from the difference of the target position in eye coordinates sent by the tracking module, with respect to the sampling time of the cameras. When the system learns to predict the target dynamics the regression vector values reach convergence and the internal model stores these values. This part of the model basically follows the description presented in sec. 1.5. Regarding the behaviour expressed during occlusions, if the object disappears behind the occluder the tracking module stops sending data and another module starts to detect the edges in the image to find where the object will reappear. At this point the saccade generator module repeats the prediction of the target dynamic by a reiteration of Equation 1.5 with the complete regression matrix, as follows:

$$\mathbf{Y}(t+1) = \begin{bmatrix} 1 & \Delta t \\ w1 & w2 \end{bmatrix} \mathbf{Y}(t) \tag{2.1}$$

Where Δt is the sampling time of the cameras and $\mathbf{Y}$(t) represents the velocity and the position of the target. In order to obtain a long term prediction, the current state $\mathbf{Y}$(t) has to be set equal to the previous iteration of Equation 2.1. The 2.1 is repeated until the predicted position is equal to the edge detected from the previous module. In this way it is possible to obtain the position and the velocity of the target reappearance. The robot switches gaze saccadicly across the occluder to continue tracking and arrives at the opposite side of the occluder slightly before the object. In Fig. 2.4 are shown the results obtained from a simulation of this model on MATLAB Simulink for a sinusoidal dynamics with angular frequency of 1 rad/sec and amplitude of 20 rad. The occlusion range was chosen between -10 rad and 10 rad. In Fig. 2.4 (top) are shown the eye position and the target position. When the target goes behind the occluder, the eye rapidly reaches the exact reappearance point predicted. In Fig. 2.4 (down) the eye velocity has a peak on correspondence with the saccadic movement, then it goes to zero until target reappearance. The velocity of the saccadic movement reaches 300 rad/sec.

2.5. Robotic implementation

To emulate the gazing behaviour of humans in an experiment when the object of interest undergoes total occlusions, we use a method for object detection and tracking with built-in occlusion detection. Two properties of the tracking system are important for this work: it must be able to detect transitions between the states of full visibility and occlusions of the tracked object and it must be able to initialize autonomously the tracker when the object of interest reappears after an occlusion. The detection of the aforementioned transitions is important for our purposes because it corresponds to the events when humans toggle their eye movement behaviour from smooth pursuit to saccadic. We use the tracking system described in (Taiana et al. 2010; 2008), exploiting the behaviour of the likelihood values it computes whens the object of interest is partially occluded. The tracking system we use is based on Particle Filtering methods and exploits knowledge on the shape, color and dynamics of the tracked object. Each particle in the filter represents a hypothetical state for the object, composed of 3D position and velocity. Particles are weighted according to a likelihood function. To compute the likelihood of one particle we first place the points of the shape model around the 3D position encoded in the particle, with respect to the camera. Then we project these points onto the image plane obtaining two sets of 2D points. The sets of 2D points lie on the image on the inner and outer boundary of the silhouette that the tracked object would project if it were at the hypothetical position. The idea is that the color and luminance differences between the sides of the hypothetical silhouette are indicators of the likelihood of the corresponding pose. Object-to-model similarity positively influences the likelihood, while object-to-background similarity contributes to likelihood in the opposite direction. When the object of interest is fully visible, the likelihood estimated by the

filter as a whole is high. When the object gradually becomes occluded, the tracker continues working, but the estimated likelihood drops, only to rise again when the object reappears. The observation model we use enables us to detect occlusions and reappearance events just by setting a threshold on the likelihood value and by reinitializing the tracker, effectively running a detection process, each time the likelihood is below that threshold. The initialization is performed by generating a new particle set, sampling a predefined Gaussian distribution.

Beyond the simulations we have performed results on the real robotic platform iCub (described in sec. 2.2). A known target (a blue ball) is suspended from the ceiling with a string. Once it is put into periodic oscillation, the robot starts estimating and tracking the ball trajectory. It uses the predicted velocity to command the eye motions. Suddenly, an occluder is put close to the ball. At moderate amounts of occlusions, the robot still detects the ball and keeps tracking it. When the occlusion is almost complete, the smooth pursuit tracking stops and the robot estimates when and where the ball will reappear, preparing a saccade. The saccade happens at the onset of reappearance and the eyes are already centered at the target and ready to keep tracking it (Falotico et al. 2009).

2.6. The visual tracking model

The space-variant resolution of the retina requires efficient eye movements for correct vision. Saccades are fast eye movements (maximum eye velocity $>$ 1000 deg/sec) that allow primates to shift the orientation of the gaze using the position error (difference between the target position and the eye position) (Leigh and Kennard 2004). The duration of the saccadic movement is very short (30-80ms), so they cannot be executed with continuous visual feedback. The saccade generation consists in a sensorimotor transformation from visual space input to the motor command space. That transformation involves many brain areas from the superior colliculus (SC) to the cerebellum. Some of these areas are similar to those involved in the smooth pursuit generation (de Xivry 2007). Usually smooth pursuit is executed for predictable target motion rather the saccades are used in correspondence of static target. In case of moving target the oculomotor system uses a combination of the smooth pursuit eye movement and saccadic movement, namely “catch up” saccades to fixate the object of interest. Recent studies investigate the mechanisms underlying the programming and the execution of catch-up saccades in humans (de Brouwer and Missal 2001; de Brouwer et al. 2002a;b).

The model presented in sec. 1.5 (and Zambrano et al. 2010) is able to predict target trajectories that present a second order dynamics. It is possible to extend this model to cope with more complex target motions with nonlinear dynamics as suggested in sec. 2.4 (Falotico et al. 2009). This model is composed by a saccade generator system and a predictive model of smooth pursuit eye movement. The smooth pursuit controller has been proposed by Shibata (Shibata and Schaal 2001). This controller

learns to predict the visual target velocity in head coordinates, based on fast on-line statistical learning of the target dynamics. This model has been modified to improve its convergence speed by using a memory based internal model that stores the already seen target dynamics (Zambrano et al. 2010). Fig. 1.3 shows the smooth pursuit model block schema. The Estimator State module generates the target velocity estimation and computes position by integrating the velocity information. The state vector is used by the Predictor to compute the target velocity in the next time step. The Inverse Dynamics Controller generates the necessary torque force that allows the Eye Plant to reach the predicted velocity. This controller corresponds to the low-level velocity controller of the robot. The control model consists of three subsystems: a RLS (Ljung and Soderstrom 1987) predictor (see sec. 1.4) mapped onto the MST, which receives the retinal slip, i.e. target velocity projected onto the retina, with delays, and predicts the current target motion; the inverse dynamics controller (IDC) of the oculomotor system, mapped onto the cerebellum and the brainstem; and the internal model that recognizes the already seen target dynamics and provides predictions that are used alternatively to the RLS predictor. The third part is based on the fact that there is a direct relationship between the angular frequency of the target dynamics and the final weights of the model. Such values depend only on the angular frequency of the target dynamics and on the configuration of the system, being independent from the amplitude and the phase of the sinusoidal motion. A memory block (Internal Model) recognizes the target dynamics and it provides the correct weights values before the RLS algorithm. For this purpose, such weight values are stored in a neural network (MLP) for future presentation of learned target dynamics. The neural network outputs are the correct weight values of the corresponding target dynamics. Such weights are set to the predictor module in order to guide the RLS algorithm to final values improving the converging speed (see sec. 1.5 and Zambrano et al. 2010). Concerning the Saccade Generator block, it has been implemented the results provided from recent studies (de Brouwer and Missal 2001; de Brouwer et al. 2002a;b). These studies show that the smooth pursuit motor command is not interrupted during catch-up saccades. Instead the pursuit command is linearly added to the saccade. From experimental data analysis it has been also shown that there is a specific equation that can generate a correct saccade, taking into account both position error $e(t)$ and retinal slip $\dot{e}(t)$:

$$ES_{amp} = 1 * e(t) + (0.1 + S_{dur}) * 0.77 * \dot{e}(t) \tag{2.2}$$

Where ES_{amp} is the exact amplitude of the saccade that will catch the moving target and S_{dur} is an estimate average saccade duration (= 0.074). Although the experimental results show that the final position error is not always cancel out by the catch-up saccade and that it is influenced by retinal slip (de Brouwer and Missal 2001; de Brouwer et al. 2002a), for this robotic implementation it has been used the exact formula. Moreover the saccade amplitude is converted in a velocity profile in order to keep the same velocity control using for the smooth pursuit system and

to obtain the linear adding of the smooth pursuit and saccadic command. The mechanism underling the decision to switch from the smooth pursuit system to the saccadic system has been also studied (de Brouwer et al. 2002b). What it has been found is that the oculomotor system uses a prediction of the time at which the eye trajectory will cross the target, defined as the eye crossing time T_{XE}. This value has been defined as the ration between the opposite of the position error $e(t)$ and retinal slip $\dot{e}(t)$:

$$T_{XE} = -\frac{e(t)}{\dot{e}(t)} \tag{2.3}$$

This time is evaluated 125 ms before saccade onset due to the visual system delay. On average, for between 40 and 180 ms no saccade is triggered and target tracking remains purely smooth. In contrast, if is smaller than 40 ms and larger than 180 ms, a saccade is triggered after a short latency. With regard to the proposed implementation the Equation 2.3 for the eye crossing time poses two problems. First of all, the equation presents a discontinuity when the retinal slip is null. Although this case, probably never happens in real systems, in principle, the smooth pursuit controller tries to reduce the retinal slip as much as possible. Thus the trigger system will command for a saccade even if it is not necessary. The second problem connected with the previous, is that the robotic system has some intrinsic limits firstly due to the noise added to the measure of the position error from the cameras. Others sources of errors are the accuracy of the motor system and the noise on the encoder. Thus the accuracy of the entire system is not less 3 degrees. For these reasons it has been added a threshold value for which the saccade will be not generated if the absolute value of the position error is smaller than 3 degree. This threshold could be modified depending on the characteristic of the specific robotic system.

2.7. Results

The model has been tested on the iCub Simulator and on Matlab Simulink. Both implementation results showed in the figures below, try to reproduce experiments on humans (described in de Brouwer et al. 2002b). These experiments aim at studying the interaction between saccades (catch-up saccades) and smooth pursuit. Fig. 2.6 show examples of responses to unexpected changes in target motion. In particular they show a typical response to an increase in target velocity between two ramps. Smooth pursuit system is able to cancel out the retinal slip during the first ramp, but has no influence on the position error on the retina. So, when the second ramp occurs, the position error increases and one or more corrective saccades are elicited to reach the target. The Fig. 2.6 is the result of a test executed on the iCub Simulator (described in sec. 2.2). The implementation confirms expected results,

according to human experimental data (de Brouwer et al. 2002b). The model has been tested on sinusoidal target motions (already tested as input in Equation 1.7). Fig. 2.7 shows the results of an example of simulation with a sinusoidal motion target with frequency of 0.2 Hz and 0.4 Hz. The target position and the eye position are aligned for five seconds, when the target position follows an already known sinusoidal motion. After this time the frequency of the sinusoidal target motion is doubled. The position error increases and some saccades are elicited. Saccades correspond to peaks in the position error time course. The model is able to cancel the retinal slip with the smooth pursuit and the position error with catch-up saccades. Preliminary tests have been executed on the iCub robot. The model has been tested on sinusoidal target motions with the dynamics described in Equation 1.7. The tracking algorithm used is based on Particle Filtering method (Taiana et al. 2008; 2010). Fig. 2.8 shows the results of an example of simulation with a sinusoidal motion target with frequency of 0.5Hz. The number of saccade elicited is greater than the number of saccade elicited in the same test executed on the iCub simulator, because of the noise. The position error, after an initial phase, decreases and after 5 seconds is almost canceled.

This work presents a model and a robotic implementation to address the problem of tracking visual targets with coordinated predictive smooth pursuit and saccadic eye movements, like in humans. The oculomotor system uses prediction to anticipate the future target trajectory during smooth pursuit. When the object motion is unpredictable there is an accumulation of retinal error that is compensated by catch-up saccades. These movements are executed without visual feedback and in order to achieve better performance they have to take in account the retinal slip.

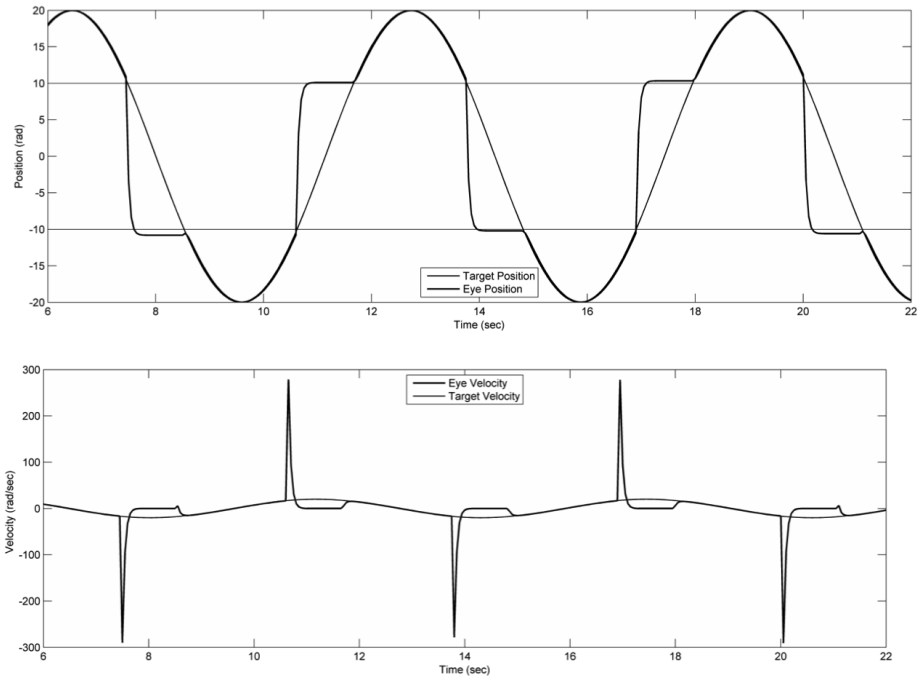

Figure 2.4.: The simulation results of the eye position and the target position (top) for a smooth pursuit tracking with occlusion of a sinusoidal target dynamics with angular frequency of 1 rad/sec and amplitude of 20 rad. The gaze saccadiclymoves across the occluder to continue tracking and arrives at the opposite side of the occluder slightly before the object. The eye velocity (down) has a peack on correspondence with the saccadic movement, then goes to zero until target reappearance.

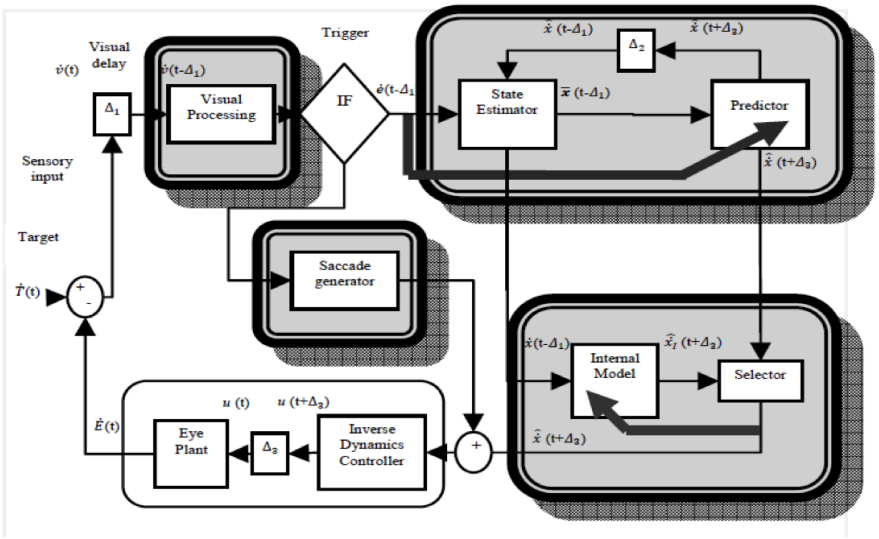

Figure 2.5.: The model schema is composed by a saccade generator system and a predictive model of smooth pursuit eye movement.

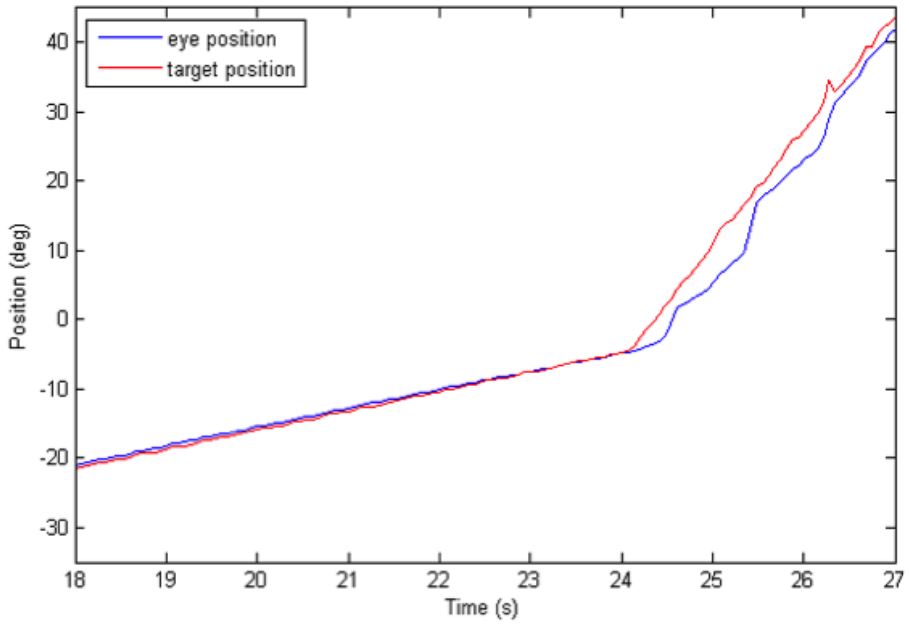

Figure 2.6.: Example of the responses to unexpected changes in target velocity between two ramps

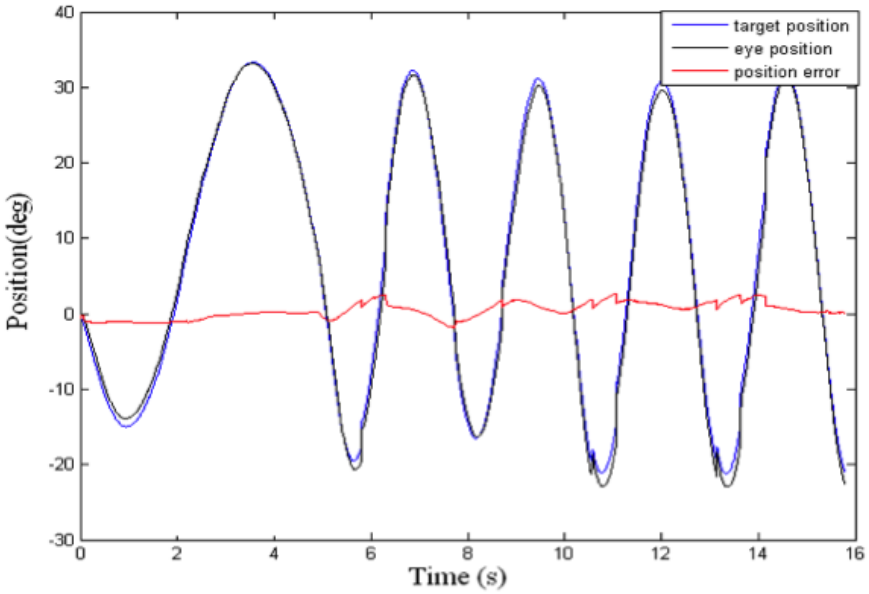

Figure 2.7.: A smooth pursuit trial, for which the combination of retinal slip and position error is such that smooth eye movement is sufficient to catch the target

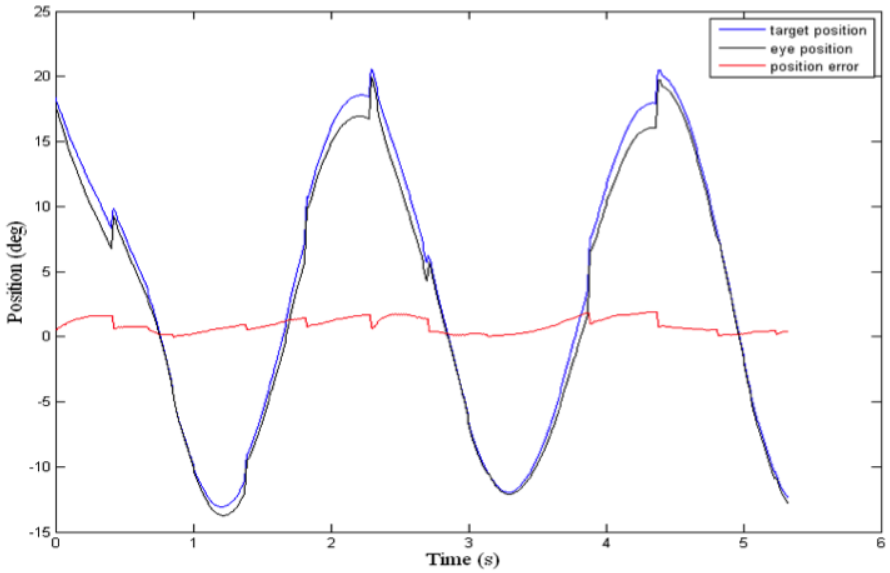

Figure 2.8.: Simulation on iCub robot of response to a sinusoidal motion of the target.

3. The gaze control

3.1. Overview

Space-varinat resolution retina imposes that when we want to examine an object in the world, we have to move the fovea to it. The gaze system performs this function through two components: the oculomotor system, which moves the eyes in the orbit, and the head movement system, which moves the orbits in space (Kandel et al. 2000). The gaze system also prevents the image of an object from moving on the retina. It keeps the eye still when the image is still and stabilizes the image when the object moves in the world or when the head itself moves. As described in chapter 1 the smooth pursuit system keeps the image of a moving target on the fovea. While the saccadic system shifts the fovea rapidly to a visual target in the peripheryn (see chapter 2). Vestibulo-ocular movements hold images still on the retina during brief head movements and are driven by signals from the vestibular system. Optokinetic movements hold images during sustained head rotation and are driven by visual stimuli. Finally, there are times that the eye must stay still in the orbit so that it can examine a stationary object. Thus, another system, the fixation system, holds the eye still during intent gaze. This requires active suppression of eye movement. When we look at an object of interest a neural system of fixation actively prevents the eyes from moving.

The foundations of cognition are built upon the sensory-motor loop - processing sensory inputs to determine which motor action to perform next. The human brain has a huge number of such loops, spanning the evolutionary timescale from the most primitive reflexes in the peripheral nervous system, up to the most abstract and inscrutable plans. This chapter, complete the loop of the gaze control, by analyzing the learning mechanisms that govern its behavior. At the subcortical level, the cerebellum and basal ganglia are the two major motor control areas, each of which has specially adapted learning mechanisms. The basal ganglia are specialized for learning from reward/punishment signals, in comparison to expectations for reward/punishment, and this learning then shapes the action selection that the organism will make under different circumstances (selecting the most rewarding actions and avoiding punishing ones). This form of learning is called reinforcement learning. The cerebellum is specialized for learning from error, specifically errors between the sensory outcomes associated with motor actions, relative to expectations for these sensory outcomes associated with those motor actions. Thus, the cerebellum can refine the implementation of a given motor plan, to make it more accurate,

efficient, and well-coordinated. Therefore we can say that the basal ganglia help to select one out of many possible actions to perform, and the cerebellum then makes sure that the selected action is performed well. A typical example of the role of the cerebellum in the gaze control is the VOR/OKR system.

3.2. The VOR/OKR system

This work is focused on oculomotor control, in particular in one of the most basic and phylogenetically oldest functions of oculomotor control: the visual stabilization. Since the oculomotor system resides in a moving head, successful visual perception requires that retinal images remain constant, at least for the time necessary for accurate analysis. The head motion is recognized by the oculomotor system and it knows how much to move the eyes to compensate for the head movement in order to maintain clear vision. The head motion is derivable from visual information because when the head moves the image of the world also moves on the retina. It is also possible to derive head velocity from proprioceptive systems of the neck and body. However, these sensory mechanisms are too slow. In contrast, the hair cells of the vestibular system sense head acceleration directly, and this sensing in turn allows those reflexes (that require information about head motion) to act efficiently and quickly. Due to the latencies of the oculomotor system, however, many evidence suggest that the brain, and in particularly the cerebellum, uses learning to overcome these delays and to obtain perfect stabilization (Ito 1984). The state of the art of these system models provides basically two different approaches to the problem of the modeling of this behavior. In one case (Shibata and Schaal 2001), Shibata and Schaal suggest the idea of feedback error learning (FEL) as a biologically plausible adaptive control concept (Kawato 1990). In this way they propose biomimetic oculomotor controller with accurate control performance and very fast learning convergence for a nonlinear oculomotor plant with temporal delays in the feedback loop. This model will be henceforward referred as FEL model. In another case (Porrill et al. 2004) Dean, Porrill and Stone propose an algorithm for the cerebellum, called decorrelation control, that offers the possibility of reconciling sensory and motor views of cerebellar function. The algorithm learns to compensate for the oculomotor plant by minimizing correlations between a predictor variable (eye-movement command) and a target variable (retinal slip), without requiring a motor-error signal. This model will be henceforward referred as decorrelation model.

From biological point of view, in the VOR movement there are evidences of adaptive behavior (Ito 1984). By manipulation of the retinal slip using magnifying spectacles the ratio between eye and head velocity (VOR gain) changes after a certain learning time. This adaptation involves the vestibular cerebellum area that participates also in the Opto-Kinetic Response (OKR). The OKR reflex is another eye movement responsible of the stabilization of images from the retinal slip information. The retinal slip based feedback control loop is too late (80-100 ms) to fix the image on the

retina. The VOR system and OKR system cooperate to achieve visual stabilization sharing the frequency range response; the first one provides image stabilization at much higher frequencies than the other one (Shibata and Schaal 2001). According to the FEL theory (Kawato 1990), Gomi and Kawato proposed a model of VOR and OKR learning for image stabilization (Gomi and Kawato 1992). In Lisberger et al. proposed models (Raymond and Lisberger 1998; Stone and Lisberger 1990a;b), the VOR learning occurs not only in the cerebellar focculus but also in the brainstem. These models are related with previous works of Lisberger and colleagues (Stone and Lisberger 1990a;b). However this idea seems not in according with the FEL theory proposed in Shibata and Shibata (Shibata and Schaal 2001). Other works that employ an adaptive system for vestibulo- ocular reflex similar to FEL are provided by Quinn et al. (Quinn et al. 1992) and Berthouze et al. (Berthouze et al. 1996). The compared models take in account different parts of the characteristics described in the literature. The adaptation mechanism, provided by the models, is the main differentiation point between the two approaches.

3.3. The image stabilization models

The FEL model (Shibata and Schaal 2001) (Fig. 3.1) underlines the importance of two basic ocular reflexes involve in non-blurred visual perception: the Opto-Kinetic Reflex (OKR) and the Vestibulo-Ocular Reflex (VOR). In particular it investigates the cooperation between these two ocular movements. OKR receives a sensory input (the retinal slip) which can be used as a positional error signal, and its goal is to keep the image still on the retina. VOR uses instead as sensory input the head velocity signal (acquired by vestibular organ in the semicircular canals), inverts the sign of the measured head velocity and, with the help of a well-tuned feedforward controller, rapidly generates the appropriate motor commands for the eyes. To achieve appropriate VOR-OKR performance, the authors of the model synthesize the VOR system as a feedforward open- loop controller using an inverse control model. The OKR is defined instead as a compensatory negative feedback controller for the VOR, involving the PD controller based on retinal slip. These two systems form what is called the “direct pathway” of oculomotor control in biology. According to the authors (Shibata and Schaal 2001), to accomplish excellent VOR and OKR performance, it is necessary to introduce an “indirect pathway”. It corresponds to a learning network located in the primate cerebellum. It acquires during the course of learning an inverse dynamic model of the oculomotor plant. The learning controller takes as input the head velocity and the estimated position of the oculomotor plant and outputs necessary torque. It is trained with the FEL (feedback-error-learning) strategy. FEL employs an appropriate way of mapping sensory errors into motor errors that, subsequently, can be used to train the neural network by supervised learning. As a computationally efficient learning mechanism, the authors suggest using recursive least squares (RLS) (Ljung and Soderstrom 1987 similarly to the

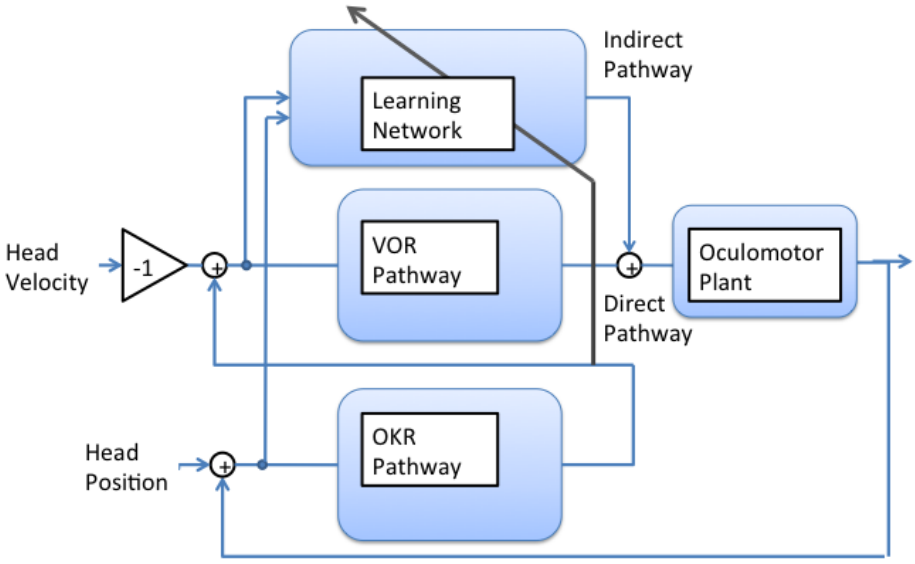

Figure 3.1.: The algorithm feedback-error-learning (FEL) acquires an inverse dynamic model of the oculomotor plant.

one used in sec. 1.4) for the "learning network", introducing a small modification in the standard RLS algorithm. For successful FEL, the time-alignment between input signals and feedback-error signal is theoretically crucial. To solve this problem the authors suggest the concept of eligibility traces, and model them as a second order linear filter of the input signals to the learning system.

The decorrelation model (Dean et al. 2002) (Fig. 3.2) investigates the structure and plasticity of the cerebellar cortex with the aim to reveal the basic cerebellar microcircuit. First the transformation of mossy-fiber input into parallel fiber activity is seen as splitting the input signal into simpler components. Second synapses between parallel fibers and Purkinje cells are seen as "weighting" signal components. Third climbing fiber input acts as a teaching signal, enabling the cerebellum to be involved in motor learning through the alteration of the weights. It is commonly assumed that this teaching signal must be motor error (the difference between actual and correct motor command), but this approach requires complex neural structures to estimate unobservable motor error from its observed sensory consequences. So the authors of the model propose a recurrent decorrelation control architecture in which the model learns without requiring motor error. By definition sensory error is caused by motor error. Values of the relevant sensory variable are therefore correlated with preceding motor commands if those commands are incorrect. The purpose of decorrelation

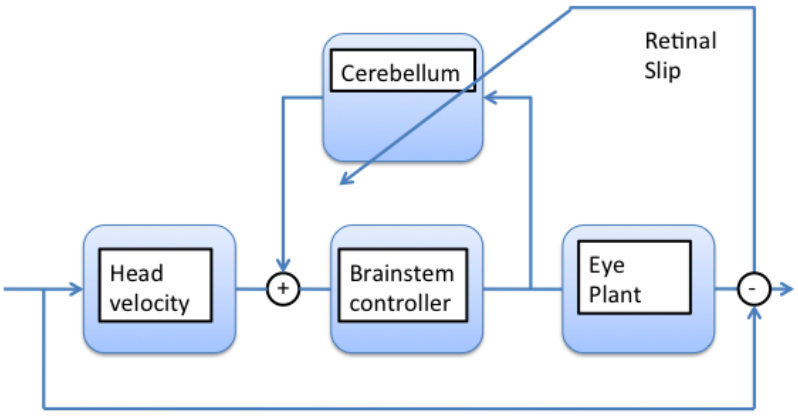

Figure 3.2.: A recurrent decorrelation control architecture that learns without requiring motor error.

control is therefore to remove any correlation between motor command (carried by the mossy-fibers) and the variable that codes sensory error (carried by the climbing fibers). The equation is:

$$\delta\omega_i = -\beta \cdot e(t) \cdot y_i(t) \tag{3.1}$$

The change ($\delta\omega_i$) in the weight (ω_i) of the synapse between the i-th parallel fiber and the target Purkinje cell is proportional (with learning-rate constant β) to the product of the sensory error e(t) (corresponding to the difference between the head velocity and the eye velocity) and the signal in the i-th parallel fiber $y_i(t)$. So this learning finally ceases when the component of motor command is decorrelated from sensory error.

3.4. Comparison results

The described models provide two different approaches to the modeling of visual stabilization system in humans. The comparison of the models performance concerns

the position error on the camera image during the post training phase (Franchi et al. 2010). Both approaches concern the neurophisiological adaptive mechanism able to fixate images on the retina compensating the head movements. The VOR reflex uses the vestibular information to estimate the head velocity and generates an appropriate motion signal that controls the eye motion in the opposite direction compared with the head motion. It has been shown (Ito 1984) that this control system has adaptive properties and this behavior resides in the cerebellum. The adaptive system uses the retinal slip as error signal and compensates for the eye dynamics, the control loop latencies and the nonlinearity due to the offset between the rotational axes of the eyeballs and the head. Despite that both models provides a bio-inspired solutions to representing these system characteristics, the proposed learning control systems are completely different. In the FEL model (Shibata and Schaal 2001) the authors propose a learning network which acquires during the course of learning an inverse dynamic model of the oculomotor plant that compensates for the missing performance of the direct pathway. Moreover the authors consider the component of another eye movement, the OKR system that collaborates with the VOR sharing the frequency bandwidth response. This component plays a fundamental role in the control loop driving the feedback error signal to the controller and compensating also for the position error. Instead in the decorrelation model (Dean et al. 2002) the OKR component is not considered and the approach is more focused on the cerebellar learning modeling. The purpose of decorrelation control is to remove any correlation between motor command (carried by the mossy-fibers of the Purkinje cells) and the variable that codes sensory error (carried by the climbing fibers and corresponding to the difference between the head velocity and the eye velocity) through a simple learning rule. The idea is that the cerebellum splits the input signal into simpler components and uses the velocity error as teaching signal, enabling the motor learning through the alteration of the synapses weights.

The differences between the two control systems lead to fully distinct results in terms of learning and generalization phases. The FEL model is characterized by fast and simple online learning technique that allows fast changing of the input dynamics (see Fig. 3.3). After the learning phase the model well responds to a large spectrum of input dynamics by varying for a short time the regression parameter vector. This adaptation velocity is due to the simplicity of the learning mechanism representation. While on the one hand this approach corresponds to high computational efficiency, on the other hand the representation could be, in some cases, too simple to well match with the oculomotor control system complexity. In the decorrelation model the learning phase has to be long (more than 300 sec) in order to explore a wide range in the input-output matching space. This guarantees a good performance on the band-passed random signal which is similar to the human walking one. Moreover this is an optimal starting point to a further learning of different input signals. The system performances largely depend on the kind of learning phases chosen. Although in this work it has not been represented, it is reasonable to assume that higher performances are obtained by a larger learning phase. Nevertheless the system

employs higher resources in terms of computational burden. Further experiments on the iCub platform confirms the results described (Franchi et al. 2010). However, for the further experiments the FEL model has been taken into account, mainly due to the OKR compontent and to the fast learing phase presented by the model.

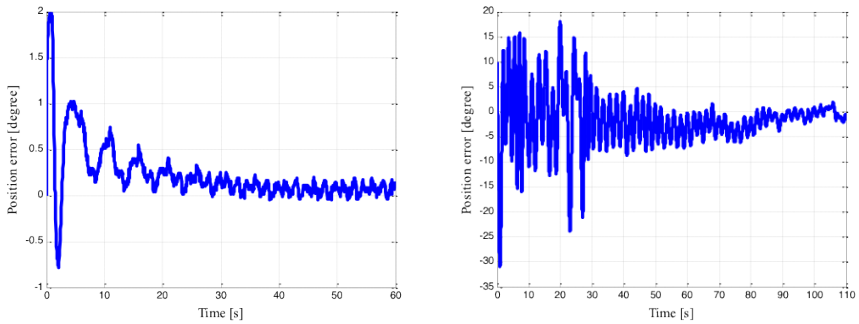

Figure 3.3.: Time course of the position error during the post training phase of the FEL model (left) and decorreletion model (right).

3.5. Basal Ganglia and action selection

As illustrated in Fig. 3.4, the basal ganglia (BG) is a group of interconnected subcortical nuclei. In the rat brain, the principle basal ganglia structures are the striatum, the globus pallidus (GP), the entopeduncular nucleus (EP), the subthalamic nucleus (STN), and the substantia nigra pars reticulata (SNr). The striatum receives somatotopic cortical input from the sensory, motor, and association areas. The major output structures are EP and SNr. They maintain a tonic inhibition on thalamic nuclei that project on the frontal cortex, in particular on motor areas. The internal connectivity of the BG has long been interpreted as a dual pathway, a direct pathway, consisting of inhibitory striatal efferents which projects to the EP/SNr, and a parallel excitatory indirect pathway, projecting to EP/SNr by way of GP and STN. This interpretation has been shown to have several shortcomings, in particular, it fails to account for several anatomically important pathways within the BG and to accommodate recent clinical data. The model proposed by Gurney, Prescott and Redgrave (Gurney et al. 2001a;b) (henceforth the GPR model) reinterprets the basal ganglia anatomy as a set of neural mechanisms for selection in a new, dual-pathway functional architecture. A selection pathway, including D1 striatum (i.e., striatal neurons with D1 dopamine synaptic receptors) and STN, operates through disinhibition of the output nuclei (EP/SNr). A control pathway, involving D2 striatum (i.e., striatal neurons with D2 dopamine synaptic receptors) and STN, modulates the selection process in the first pathway via innervations from GP. Moreover, Humphries and Gurney (Humphries and Gurney 2002) embedded the two circuits into a wider anatomical context that included a thalamo-cortical excitatory

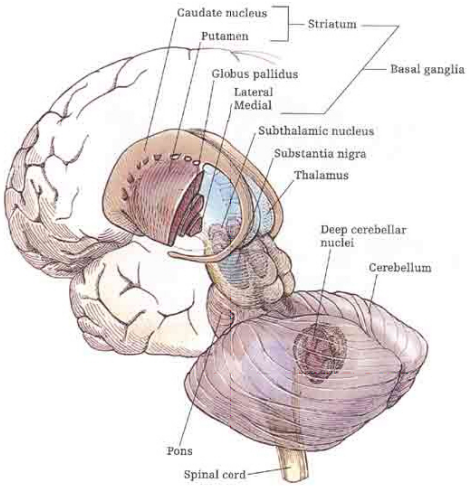

Figure 3.4.: The basal ganglia and the cerebellum may be viewed as key elements in two parallel reentrant systems that receive input from and return their influences to the cerebral cortex through discrete and separate portions of the ventrolateral thalamus.

recurrent loop whereby the output of the basal ganglia can influence its own future input. Within the selection pathway, the more salient an action is, the more the D1 striatal neurons inhibit the output nuclei neurons of the same channel. The tonic inhibitory output of each channel in the GPi/SNr, therefore, decreases with increasing inhibition provided by the striatum (and, by definition, with increases in the salience level). With a sufficiently high level of salience the output channel can effectively be turned off, removing its tonic inhibition. This causes complete disinhibition of the targets of that channel (a subset of cells in the BG target nuclei and/or a subset of those nuclei). Any subsequent excitatory input reaching these targets such as, for example, a motor command from the cortex, could then cause the target cells to fire. This mechanism of selection has been termed 'selective disinhibition'. Furthermore, the diffuse projections of STN neurons to GPi/SNr across multiple channels allows STN to increase the output level of non-selected channels. This emphasizes the difference in output of the selected and non-selected channels. However, because each GPi output channel receives input from all STN channels, a mechanism for scaling the level of excitation is necessary. The control pathway has several functions, one of which is to limit, via the GPe–STN negative feedback loop, the overall level of activity (Gurney et al. 2001a). This limit is kept roughly constant as BG recruits more channels so that the selection process can continue properly. Analysis and simulation of a quantitative model of the functional anatomy showed that the BG were capable of outputting signals consistent with action selection (Gurney et al. 2001a). This model will henceforth be denoted as the intrinsic model. Further, the ability of the model to perform action selection was critically dependent on the level of dopamine. When dopamine levels were too high, multi-

ple channels were selected too easily: this may correspond to many actions being executed and is consistent with behavioural states associated with attention deficit hyperactive disorder (ADHD). Very low levels of dopamine resulted in no selection occurring. This may correspond to immobility and the inability to initiate actions, as observed in Parkinson's disease patients. Thus, direct parallels could be drawn between the model's behaviour under abnormal dopamine conditions and disorders known to be caused by dysfunction of the BG.

The extended model uses leaky-integrator artificial neurons. Let u be the total afferent input and k be the constant determining the rate of activation decay. The activation a of a leaky integrator is then:

$$\dot{a} = -k(a-u) \tag{3.2}$$

where $\dot{a} \equiv da/dt$. In all that follows, we are describing the activation at equilibrium $\tilde{a}$ which is just $\tilde{a} = u$. The output y of the neuron, corresponding to the mean firing rate, is bounded below by 0 and above by 1. In simulation, this is achieved by using a piecewise linear output function. However, as we previously demonstrated (Gurney et al. 2001a), it is possible to ensure that y never exceeds 1 so that the output relation can be written as:

$$y = m(a-\varepsilon)H(a-\varepsilon) \tag{3.3}$$

where ε is the output threshold, *H()* is the Heaviside step function, and m is the slope of the output function. Motor cortex receives sensory input S_i from somatosensory cortex, and input from VL thalamus y_i^v , where i is the channel index. The strength of the synaptic connections from VL thalamus and somatosensory cortex are denoted by ω_{vl} and ω_s , respectively (weights are assumed to be given as absolute magnitudes throughout this section). If $\tilde{a}_i^m$ is the equilibrium activation of channel i in motor cortex then:

$$\tilde{a}_i^m = \omega_{vl} y_i^v + \omega_s S_i \tag{3.4}$$

Then, if ε_m is the output relation threshold term (see equation 3.3) the output yim of motor cortex is given by:

$$y_i^m = m(\tilde{a}_i^m - \varepsilon_m)H(\tilde{a}_i^m - \varepsilon_m) \tag{3.5}$$

The thalamic reticular nucleus receives input from three sources: motor cortex y_i^m, VL thalamus y_i^v and the BG output nuclei, y_i^b . Let the synaptic strengths from

the three sources be ω_m , ω_v and ω_{bg} , respectively, and let $\tilde{a}_i^t$ be the activation at equilibrium of the i-th channel of TRN, then:

$$\tilde{a}_i^t = \omega_v y_i^v + \omega_m y_i^m + \omega_{bg} y_i^b \tag{3.6}$$

Thus, if ε_t is the output relation threshold term, then the output y_i^t of TRN is given by :

$$y_i^t = m(\tilde{a}_i^t - \varepsilon_t) H(\tilde{a}_i^t - \varepsilon_t) \tag{3.7}$$

Ventrolateral thalamus (VL) receives input from motor cortex y_i^m , the BG output nuclei y_i^b and the TRN y_i^t. The inhibitory input from the TRN has two distinct components. Within- channel input is assigned the weight ω_T^*. The between-channel input contacts all channels in VL thalamus except the corresponding channel i. Hence, the total between-channel output of the TRN Y_i^t is given by:

$$Y_i^t = m \sum_{j \neq i}^{n} (\tilde{a}_i^t - \varepsilon_t) H(\tilde{a}_i^t - \varepsilon_t) \tag{3.8}$$

where n is the total number of channels. Let the strength of the between channel connection be ω_b, the motor cortical input be ω_x, and BG input be ω_o, then the activation at equilibrium of the i-th channel in VL thalamus is:

$$\tilde{a}_i^v = \omega_x y_i^m - (\omega_o y_i^b + \omega_T^* y_i^t + \omega_b Y_i^t) \tag{3.9}$$

Then, if ε_v is the output relation threshold term, the output y_i^v of VL thalamus becomes:

$$y_i^v = m(\tilde{a}_i^v - \varepsilon_v) H(\tilde{a}_i^v - \varepsilon_v) \tag{3.10}$$

Input to the striatum is a combination of sensory input (from somatosensory cortex) and motor cortical input, which we denote by S_i and y_i^m, respectively. The strength of the synaptic connections from somatosensory and motor cortex are ω_{sc} and ω_{mc} . Thus, the salience level c input to the i-th striatal channel is given by:

$$c_i = \omega_{bg} S_i + \omega_{mc} y_i^m \tag{3.11}$$

We retain the disparate action of dopamine used in the intrinsic model in the two separate pathways (selection and control) by using a multiplicative factor in the synaptic weight. Thus, let λ_e and λ_g parametrize the tonic level of dopamine in the control and selection pathways respectively, where $0 \leqslant \lambda_e, \lambda_g \leqslant 1$. Then the action of dopamine in the control pathway can be characterized as a modification to the synaptic weights: $(1 - \lambda_e)\omega_{sc}$ and $(1 - \lambda_e)\omega_{mc}$. Similarly, for the selection pathway $(1 - \lambda_e)\omega_{sc}$ and $(1 - \lambda_e)\omega_{mc}$. The activation functions for D1 and D2 striatal neurons, respectively, are then:

$$\begin{aligned} \tilde{a}_i^v &= \omega_x y_i^m - (\omega_o y_i^b + \omega_T^* y_i^t + \omega_b Y_i^t) \\ \tilde{a}_i^v &= \omega_x y_i^m - (\omega_o y_i^b + \omega_T^* y_i^t + \omega_b Y_i^t) \end{aligned} \tag{3.12}$$

The output relation for neurons in the selection pathway is:

$$y_i^g = m(\tilde{a}_i^g - \varepsilon) H^{\uparrow}(\lambda_g) \tag{3.13}$$

where $H^{\uparrow}(\lambda_g) = H(\tilde{a}_i^g - \varepsilon)$. The up-arrow emphasizes that the value of ε indicates the difficulty of the UP/DOWN state transition: if ε is given a positive value, then the neuron must receive input of at least this level to have a non-zero output. Similarly, the control pathway's output relation is:

$$y_i^e = m(\tilde{a}_i^e - \varepsilon) H^{\uparrow}(\lambda_e) \tag{3.14}$$

Similar to the striatum, the equations describing STN activation and output have to be rewritten to accommodate the split input from somatosensory cortex S_i and motor cortex y_i^m, which replaces the original single salience input. Let the strength of the synaptic connections from somatosensory and motor cortex be ω_{st} and ω_{mt}. Then the equilibrium activation $\tilde{a}_i^+$ of the i-th STN channel is given by:

$$\tilde{a}_i^+ = \omega_{st} S_i + \omega_{mt} y_i^m + \omega_g y_i^P \tag{3.15}$$

where ω_g is the weight of the GP–STN pathway and y_i^P is the output of GP. If ε' is the output relation threshold term, the output y_i^+ of STN remains:

$$y_i^+ = m(\tilde{a}_i^+ - \varepsilon') H(\tilde{a}_i^+ - \varepsilon') \tag{3.16}$$

where ε´ is given a moderate negative value to simulate the tonic output of STN. However, as STN output is diffuse across all channels in its target structures we need to consider the total STN output Y^+, which is given by:

$$Y_i^+ = m\sum_{j=i}^{n}(\tilde{a}_i^+ - \varepsilon')H(\tilde{a}_i^+ - \varepsilon') \tag{3.17}$$

The authors (Humphries and Gurney 2002) emphasize that the descriptions of the BG nuclei (striatum, STN, GPe, and GPi) given here are identical to those used in the intrinsic model (Gurney et al. 2001a), except for the split somatosensory and motor cortex input which replaces the single salience input into striatum and STN. A GPe channel receives input from the corresponding striatal D2 population channel yie (in the control pathway). It also receives input from all the STN channels Y^+. Let the striatum D2 to GPe connection strength be ω_{ep} and that of the STN to GPe connection be ω_{sp}. Then the activation at equilibrium $\tilde{a}_i^P$ of the i-th GPe channel is given by:

$$\tilde{a}_i^P = \omega_{sp}Y^+ - \omega_{ep}y_i^e \tag{3.18}$$

If ε_P is the output threshold term, then the output y_i^P of the i-th GPe channel is:

$$y_i^P = m(\tilde{a}_i^P - \varepsilon_P)H(\tilde{a}_i^P - \varepsilon_P) \tag{3.19}$$

A GPi channel receives input from three sources: the corresponding striatal D1 population y_i^g and GPe channel y_i^P, and diffuse STN input Y^+. The strength of the synaptic connections from striatum D1, GPe, and STN are given by ω_{gb}, ω_{pb}, and ω_{sb}, respectively. The equilibrium activation of the i-th GPi channel $\tilde{a}_i^b$ is thus given by:

$$\tilde{a}_i^b = \omega_{sb}Y^+ - \omega_{eb}y_i^P - \omega_{gb}y_i^e \tag{3.20}$$

Letting ε_b be the output threshold term, the output y_i^b of a GPi channel is:

$$y_i^b = m(\tilde{a}_i^b - \varepsilon_b)H(\tilde{a}_i^b - \varepsilon_b) \tag{3.21}$$

3.6. The basal ganglia model for the gaze system integration

The selection problem is just as relevant in cognitive aspects of behaviour. There is a mechanism (action selector) that arbitrates between competing choices. The action selection is viewed in terms of signal selection, by encoding the propensity for selecting a given action as a scalar value (the salience). The model implemented has some features which are desirable in an action selection mechanism Humphries and Gurney 2002. First, the selection depends on the relative salience levels of the competing actions. Therefore, the action with the highest salience is selected and expressed. Second, the termination of an action, in a normally functioning BG, occurs when an action is interrupted by a competing action with a higher salience. This condition ensures that the animal progresses smoothly from one action to another without a conflicting use of motor resources occurring. Third, the model presents clean switching: the competition between actions should be resolved rapidly and decisively. Fourth, once an action has been successfully selected, it is undesirable that its expression be hampered or temporarily interrupted by losing competitors (absence of distortion). Any losing competitor should be sufficiently suppressed so that it cannot interfere with the selected action. Furthermore, short-term increases in salience on a non-selected channel should also be suppressed, unless the increase is of a sufficient magnitude to warrant selection. Finally, when the competition for selection is between actions with almost equal saliences, then it is essential that the selected action continues after its salience has dropped below the level of its immediate competitors (persistence). Otherwise after selecting an action, the relative salience decreases and the selector should changes rapidly to the other one, therefore constantly oscillating between two behaviours: a phenomenon known as 'dithering'. The BGs are a set of interconnected nuclei, predominantly located in the forebrain. All the brain areas involved are represented as leaky-integrator artificial neurons. Respect to the winner-tak-all approach, a classical action selection mechanism, the elenced BG proprieties allow better performances in specific tasks Girard et al. 2003. In Fig. 3.5 the different channel saliences (red) and outputs (blue) in function of time are shown: the lowest value wins. At the beginning Channel 1 has the highest value and it is selected; the other channels are inhibited. As the Channel 2 salience increases Channel 1 is inhibited and Cannel 2 is selected. Despite the fact that Channel 1 salience has the same value it is still inhibited due to the absence of distortion propriety. The model has been implemented with three channels that correspond to the three different behaviours previously described: saccade, smooth pursuit (with catch-up saccade) and fixation (VOR).

In the case of oculomotor system, there are different sub-systems that are in competition for a common resource, the eye muscles. These functional units are physically separated within the brain but are in competition for behavioural expression. The principle of parallel but distinct pathways for pursuit and saccades extends to circuits involving the basal ganglia and thalamus. Cortical areas such as the FEF

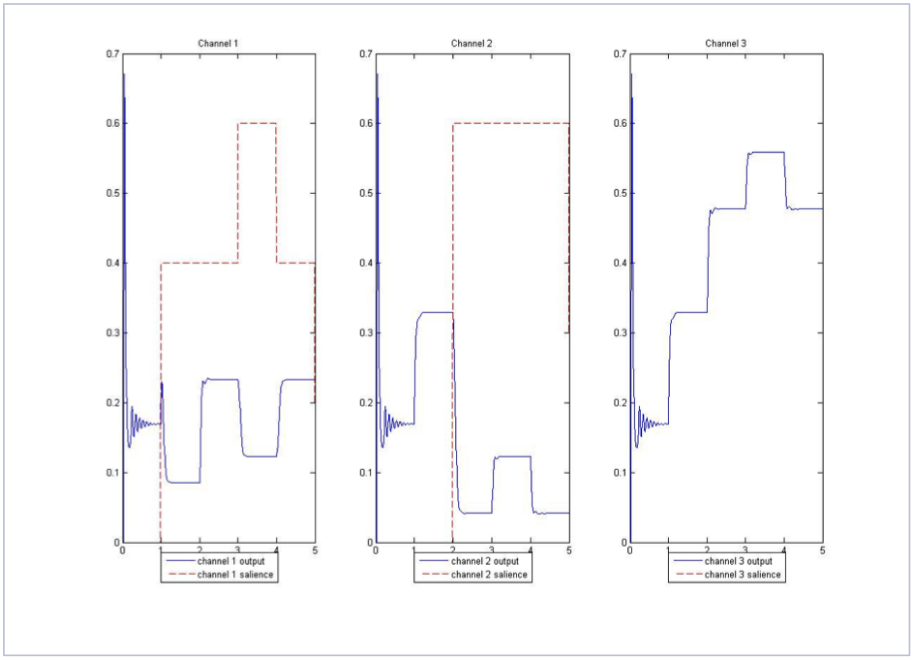

Figure 3.5.: Example of the BG model output for a 3-channel architecture.

project to the substantia nigra pars reticulata (SNr) via the caudate nucleus (CN) of the striatum, and a series of classic studies has shown how tonic inhibition exerted on the superior colliculus (SC) through this pathway is involved in regulating the triggering of saccades (for a review see Krauzlis 2004 and Krauzlis 2005). Recently, it has been demonstrated that the caudate receives input from the FEFsem, as well as from the FEFsac. The picture that emerges from these recent studies is quite different from the traditional view of the pursuit system (Fig. 3.6). In short, the pursuit system has started to look much more like the saccadic system. Both pursuit and saccades are gated motor responses that involve a break from ocular fixation. The operation of the gating mechanism for pursuit has long been discussed, but the site of the mechanism is unknown. Based on the partial overlap in the brain stem pathways for pursuit and saccades, we can now speculate that the gating of pursuit involves some of the same players in the premotor nuclei (PPRF, riMLF, cMRF, and OPNs) that regulate the gating of saccades, but with the circuitry cast into functional states that have not yet been identified. However, the recent data on the role of premotor brain stem structures in the control of pursuit provide new possibilities. In particular, the inhibitory relationship between OPN activity and pursuit suggests that they may be involved in gating pursuit, as well as saccades (Missal and Keller 2002). The exact circuit is not yet known, but Fig. 3.7 shows one recent proposal (Keller and Missal 2003). In this scheme, OPNs regulate the gain of pursuit through their inhibitory effect on pursuit neurons (PN) in the vestibular and prepositus nuclei, analogous to the way that they are believed to gate the occurrence of saccades through inhibitory effects on excitatory burst neurons (EBN)

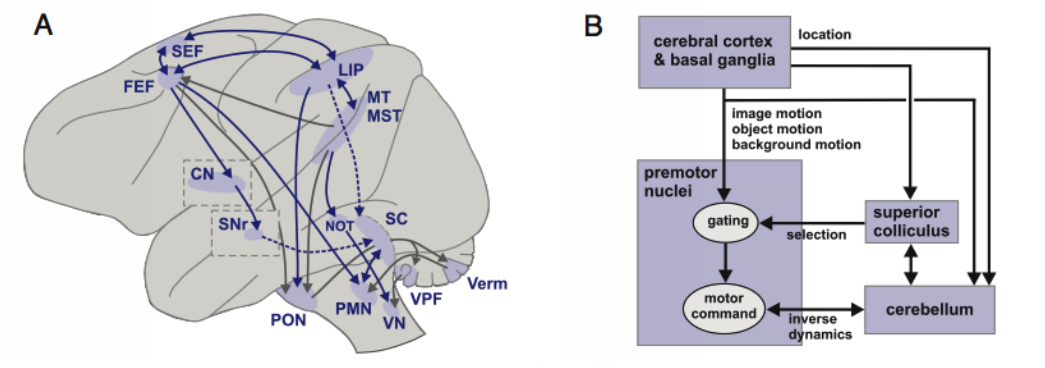

Figure 3.6.: Revised outline of the descending control pathways for pursuit eye movements (from Krauzlis 2004). A: schematic anatomical diagram of the descending pathways. Dashed arrows indicate presumed connections; B: functional diagram of the pathways controlling pursuit. Descending pathways from the cerebral cortex and basal ganglia provide sensory and command signals to the premotor nuclei, superior colliculus, and cerebellum. The pre-motor nuclei act to gate the descending signals and to construct the motor command. The superior colliculus contributes to the gating of pursuit and the cerebellum adjusts the final motor commands.

(see as example the saccadic system model proposed in Tabereau et al. 2007).

3.7. The integrated gaze system

In this phase a unified oculomotor system has been proposed to coordinate the different eye movements. In particular it has been possible to underline three different situations. The first corresponds to the moment in which the new desired focus of attention is identified: it happens thanks to a sensory processing module (a saliency map) which receives as input raw bottomup sensory signals from all available modalities and outputs the target for next saccade. After that the model output reaches the interesting target through the shift of gaze executed by its head-eye system. During the second kind of situation instead the pursuit eye movements are active to allow the robot to follow moving objects with the eyes: in particular the robot pursues moving targets by using a combination of smooth eye movements, which reduce the error between eye velocity and target velocity (retinal slip), and catch-up saccades, which reduce the error between eye and target positions. Finally the third situation concerns eye-head coordination after saccades: in particular, a gaze control model which lets to focus interesting target despite head motion has been implemented. In this case stabilization is possible thanks to the Vestibulo-Ocular Reflex (VOR), which lets to stabilize the image on the retina, and the Opto-Kinetic Response (OKR) which lets instead to fix and observe perfectly the interesting target.

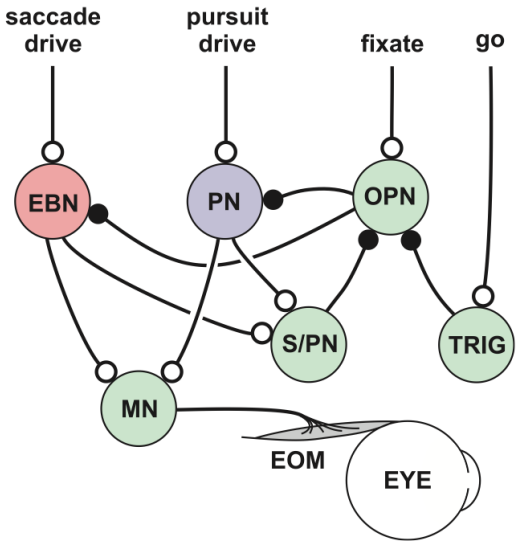

Figure 3.7.: Possible diagram of how premotor nuclei contribute to the gating effect in smooth pursuit, saccade and fixations (from Keller and Missal 2003; Krauzlis 2004).

Normally the dynamical neural network is active and lets to select the interesting target which is observed by the robot through the shift of its gaze. The pursuit of a moving object starts when the velocity of this object becomes bigger than a fixed threshold; as a consequence of this the sensory processing module stops and the combination of smooth eye movements and catch-up saccades activates. Anyway the saliency map can reactivate at the time that the robot is observing the target but suddenly it is attracted by a new object: in this case the sensory processing module outputs a new interesting target, and the robot tries to reach it through a new and different shift of gaze. When instead the amplitude of the saccades becomes bigger than a fixed threshold, it is necessary to activate the eye-head coordination and stop all the other movements; so the combination of VOR and OKR lets to stabilize the image of interesting target despite head motion. Anyway when the value of the velocity of the target becomes too high, a new pursuit starts and it is necessary to reactive the combination of smooth eye movements and catch-up saccades arresting the eye-head coordination. All these kinds of behaviours are coordinated by a basal ganglia (BG) model, that is able to solve the action selection problem. In Fig. 3.8 the implementation of the action selection mechanism for the eye movements control is shown. The architecture follows the schema presented in Fig. 3.6 and in Fig. 3.7. As a possible improvement of this work, a reinforcement learning mechanism can be added in order to let the system learn the best action to adopt in the different cases.

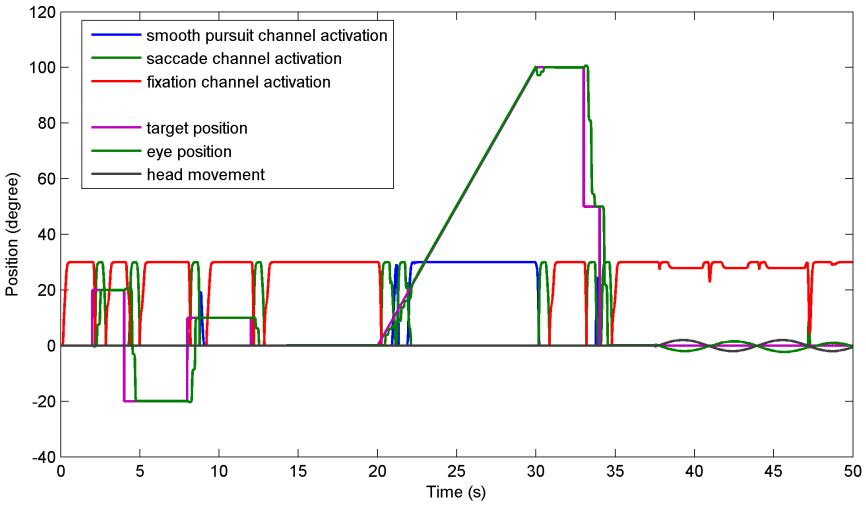

Figure 3.8.: Experimental results of the action selection mechanism for the eye movements control. The three channels activation are shown, for the smooth pursuit, the saccade and the fixation eye movements.

Part II.

A case study: gaze control during locomotion

4. Trajectory planning models

4.1. Overview

The human locomotion is a complex motor task that coordinates the activity of many different muscles and joints across each step. In terms of general behavior, this complexity can be modeled using simple rules due to the high redundancy presented by the motor system. This chapter presents a detailed analysis on recent neuroscientific models for the trajectory formation during locomotion task. With the aim to implement one of the presented approaches in a humanoid platform, these models have been applied on human data and compared. The gaze role has been highlighted with respect to the neuroscientific models compared (Zambrano et al. 2012).

4.2. Human trajectory planning models

In humans, during vision-guided walking task, gaze has an important role. It assists the locomotion allowing collision prediction, by planning the path to navigate in the environment or by providing cues in the surface on which humans are walking (Lewis et al. 2005; Marigold and Patla 2007). Land et al. (Land and Lee 1994) showed the gaze role for driving tasks in which humans are able to control the steering using visual information from road features. During a straight path, gaze aligned with environmental features lying in the subject's current plane of progression. However, prior to changing the direction of walking, gaze makes saccadic eye movements to aligning itself with the end point of the required path (Hollands et al. 2002). Saccadic eye movements typically anticipate step initiation in several locomotor tasks (Imai et al. 2001; Patla and Vickers 1997). In obstacle avoidance tasks, saccadic eye movements precede the leg that is preparing to move to the target during its stance phase. This behavior provides information before the foot lifts (Di Fabio and Greany 2003). Patla and Vickers (Patla and Vickers 1997) have identified three gaze behaviors: obstacle fixation, travel fixation and fixation in the 4-6 m region. Gaze obstacle fixation results needed for limb elevation control. The role of gaze fixations becomes more useful during precision-stepping tasks in which an accurate foot placement is needed to reduce the risk of falls (Patla and Vickers 1997). During these tasks gaze gathers information regarding anchors or key position (Di Fabio and Zampieri 2003; Di Fabio and Greany 2003). Marigold and Patla (Marigold

and Patla 2007) demonstrated that gaze fixations are task-relevant and that they are directed to regions that maximize the amount of information, which the human nervous system can integrate to guide safe foot placement. These results yield to the evidence that humans use the gaze to extract geometrical features of the environment and to plan the trajectory of the body. The human locomotion is a complex motor task that coordinates the activity of many different muscles and joints across each step. However, despite the high redundancy presented by the motor system and which is involved in such movements, stereotyped behaviors are observed. These behaviors can be studied following different approaches. In the next sections, the recent state of the art the human trajectory formation models, is reported. These models can be essentially divided in two different classes: *steering models* and *optimization models*. In the first class can be included the works made by Warren and Fajen (Warren 2006) and by Wilkie and Wann (Wilkie and Wann 2011). In this approach the locomotor trajectory is viewed in the framework of the dynamical systems. In the second class, indeed, is reported the optimal control principle approach that has been used to characterize the human walking (Pham et al. 2007). According to the robotic implementation specifications, the models are compared with respect to the trajectory error computed on human data.

4.3. Steering models

The main contribution of Warren and Fajen to the study of the human locomotion was the development of a general framework, called *behavioral dynamics* that can be used to anticipate human behaviour in different and complex locomotor tasks (Warren 2006). In this context, the human behaviour is described by the effect of the interaction between an agent and the environment. The dynamics of the behaviour and its proprieties of stability and flexibility emerge from the information exchange between the two mutually coupled dynamical systems. The formal description of the locomotion is given by a system of differential equations whose vector field correspond to the observed pattern of behaviour. In this perspective, an object-oriented locomotor task can be described considering the target as an attractor and the obstacle as a repeller. By applying this framework, the works developed by the authors model different kind of tasks such as the steering to a goal, the static or moving obstacle avoidance and the route selection (Fajen and Warren 2003; 2007). Moreover, the authors analysed the different kind of perceived information in the visual field as the contribution of the optic flow in the human walking control (Warren et al. 2001). Considering the simple task of steering to a stationary goal, the behaviour is described by a second order linear system (Eq. 4.1) in which the current heading direction ϕ, varying according to the steering angle, the heading angle error between the agent and the target $(\phi - \psi_g)$:

$$\ddot{\phi} = -b\dot{\phi} - k_g(\phi - \psi_g)(e^{-c_1 dg} + c_2) \tag{4.1}$$

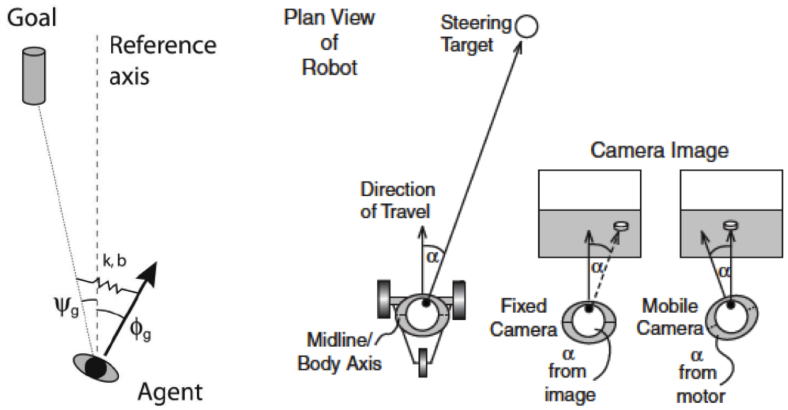

Figure 4.1.: Left. Representation of the Warren and Fajen model parameters. The dynamical system can be viewed as a second order linear system representing the spring that link the heading direction to the target. (Warren 2006). Right. An agent with fixed or mobile gaze is showed, representing the advantage of the mobile gaze in extending the visual field (Wilkie and Wann 2011).

This system could be viewed as an agent attached to the goal by a damped spring, where b represents the "damping" rate and indicates the resistance to the turning rate. The "stiffness" term k_g reflects the finding that the angular acceleration increases linearly with the heading error (Fig. 4.1 left), while dg represents the distance to the goal, c_1 (in units of 1/rad) is the rate of decay and c_2 (in units of 1/rad) a minimum value to ensure an efficient response also for distant goals. In case of obstacle avoidance, the authors finding was that the direction and the distance of the obstacle influenced the path (Fajen and Warren 2003). That case can be seen as a spring with inverse sign and whose stiffness is modulated as the distance to the obstacle (Fig. 4.1). The angular acceleration decreases exponentially with both heading error and obstacle distance:

$$\ddot{\phi} = -b\dot{\phi} - k_o(\phi - \psi_o)(e^{-c_3|\phi-\psi_o|})(e^{-c_4 do}) \tag{4.2}$$

In that case, do is the distance to the obstacle and c_3 and c_4 are decay rates (in units of 1/rad) of the stiffness due to the angular error and obstacle distance respectively (Eq. 4.2). Despite the fact that the main input to the system comes from the visual system and that it has been studied, the role of the optic flow in detecting the heading angle (Warren et al. 2001), these works exclude the importance of gaze as a fundamental component of the locomotion control. As argued by recent works presented by Wilkie and Wann (Wilkie and Wann 2011; Wilkie 2003; Wilkie and Wann 2005; Wilkie et al. 2008; 2010; Wann and Swapp 2000), there are at least two problems within the Warren and Fajen model: i) it assumes that only the heading direction is used to control the steering, when in some cases, it does

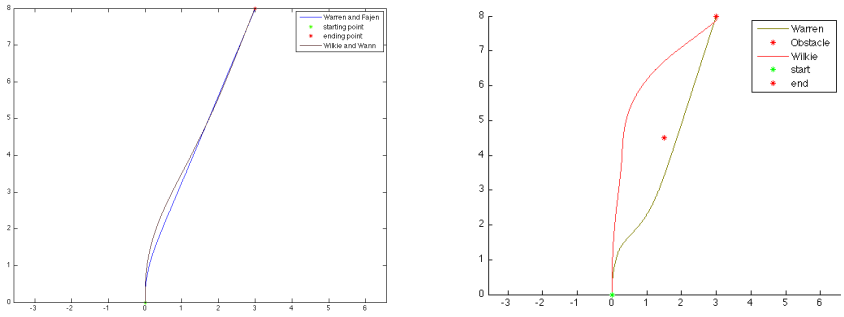

Figure 4.2.: Left. This picture shows the simulation results of the Warren and Fajen steering model compared with the Wilkie and Wann one. Right. Comparison of the model results in the presence of one obstacle.

not specify required steering angle; ii) it considers gaze as a complication. The authors contested the simple evidence that, if humans are evolved with a mobile gaze, this should be an important advantage also in the control of the locomotion. In particular, the mobile gaze can provide a larger visual field and by orientating gaze toward the desired steering goal, the agent can take information about the target using a weighted combination of visual and non-visual sources. The formulation of the steering model made by Wilkie and Wann considers a dynamical system (Eq. 4.3) in which the steering angle between the agent and the target is reduced by the effects of three main components:

$$\ddot{\theta} = k_1(\dot{\alpha}) - k_2(\alpha) - b\dot{\theta} \tag{4.3}$$

Where θ is the rate of the current steering response damped by the parameter b. Note that θ is equivalent to the steering angle $(\phi - \psi_g)$: used in (Eq. 4.1) and (Eq. 4.2), we used different notation to be in coherent with the Fig. 4.1 (right). The authors showed that the rotation input damped by the parameter k_1, could be provided by different kind of visual and non-visual information (Wilkie et al. 2010; Wann and Swapp 2000). To ensure the target reaching, the authors also added the error with respect to the target angle, a, damped by the parameter k_1, that can change with respect to the different kind of task. For instance, during walking, the target offset can be instantaneously nullified, but when we travel at higher velocities, like driving or biking, it is not safe to null a rapidly. In order to compare the descripted models we made a series of simulation using MATLAB (Fig. 4.2). For all the cited models we used as starting point $[x_s, y_s]$ the position in 2D coordinates [0, 0], and we located the target $[x_t, y_t]$ at the 2D position [3, 5]. The obstacle $[x_o, y_o]$ was located at the coordinates [1, 4]. The model computes steering angle, angular velocity and acceleration. Despite the conceptual differences of the steering models presented, the simulation results show that the trajectory obtained in a simple steering to a

target task, are noticeably similar. Both models have the main steering component at the beginning of the trajectory and then they reach the target with a smooth path (Fig. 4.2 left). The Wilkie and Wann's model has been also tested in the presence of multiple goals (Wilkie et al. 2008). In that case, the humans look at the nearest target until they steer it, then they switch gaze to the following nearest one. An experiment was made by the authors, in order to enhance the role of gaze in the steering behaviour (Wilkie et al. 2008), at high velocity, precisely during biking. The velocity condition keeps the subject attention to be focused, therefore the gaze is emphasised into the target. This observation encourages the examination of the extendibility of the model in a normal velocity locomotor task. As a result, the obstacle avoidance task is simulated and presented in Fig. 4.2 right. In the present work, an extension of the Wilkie and Wann model is proposed, by adding other input components β and $\dot{\beta}$ (see Eq. 4.4). These components represent the angle and its rate of change with respect to an intermediate obstacle, damped by two parameters k_3 and k_4 respectively. These components should have an opposite sign regarding the components original identified for a direct steering towards a goal.

$$\ddot{\theta} = k_3(\dot{\beta}) + k_4(\beta) - b_1(\dot{\theta}) \tag{4.4}$$

By starting from the same position, the Wilkie and Wann's model predicts in this more complex task an external path rather than the internal one showed by Warren and Fajen's model. This behaviour could be easily controlled if a fast velocity execution of the task is taken into account for the simulation.

4.4. Optimization models

In the framework of the optimal control, the problem of the human behaviour modeling is solved in terms of optimization theory (Flash and Hogan 1985; Todorov 2002; 2004). The system dynamics is a consequence of the control of a specific objective or cost function. Recent neuroscientific evidences suggest the existence of invariant proprieties in locomotor tasks (Pham et al. 2007; Hicheur et al. 2007; Arechavaleta et al. 2008). According to the framework of the optimization control, the formation of the locomotor trajectory seems related to the principle of the minimization of the jerk (third-order derivative of the position) that leads to maximizing the motion smoothness. The minimum squared principle (MSD) is defined as the trajectory that minimizes the nth order MSD cost function given by:

$$\int_0^1 \left(\left(\frac{d^n x}{dt^n} \right)^2 + \left(\frac{d^n y}{dt^n} \right)^2 \right) dx \tag{4.5}$$

The problem consists of finding the function that minimizes this functional for *n=3*, given the boundary conditions:

$$\begin{array}{llllll} x(0)=x_0, & x(1)=x_1 & \dot{x}(0)=v_0^x, & \dot{x}(1)=v_1^x, & \ddot{x}(0)=a_0^x, & \ddot{x}(1)=a_1^x \\ y(0)=y_0, & y(1)=y_1 & \dot{y}(0)=v_0^y, & \dot{y}(1)=v_1^y, & \ddot{y}(0)=a_0^y, & \ddot{y}(1)=a_1^y \end{array} \tag{4.6}$$

Generally, the optimization problem involves a system which can be described by a set of nonlinear differential equantions:

$$\dot{\mathbf{s}}(t) = f[\mathbf{s}(t), \mathbf{u}(t), t] \tag{4.7}$$

Where $\mathbf{s}$(t) is a n vector function of state variables and $\mathbf{u}$(t) is an m vector control function. In this case we define the state vector as $\mathbf{s}^T(t) = [x, y, u, v, z, w]$ and the control vector $\mathbf{u}^T(t) = [\delta, \gamma]$. The components of these vectors are defined by the system equations:

$$\begin{aligned} \dot{x} &= u \\ \dot{y} &= v \\ \dot{u} &= z \\ \dot{v} &= w \\ \dot{z} &= jerk_x = \delta \\ \dot{w} &= jerk_y = \gamma \end{aligned} \tag{4.8}$$

This problem can be solved by defining a n component co-state (Lagrange multipliers) vector $\lambda(t)$ and a scalar Hamiltonian:

$$H[\mathbf{s}(t), \mathbf{u}(t), t] = L[\mathbf{s}(t), \mathbf{u}(t), t] + \lambda^T(t) f[\mathbf{s}(t), \mathbf{u}(t), t] \tag{4.9}$$

The necessary conditions for a minimum are:

$$\begin{aligned} \mathbf{s}(t) &= f[\mathbf{s}(t), \mathbf{u}(t), t] \\ \dot{\lambda}(t) &= -\tfrac{\partial H}{\partial \mathbf{s}} \\ \tfrac{\partial H}{\partial \mathbf{u}} &= 0 \end{aligned} \tag{4.10}$$

The Hamiltonian is:

$$H = \lambda_x u + \lambda_y v + \lambda_u z + \lambda_v w + \lambda_z \delta + \lambda_w \gamma + \frac{1}{2}(\gamma^2 + \delta^2) \tag{4.11}$$

By the Eulero Lagrange equations:

$$\begin{array}{lll} \frac{d\lambda_x}{dt} = -\frac{\partial H}{\partial x} = 0, & \frac{d\lambda_y}{dt} = -\frac{\partial H}{\partial y} = 0, & \frac{d\lambda_u}{dt} = -\frac{\partial H}{\partial u} = -\lambda_x, \\ \frac{d\lambda_v}{dt} = -\frac{\partial H}{\partial v} = -\lambda_y, & \frac{d\lambda_z}{dt} = -\frac{\partial H}{\partial z} = -\lambda_u, & \frac{d\lambda_w}{dt} = -\frac{\partial H}{\partial w} = -\lambda_v \end{array} \tag{4.12}$$

And:

$$\frac{\partial H}{\partial \delta} = \lambda_z + \delta = 0 \quad \frac{\partial H}{\partial \gamma} = \lambda_w + \gamma = 0 \tag{4.13}$$

That implies:

$$\lambda_u = \frac{d\delta}{dt} \quad \Rightarrow \quad \lambda_x = \frac{d^2\delta}{dt^2} \quad \Rightarrow \quad \frac{d^3\delta}{dt^3} = 0 \quad \Rightarrow \quad \frac{d^6x}{dt^6} = 0 \tag{4.14}$$

Which is:

$$x(t) = a0 + a1 * t + a2 * t^2 + a3 * t^3 + a4 * t^4 + a5 * t^5 \tag{4.15}$$

and the same for the other axis.

We can solve the problem by applying the boundary conditions. As the MSD cost function and the conditions are uncoupled in x and y the optimum function is given by the polynomial of degree *2n-1* in time (Flash and Hogan 1985). The six boundary conditions then yield a 6th-oder linear system that in turn determines the six coefficients.

Fig. 4.3 shows an implementation of this method for a simple task of target reaching, as described in the previous section. The velocity profile shows a classical bell shaped curve with non zero initial velocity and null velocity at the end. The model proposed by Pham (Pham et al. 2007) does not consider the possibility to add obstacles in the model. The optimal control problem in that case can be seen as the problem to find a curve that pass through a specific point in a specific time. The solution proposed by Flash and Hogan (Flash and Hogan 1985) for the problem of via point (p) constraint trajectory optimization in arm movement, has been implemented in this work (Fig. 4.3). The problem in this case, is to generate the smoothest motion from the initial position to the final position in a given time. The head trajectory must move to the final position through a specified point at an unspecified time. In case of minimum jerk with interior point, the cost function changes by adding the interior point constraints. A vector of Lagrange coefficients and Hamiltonian is defined for $t \leq t1$ and other coefficients and Hamiltonian for $t \geq t1$. Now there are two Hamiltonians that are similar to the Hamiltonian defined in the point to point

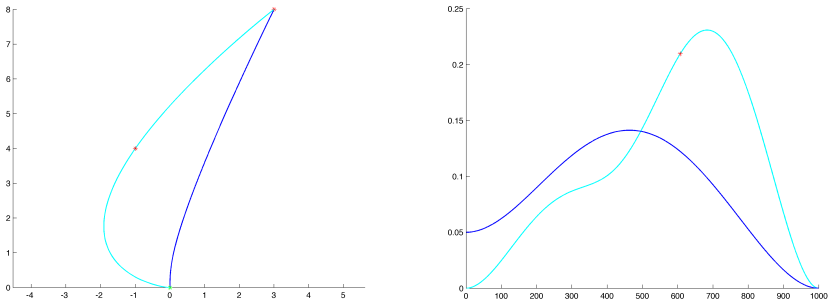

Figure 4.3.: Minimum jerk trajectory formation from a simple reaching task (top blue line). Via-point implementation (cyan) trough the point [-1,4] (red dot). Classical bell shaped velocity profile (bottom) for minimum jerk (blue line) and for via-point (cyan) with the time of passage (red dot).

problem. That means we should come to the solution of two fifth degree polynomials. We have one polynomial defined for $t \geq t1$ and another for $t \leq t1$. Totally we have 12 unknowns for axis. So we need 12 equations. We have 6 boundary conditions (position, velocity and acceleration at the beginning and at the end). In case of (Flash and Hogan 1985) the authors considered the velocity and the acceleration at the beginning and at the end equals to zero. Two equations come from the requirement of the continuity of velocities and accelerations at *t1*:

$u^+(t1) = u^-(t1), z^+(t1) = z^-(t1)$

Other two equations come from the Lagrange multipliers. From the Eulero-Lagrange equations we came to the conclusion that: $\lambda_x = \ddot{\delta}$, and $\lambda_z = \delta$. λ_u and λ_z must be continuos in *t1* (equations C9 in Flash and Hogan 1985), λ_x instead should consider the inner point as said in (equations C8 in Flash Hogan 1985):

$$\begin{aligned} \lambda_x^- &= \lambda_x^+ + \pi_1 \\ \lambda_y^- &= \lambda_y^+ + \pi_2 \end{aligned} \tag{4.16}$$

So now we have the equations of the movement $x^-$and x^+ (and y^- ,y^+ for the other axis) with two unknowns π_1 and the coefficient a_5 in the Equation 4.15. From that point by considering the continuity in position, we can have a system of two equations and two unknowns. Thus we can obtain π_1 and a_5 and substitute them in:

$$\pi_1 u(t1) + \pi_2 v(t1) = 0 \tag{4.17}$$

We obtain the value for *t1* and then the total expression for the entire movement in x(t) and y(t). The method generates two plane trajectories, one from the starting

point to (p) and the other form this point to the target assuring the continuity of velocity and acceleration in (p) and the minimum jerk with the passage time. This solution has been proposed by Flash and Hogan (Flash and Hogan 1985) for the arm movement, but the invariant proprieties in human locomotion suggest the possibility to adopt this solution for obstacle avoidance locomotion task. Their solution considers only the case of zero velocity and zero acceleration at the beginning and at the end of the movement. This relation was further studied from the point of view of compositionality of geometrical invariance, in the work made by Bennequin et al. (Bennequin et al. 2009), and it was compared quantitatively with the relation that exists for hand movements .

4.5. Experimental protocol

In this section the results obtained from the trajectory analysis of the performed experiment have been reported and discussed. The experimental protocol will be discussed also in the chapter 5. 10 subjects participated in an experiment with an optoelectronic VICON motion-capture system with 12 MX cameras. The locomotor behaviours have been captured at 120 Hz sampling frequency. Participants wore a tight black suit with 48 light-reflective markers located on body landmarks following the VICON Plug-in Gait model. Rotation and translation of the body segments were calculated from the 3D Euclidian position of the markers according to a space-fixed reference frame defined by the motion capture system (Xs, Ys, Zs). The vertical axis (Zs) coincided with the opposite direction of gravity. The Ys axis coincided to the long extension of the walking task with positive values from the box towards the Starting Point (see Fig. 4.4). The Xs axis coincided with the short extension of the walking task, with positive values from the box to the Starting Point. Participants were instructed to walk naturally. They had to walk along the trajectory involving avoidance obstacle, step on and over a box. We asked to the subject to perform the task in two different conditions: Natural Velocity (NV) and Fast Velocity (FV) conditions. Each trajectory condition was performed 10 times. In FV condition the subject had to walk as fast as possible without running. Trajectory was shown by finger to the subject. We asked the participants to start with the right feet. The size of the space to cover the trajectories was about 5 m x 4 m. The trajectory was not drawn on the floor. Movement of the participant's right eye was recorded using a video-based eye tracker system at 50 Hz sampling rate. The eye tracker was calibrated together with the motion capture system in space and in time. For that, we used an elliptic calibration grid of 1.45 m width and 1 m. height, composed of 17 markers forming an ellipsoidal grid. The temporal synchronization was done using a manual clapperboard with some reflective markers attached to it.

For the experimental validation of the proposed models only the first quarter of the trajectory has been taken into account (from the Starting Point to the Ending Point showed in Fig. 4.4). The first quarter represents the moment in which the

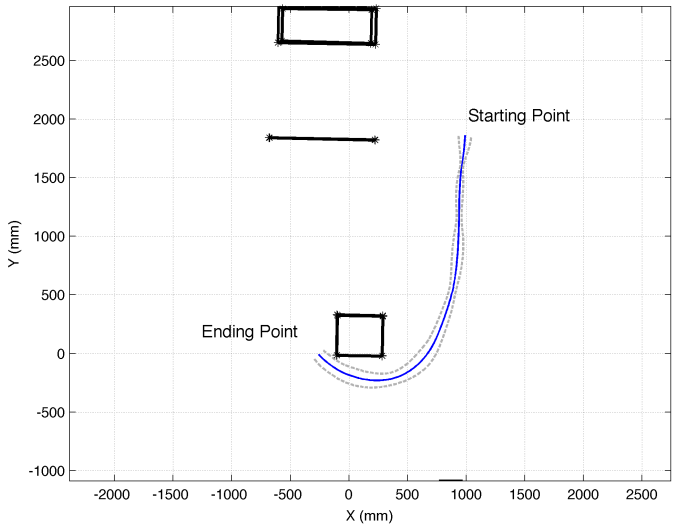

Figure 4.4.: Average (blue line) and standard deviations (grey dashed lines) of the head trajectory for 10 trials of one subject

subject overcomes the first obstacle. The comparison between the models has been computed with respect to the average of the ten trajectories performed by each subject $(x_{av}(t), y_{av}(t))$. As performance index it has been chosen the sum of the instantaneous trajectory error (TE) defined as:

$$TE(t) = \sqrt{(x(t) - x_{av}(t))^2 + (y(t) - y_{av}(t))^2} \tag{4.18}$$

Where x(t) and y(t) represent the trajectory generated by the examined model. The sum of the trajectory error (STE) represent the total error performed by the model with respect to the real trajectory. The maximum trajectory error (MTE) has been also computed and showed in the next session.

4.6. Comparision results

The results of the comparison are presented in Table 1. Both the Warren and Fajen model and the Wilkie and Wann model have been fitted on the curves. In order to represent the proposed scenario in the steering model framework, it has been considered that the agent can always see the Ending Point and the obstacle position. The obstacle has been represented as five point obstacles (the center and the four corners). The best fitting of the trajectory is obtained by tuning the model's parameters. The averages of the resulted parameters for the Warren and Fajen model were: b= $1.95, k_g = 9.2, c_1 = 2.54, c_2 = 0.37, k_o = 261.7, c_3 = 0.42, c_4 = 1.4$.

For the Wilkie and Wann model the averages of the obtained parameters were: $b_1 = 1, k_1 = 609, k_2 = 2.28, k_3 = 237.51, k_4 = 0.39$. The results of the two steering models implemented are showed in Fig. 4.5. The figure shows the average of the head

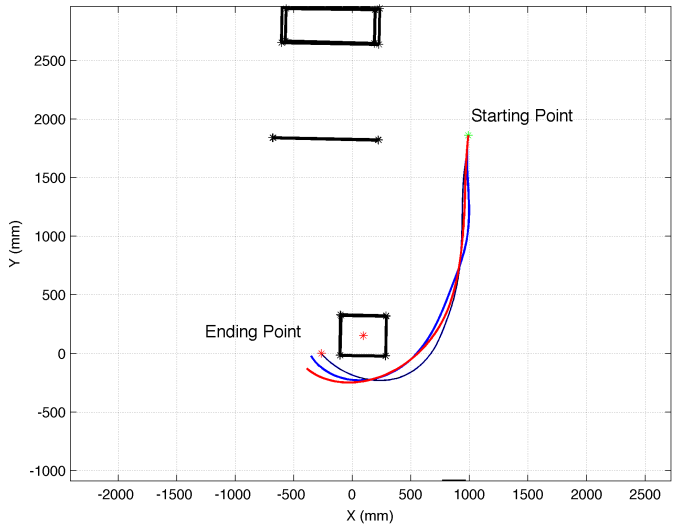

Figure 4.5.: Results of the fitting of the Warren and Fajen model (blue line) and the Wilkie and Wann model (red line) on the average head trajectory (black line) of one subject

trajectory of one subject (black line) and the trajectories obtained from the models (in blue the Warren and Fajen model and in red the Wilkie and Wann model). Both the steering models do not perfectly reach the target. Regarding the optimization model, it perfectly reaches the target since the boundary conditions necessary to obtain the equation coefficients, yield to a perfect fitting with the subject data. In case of the minimum jerk model it has been used the velocity and the acceleration data at the beginning and at the end of the considered trajectory. The solution proposed by Flash and Hogan (Flash and Hogan 1985) has been also implemented. According to the authors (Flash and Hogan 1985), the via point position in that case has been chosen as the value of the original head trajectory with maximum curvature (see Fig. 4.6).

From the obtained results, summarized in Tab. 4.1, the steering models represented the best fitting of human data in the presented context. In particular the model proposed by Wilkie and Wann had the best performance. Moreover this model was simpler with respect to the Warren and Fajen model and this is useful during the tuning of the model's parameter for the best data fitting. The possibility to include gaze control in this framework should be also taken positively into account. However these models cannot predict the correct velocity profile. The temporal relation in the obtained trajectory should be useful information especially in the robotic context. The solution given by the optimal principle approach seems to

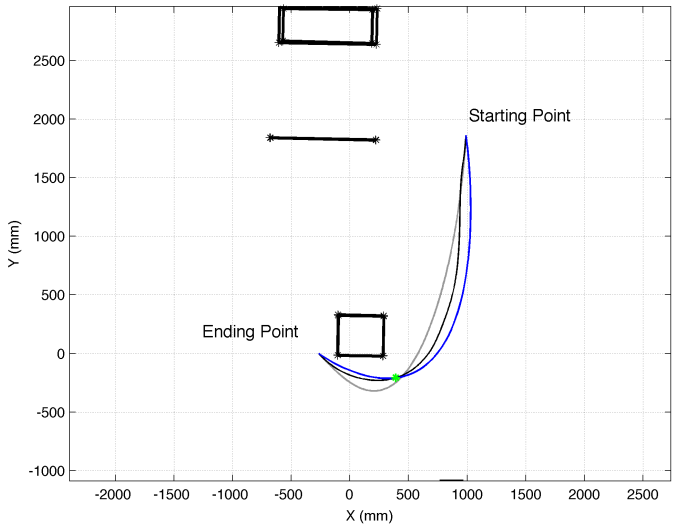

Figure 4.6.: Results of the optimization models. The black line represents the averaged head trajectory among ten trials of one subject. The blue line is the minimum jerk model proposed by Pham (Pham et al. 2007) while the grey line is the minimum jerk solution with via point proposed by Flash and Hogan (Flash and Hogan 1985)

fulfill both the behaviour and the velocity profile of the trajectory dynamics. This is possible due to the fact that we used original velocity and acceleration data as boundary values. The model predicts the correct shape showed by the subjects by using the final orientation of the human velocity data. However the proposed solutions do not correctly fit the human data. The similarity between the Flash and Hogan solution and the human data suggests that a not constrained boundary condition solution could correctly predict the head trajectory. Obstacle avoidance, via-points selection, not constrained boundary conditions and the gaze role, are open questions for the optimization principle approach to the human locomotion modeling.

Model Name	STE (mm)	MTE (mm)
Warren and Fajen	21335	173.54
Wilkie and Wann	21768	172.27
Pham et al.	49130	338.67
Flash et al.	42957	314.77

Table 4.1.: Comparison results in terms of sum of trajectory error (STE) and maximum trajectory error (MTE)

5. Gaze fixations during locomotion

5.1. Overview

This chapter aim at defining a model of the generation of walking trajectory from gaze. This includes modeling of gaze control in humans and his relationship with trajectory planning for locomotion. Our approach is based on the strong stereotype observed on the locomotor trajectory as classically observed also for the arm movements. Firstly several known neuroscientific models have been compared in order to explore the different aspects of the human trajectory planning in relation with the gaze. Secondly we used the results obtained from the experiments conducted, to precise the relation between gaze and the variability structure of the trajectory. Based on this study, a new model is proposed as general framework for the modeling of the locomotor trajectory planning in complex tasks.

The work can be divided in four parts: firstly, we noted that gaze is an important factor for the generation of a trajectory; however several aspects of gaze are reported: (i) a role for motor prediction, (ii) saccades to important cues (or else), allowing standard prediction, and (iii) fixation on specific elements in the environment, as obstacles or imposed via-points, for steering. In our study we assume that this third component of gaze behaviour is used for internal computation of the future trajectory. And we aim to exploit this information in addition to the motor prediction. We characterized better what are the fixation points, and defined the notion of LFP (Landmark Fixation Point). Secondly, we noted that the generation of locomotor trajectory for animals, in particular for humans, is not simple execution of a fully planed trajectory in advance; in particular some elements along the trajectory seem to be more anticipated than other. Thus we made the hypothesis that these elements correspond to the minimum of variability in the geometry and the kinematic of the trajectory. We determined the points where the geometric trajectory has less variation over repetition (MVPP) and points where velocity has less variation over repetition (MVPV). Third, we analysed the relation between LFPs times and MVPPs times, and fourth, we used this relation to construct a model of generation of trajectory.

5.2. Gaze and movement

Gaze drives and guides our movements. The relationship between gaze and actions has been studied in different kind of tasks from object manipulation (Johansson et al. 2001; Land 2004; 2009) to driving (Authié and Mestre 2011; Land and Lee 1994), biking (Wilkie et al. 2008) and walking (Land 2009; Land and Lee 1994; Marigold 2008; Marigold and Patla 2008; 2007; Marigold et al. 2007; Wilkie 2003; Wilkie et al. 2010; Wilkie and Wann 2003; 2005; 2006; 2011; Wilkie et al. 2008). Many works in literature demonstrated the direct relation between the gaze fixation pattern and the task, by which the gaze anticipates human actions (Johansson et al. 2001; Marigold 2008; Marigold and Patla 2007; 2008; Marigold et al. 2007). Humans use saccadic movements in order to direct the object of their interest in the centre of the retina, the fovea, which is the highest visual acuity area (Burbeck and Yap 1990; Levi and Klein 1996). In most of the cases, human eye movements are directed towards locations of the visual scene that catch their attention. These locations could reflect properties linked to the information content of the scene (many examples, (Authié and Mestre 2011; Land and Lee 1994) and to the previous knowledge about the environment (Baldi 2009; 2010; Rothkopf et al. 2007). In case of the gaze and hand movement relationship, we can easily distinguish in literature, two main kind of studies. In the first case, the gaze role has been analysed in relation to object manipulation tasks (Baldi 2010; Johansson et al. 2001; Land 2004; 2009). In this case it has been shown that the gaze is used to provide information to carry out the task. Within these task-oriented objectives, the subjects fixated only objects that are related with the ongoing activity and showed anticipative behaviour by switching the gaze, from the present object to the next one, before the manipulation is completed. These findings suggest that the kind of information required accomplishing the task, such as some object attributes, like location or grasping features, are taken in advance by the vision systems in order to guide the next action. In the second case, it has been analysed the relationship of the gaze and the control of the hand trajectory. The role of the gaze has been correlated with specific features of the hand trajectory (Reina and Schwartz 2003; Viviani and Flash 1995; Viviani and Terzuolo 1982). When writing, the hand shows a specific link between the curvature and the velocity of the executed motion. This is knows as 2/3 power law and depicts the evidence in which the velocity slows down when the curvature of the hand trajectory increases. However the ratio between velocity and curvature assumes different values during different phases of the motion, suggesting a segmentation of the trajectory into units of action. In closed loop drawing (Reina and Schwartz 2003; Viviani and Flash 1995; Viviani and Terzuolo 1982) the whole trajectory seems segmented in parts, separated by points where the angular acceleration reaches local maxima. In this tasks the gaze fixations anticipated the point in which the hand reaches the highest curvature. These evidences propose a specific link between the hand and eye kinematics. In case of navigation inside the environment, the kind of information available changes. Vestibular responses and optic flow are typical

suitable data generated by the self-motion (Berthoz 2000). Gibson (Gibson 1950) was the first supporting the idea that the focus of expansion is used to control the movement direction. He argued that the pattern of lights that reaches the eye, specifies the heading direction. Thus, in order to reach a target, it is sufficient to keep the focus of expansion on it. Driving is a typical task adopted to study the influence of optic flow in the gaze pattern. In this framework, it has been specified that when there is a rotation and a translation typical of curvilinear trajectories, the focus of expansion no longer exists (Gibson 1950). However, Land and Lee (Land and Lee 1994) observed that drivers oriented the gaze toward a specific point derived from the intersection between the inner edge line of the road and the tangent to this one, the tangent point. The fixations on the tangent point were made from one to two seconds before turning the wheels to steer, and frequently during the turn. In a recent study (Authié and Mestre 2011), the authors confirmed that the tangent point remains an important location in the visual scene for gaze direction. However they observed a systematic optokinetic nygstagmus behaviour (OKN) near the tangent point, by showing an active mechanism to extract the best useful information for the ongoing task. This kind of analysis manifests a highlighted optic flow influence due to the high motion velocity. In that sense the strategy that humans adopt during slow motions, such as walking, partially confirm these findings (Warren 1998; 2006; Warren et al. 2001). The authors suggested that the head, and not the gaze, guides the human walking (Warren et al. 2001). However, the importance of the active gaze has been recently revaluated during locomotion (Wilkie and Wann 2003; 2011; Wilkie et al. 2008). The eye movements seem crucial to getting optic flow information for navigation. The anticipative role of gaze has also been studied in terms of correlation with the consequent reorientations of body links (Hollands et al. 2002; 2004; Kadone et al. 2010; Patla and Adkin 1999). The resulting frame of reference reflects a top down organization that begins form the gaze motion. In human bipedal locomotion tasks, the gaze fixations have been studied to show their role for navigating, planning and approaching and avoiding obstacles (Hollands et al. 2002; 2004). Several works supports the idea that peripheral vision is sufficient for guiding actions also in presence of unpredictable obstacles (Marigold and Patla 2007; 2008; Warren et al. 2001). This argument is also reinforced by the work proposed by (Franchak and Adolph 2010), where young and adult subjects were studied in free walking environment. The authors showed that gaze fixations are not required for navigation of obstacles. The contribution of the optic flow information coming from peripheral visual field has been also linked to the path chosen by the subject (Jansen et al. 2011). The authors related the energy conservation principle in human locomotion (Donelan et al. 2004) with the need of safety approach to the obstacles. The results suggest that the humans use optic flow information to approach obstacles in order to keep the safest distance. Recent studies on the human locomotion show invariance proprieties of the generated trajectory compatible with the 2/3 power law (Hicheur et al. 2007; Pham et al. 2007). These findings are consistent with the optimization principles governing other human motions (Flash and Hogan 1985; Todorov 2004). The stereotyped behaviour has been founded both in terms of geometrical path and

in the kinematics with high variability in feet placement. In a successive work it has been also compared the performed trajectory with and without visual feedback (Pham 2009). As main result, the authors show that the averages of trajectories performed with visual feedback are comparable with trajectories performed without visual feedback, indicating the existence of a common optimality principle for both conditions. However the trajectory variability is affected by the visual feedback, indicating an on-line visual guided trajectory correction. In summary, during simple locomotion tasks, humans direct their gaze where they are going to step on (Marigold and Patla 2007), on the landing area after an obstacle (Land 2009) or where they can anticipate specific features of the trajectory (Kadone et al. 2010). In general, it corresponds to places where they can get information to guide their movements (Marigold and Patla 2008; Rothkopf et al. 2007; Wann and Swapp 2000). Despite these evidences no works in literature show a specific relationship between the gaze and the stereotyped behaviors performed by humans during locomotion tasks. Do humans use gaze fixations to get information from the environment or are there specific gaze fixation patterns correlated with the trajectory? Are there specific landmarks, points in which subject prefers to look at, that the subjects fixate during walking? In order to answer to these questions, a new paradigm for the gaze analysis during locomotion tasks in a 3D environment with obstacles is proposed. We examined the role of gaze during walking when the gaze is shared between several locomotor activities: turning around and avoiding an obstacle, stepping over and stepping on an object. To our knowledge at the moment, there is no study that adopts this complex protocol. We examined whether in a natural walking task, humans use fixations to guide their movements. If the gaze activity is correlated with the performed trajectory, stereotyped behaviours both in gaze fixations and in walking trajectories should be found. Moreover, we asked to the subjects to perform the same task in a fast velocity condition in order to constraint them to fixate only those points related to the task. Our hypothesis is that the gaze is involved in the segmentation of complex trajectories and it also helps to the correction of the trajectory variability toward specific control points. If the hypotheses are true, similar results should be found also in the fast velocity condition.

5.3. Methods

Participants 10 male subjects ranging in age from 24 to 33 years old (M=28.5) participated in the experiment. Participants did not have any sensory, perceptual or motor disorders. Participants wearing glasses or reporting to wear glasses to walk were excluded to avoid any recording problem with the eye tracking system. They were naive to the purpose of the experiment. The participants signed an informed consent form in agreement with the standards established by the Declaration of Helsinki.

Experimental Setup An optoelectronic VICON motion-capture system with 12 MX cameras was used to record the locomotor behaviours at 120 Hz sampling frequency (VICON motion systems Inc., Oxford, UK). The working volume was about 3.5x7x5 m^3. Participants wore a tight black suit with 46 light-reflective markers located on body landmarks following the VICON Plug-in Gait model (Fig. 5.1). To assess position and orientation of the head in space, four head markers were located over the right and left temple on the back and on the front of the head in the horizontal plane while the participant stands-up. We used the centroid of the four markers as the head position. We used the midpoint of the left and right shoulder markers as the trunk position. These markers were respectively located on the left and right acromio-clavicular joint. The centroid of the four markers located on the left and right anterior and posterior superior iliac spine was considered as indicating pelvis position. Two markers were located on each foot, placed on the toe (second metatarsal head) and on the heel at the same height as the toe marker. The positions of the makers were reconstructed and labelled using VICON iQ software. Movement of the participant's right eye was recorded using a video-based eye tracker system at 50 Hz sampling rate. The system was mounted on lightweight goggles that were fitted on the head tightly to avoid unexpected movements.

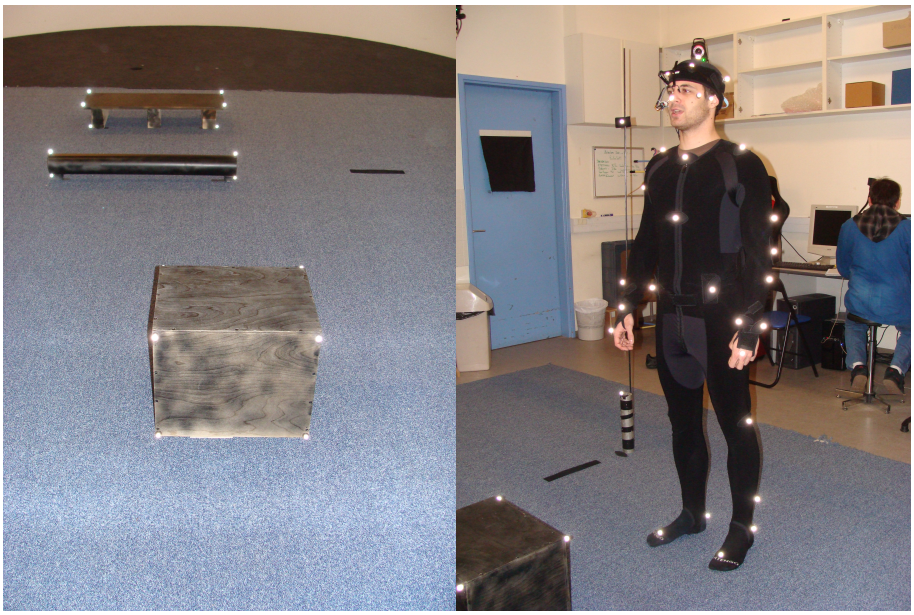

Figure 5.1.: Experimental setup: VICON motion-capture system with 12 MX cameras. The working volume was about 3.5x7x5 m^3. Three obstacles have been used (a box, a tube and a step). 10 participants wore a tight black suit with 46 light-reflective markers located on on body landmarks following the VICON Plug-in Gait model. Movement of the participant's right eye was recorded using a video-based eye tracker system at 50 Hz sampling rate.

Calibration procedure The eye tracker was calibrated together with the motion capture system in space and in time. For that, we used an elliptic calibration grid of 1.45 m width and 1 m height, composed of 17 markers forming an ellipsoidal grid. It was placed in front of the participant while he was standing in front of it at about one arm distance, which allowed full view of the grid without moving the head. The participant had to look at the markers one by one, in order to provide correspondences between the position of the centre of the pupil on the eye camera image and the direction of the markers from the eye obtained by the motion capture system. To ensure that the eye tracker stably remained on the head during the trials, calibration was done at the beginning and at the end of each experiment. The position of the eye in the head was defined by in the post-processing phase. The subject was asked to fixate two aligned markers positioned in the same subject eye height in order to be able to see just one of them. The line that intersects the two markers was computed. The eye position is then defined by the intersection of two lines computed in two different moments. At the beginning and at the end of each task the subjects have to fixate a maker positioned in front of them at the same height of the their eyes called anchor point. During this fixation on the anchor point they had to execute a sinusoidal movement with the head in order to assess the calibration phase of the eye tracker. This method was used to both detect displacements of the glasses in each trial and evaluate the system error. The system error was evaluated by taking a total number of ten samples for trial during the first and the second calibration phase, at the beginning and at the end of each trial, respectively. The first calibration phase gave an average gaze error of 0.131 ± 0.173 degrees and for the second calibration phase the error was 1.142 ± 0.692 degrees. The second calibration phase gave a bigger error due to position of the subject from the anchor point. The gaze error increased as the eye angle and the head angle difference increased. However, the system error average was less than 1 degree (0.6368 ± 0.4327 degrees). The maximum error was 3.052 degrees. It should be considered that for the second calibration phase, the position of the anchor point is oriented at 60 degrees in the right respect to the ending point, while the maximum horizontal eye angle recorded during the walking task was less than 50 degrees. The temporal synchronization was done using a manual clapperboard with some reflective markers attached to it. When the clapper is closed a light bulb comes on and this event is viewed both from by the eye tracker camera and by the VICON system that recognize the minimum distance between the clapper makers. At the beginning of each trial, the experimenter clicked the clapperboard in the captured area to generate a temporal event signal recorded by the two systems.

Tasks Participants were instructed to walk at two different velocities: natural (NV) and fast (FV). The instruction for the fast velocity condition was to walk as fast as possible without running. Three objects were positioned in a specific location of the environment: a box (LxWxH: 0.388x0.347x0.312 m^3), a tube (LxH: 0.897x0.123 m^2) and a step (LxWxH: 0.834x0.306x0.143 m^3). At the end position

of the walking trial, an anchor point composed by a pole with a sheet on top of it (0.1x0.2 m^2) was positioned. The sheet was positioned at the same height of the subject eye. A light-reflective marker was added in the middle of the sheet. A light-reflective marker was also added at each vertex of each obstacle. Fig. 5.2 (top) shows a top-down view of the scenario. Fig. 5.2 (down) shows the 3D view of the scenario. In order to clarify the subject motion in the task, three different subject poses have been shown. The stick figure has been obtained by connecting specific subject markers with solid lines. The participants were instructed to execute the first calibration phase before each trial and subsequently start walking with always the right foot. They had to turn around the box clockwise, then step over the tube and step on the obstacle step using only one foot. From then on, they came back passing near the step and the tube, turned around the box counter clockwise until a pole. The trial ended with the second calibration phase with the subjects near the anchor point. The laboratory environment had computers, cluster servers, cameras and the experimenters. A total number of 20 trials were recorded, 10 times for each velocity condition in a randomized order. The first trial was always a NV condition.

Data processing Rotation and translation of the body segments were calculated from the 3D Euclidean position of the markers according to a space-fixed reference frame defined by the motion capture system (Xs, Ys, Zs). The vertical axis (Zs) coincided with the opposite direction of the gravity. The Ys axis coincided to the long extension of the walking task with positive values from the box towards the step (see Fig. 5.2). The Xs axis coincided with the short extension of the walking task, with positive values from the box to the ending point. Temporal sequences were re-sampled into frequency of 50Hz to be synchronized with the eye tracker data. All the trials were normalized in time respect to the total duration of the trial.

Gaze projection on the environment To evaluate the gaze behaviour, horizontal angles (in degrees) were computed from the gaze and body segments in space. The horizontal angle was computed as the unwrap arc-tangent function of the ratio Ys/Xs, where Xs and Ys were the X and Y coordinates of the vector defining the orientation of each body segment in the horizontal plane. The vertical angle of gaze was also evaluated. It was computed as the arc-tangent function of the ratio between the norm of the Z coordinate of gaze vector in the XY plane. An angle equal to zero means that gaze vector was aligned with the horizontal plane. A negative sign means that gaze vector was oriented below the horizontal plane that crosses the eye. We defined gaze point as the position of the gaze in 3D coordinates computed from the projection of the gaze vector on the environment. The obstacle intersections were considered. The working volume defined the limits of the gaze projection. All fixations that fell over the working volume were considered as intersection on the defined volume.

Fixation definition According to the previous studies (Hollands et al. 2002; Johansson et al. 2001; Marigold and Patla 2007; Patla and Vickers 1997), a fixation was defined as the position of gaze stabilized on the Xs, Ys, Zs coordinates in space during about 100 ms (5 frames at 50Hz). In addition, we propose to extend this definition in considering the projection of gaze on the obstacles. The human visual acuity is greatest from 1 degree of radius from the centre of the fovea (Burbeck and Yap 1990; Levi and Klein 1996). This value has been taken as reference due to be greater or al least comparable with the presented system error. The gaze position is defined by the interceptions between gaze vector and the floor, the walking volume limits or the obstacle faces. We computed the horizontal and vertical angles between two successive projected coordinates of gaze, respect to the newest eye position. If the angular differences between the two successive points were both (horizontal and vertical) less that 1 degree, then the checked point was considered part of the fixation. Therefore, the average of those points was taken as the reference for the next gaze position. However the angle difference condition was necessary but not sufficient for the fixation definition. The algorithm also computed the distance between the eye position and projected point positions. That condition prevented the possibility to encounter an object that intercepted the gaze vector in one frame and not in the next one, by adding a threshold on the difference between two consecutive distances. A fixation was recognised if at least 5 consecutive points respected these conditions. Fig. 5.3 shows an example of the one subject behaviour of one trial at normal velocity (Fig. 5.3 top) and fast velocity conditions (Fig. 5.3 down). The head trajectory from the starting position to the ending position is shown. The gaze vector that connects the right eye to the gaze point on the environment is also shown. Only the gaze points considered part of a fixation are shown.

Landmark definition The landmarks, the most viewed points, have been identified by choosing a threshold on the gaze point number in a single volume. In this case we considered only the gaze points member of a fixation. All the trials for each subject, in each condition, were analysed separately. The trials were also divided in four phases in order to avoid multiple fixations in the same area, due to the fact that the subject had to come back to the ending point during the trial. The four phases have been defined by analysing the gaze angle during the trial. Initially the subject is oriented with a gaze angle of about -3*π/2 rad respect to the environment reference frame defined in the previous section. The first phase ends when the subject gaze cross the -π rad. That happens when the subject cross the box and is approaching to the straight line towards the tube and the step. The second phase ends when the subject steps down from the obstacle and turns his gaze back, crossing the -2*π rad. The third phase corresponds to the inflection point, before the avoiding of the obstacle. In this case the gaze angle reaches the minimum by considering the clockwise turning until that moment. The last phase ends with the end of the trial. The threshold was defined by considering the histogram of the distribution of the gaze points in the volumes. The walking scenario was divided in 0.03x0.03x0.03

m volumes. It corresponds to the estimated system error (1 degree) applied to a vertical gaze projection on the floor for a middle height subject (1.7 m). It turns out the minimum area that a middle height subject can look at, by fixating down on his vertical axis. The number of gaze points that fall in each volume was then computed. By considering ten trials per subject, there were a many volumes with just one gaze point and there were a few volumes with more that one. Therefore the distribution was exponential and, from that, the self-information content with the Shannon formula was computed.

$$I(v) = -log(p(v)) \tag{5.1}$$

Where *p(v)* is the probability associated to that event. A possible solution could be to compute the probability associated to the single volumes as the ratio between the number of gaze points that falls in that volume and the total number of gaze points. This method could extract the self-information content of the single volumes, but it contains at least two problems. Firstly, it doesn't consider that some volumes could contain more self-information as a group than as a single volume. So by considering the neighbour volumes, it is possible to extract a wide area of interest with a large number of points. Secondly, if one subject, during a trial, decides to spend more time on a single area where he does not look at in the other trials, this should be considered as an outlier for this kind of analysis. The parameter taken in account is a measure of the variability in terms of the number of trials in which, the same subject points to the same area. In this case, for each volume in the environment, we computed the number of trials in which the subject looks at one volume and his neighbour. As an example, let us consider the planar case with one area and his eight neighbours. If the subject, during his ten trials, looks, at least one time, to each of them, the score for the middle area is 10. By applying this method, a score was assigned at each volume in the environment and it was taken into account to compute the probability associated to those events. As a consequence, there were many volumes with a low score and a few volumes with high score. The self-information related with those volumes with low score, was low. But the self-information content for those volumes that was looked in each trial was high. So, it was possible to assume that, above the average of the computed scores, the self-information content is high. The average was assumed, therefore, as a threshold for each condition. Only those volumes that have more than this specific threshold of score of gaze points inside were considered.

Trajectory analysis The subject's trajectory executed has been computed by considering the average of the 3D position of the pelvis markers, the Left Anterior Superior Iliac Spine (LASI) and the Right Anterior Superior Iliac Spine (RASI). The 2D locomotion trajectory has been computed as the projection of the middle point of these two pelvis markers. In order to compare the subject trajectories among trials

and conditions, normalization on the trial duration has been adopted, as reported in (Hicheur et al. 2005; 2007; Pham 2009; Pham et al. 2007). The normalization has been computed by resampling the trajectory of each trial in 1 thousand samples. The average trajectory, $(x_{av}(t), y_{av}(t))$ for each subject in each condition, has been defined as:

$$x_{av}(t) = \frac{1}{N}\sum_{i=1}^{N} x_i(t) \quad y_{av}(t) = \frac{1}{N}\sum_{i=1}^{N} y_i(t) \tag{5.2}$$

Respect to the cited method, the trajectory variance has been considered by computing the distance of the projected 2D samples of the i-th subject trajectory from the tangent line (defined by the vector equation: $x = a + tn$) of the average trajectory curve.

$$dist_i(x = a + tn, p) = \|(a - p) - ((a - p)n)n\| \tag{5.3}$$

Where a is a point on the tangent line and n is a unit vector. Then for each distance the classical un-biased standard deviation has been computed:

$$std_i = \sqrt{\frac{1}{N-1}\sum_{i=1}^{N} dist_i(x = a + tn, p)} \tag{5.4}$$

5.4. Trajectory fitting

Fig. 5.4 shows an example of the Minimum Variance Point in Position (MVPP) found for one subject in ten trials in NV and FV conditions. MVPPs were located with respect to the local minimum of the standard deviation curve. An average of 5.9 MVPPs were found in all the ten subjects for NV condition and 5.2 for the FV condition. As a general funding it is possible to say that these points are often located on the approaching phase of the obstacles. We found MVPP before and after the steering phase around the box, before the approaching to the tube and to the step and around the inflection point in the returning phase. Fig. 5.5 shows the resulted MVPP found (green dots) for ten trials in one subject on NV condition. The red line is the average of the standard deviation of the trajectory position (blue line). The black line is the curvature of the average of the trajectories. The variance of the trajectory position increases together with the curvature. Most of the MVPPs correspond to minimum points in curvature. The minimum variance points can be also computed respect to the standard deviation of the trajectory velocities (Fig. 5.5 red curve).

The method proposed by Todorov (Todorov 1998) for arm movements, accepts as input the 2D position, velocity and acceleration for the starting point and the 2D position, velocity and acceleration for the ending point. Moreover it accepts specific via-points to be included in the vector of the positions. Note that those via-points are just 2D position points and we do not add velocity information on those points. The method needs the duration of the entire movement and it can accept also the passage time on the via-points. If the passage time is not defined the method computes it respect to an iterative optimization function. This is the main difference respect to the method proposed by Flash and Hogan (Flash and Hogan 1985), however the final solution is very similar. Finally, as results the Average of Trajectory Error (ATE) (see sec. 4.5) will be used as indicator of the fitting (Equation 4.18 divided by the movement duration).

Trial 1. The input vector contains the position points to pass (MVPP) to the minimum jerk model. (Fig. 5.6 left) ATE was 201.3449. Note that for this subject exists a MVPP just after the box. This helps for the first part of the trajectory but after the step there is no indication of the presence of an obstacle so the curve is too short. Due to the fact that the total time is a parameter of the method, any changing in it determines the final trajectory. Fig. 5.6 right shows a segmented version of the Trial 1 (Seg 1). This segments correspond to the three phases of the task: 1) avoiding the box, 2) crossing over the tube and the step and turning back, 3) avoiding the box in the other sense. The three ATEs that we found were 172.8285 + 60.4246 + 52.2142. This result corresponds to an average of 95.1558. This is a much better result, indicating that the segmentation of the trajectory is needed in presence of multiple obstacles. This is possible due to the fact that after segmentation, the model has the velocity and acceleration information of these inner points. He has just to compute velocity and acceleration in the "middle" via-points.

Trial 2. Fig. 5.7 adds 3 points more respect to the other approach. In that case we added the High Curvature Points (HCP) in correspondence of the box. The HCPs are the empty circles in the figure. This could help to represent the obstacles (Fig. 5.7 left). Total ATE is 170.9363 and for the 3 phases: 122.9364 + 80.6749 + 46.2803 = 83.2972. In the same Trial 2 we tried another segmentation (Seg 2). This time we used the HCPs to segments the trajectory (Fig. 5.7 right). Results: 114.8019 + 103.987 + 63.8505 = 94.2131.

Trial 3. In Trial 3 we used a different approach. Fig. 5.5 shows three curves. The blue one is the standard deviation of the trajectory. The black one is the absolute value of the curvature. The three HGPs are visible there. The red line is the standard deviation of the velocity curves. This curve does not have a regular shape. What is interesting is that near to the MVPPs there are some peaks also in velocity

(MVPV Minimum Variance Point in Velocity). In Trial 3 instead to use HGPs, we used these MVPVs. For total trajectory ATE was: 151.0087 (Fig. 5.8 left). The segmentation with the three original phases (Seg 1) produces: 160.6550 + 55.8285 + 49.5890 = 88.6908. The other segmentation (Seg 2, with the MVPV as segmented points) produces (Fig. 5.8 right): 97.6270 + 70.1973 + 37.6018 = 68.4753. This result is the best value that we obtained. In order to compare these results with the previous model performances, we reported in Tab. 5.1 the results of the fitting in terms of ATE. As it is possible to see the best fitting has been obtained with the optimization model approach by using Todorov's model with MVPP as via-points and MVPV as segmentation points.

Model Name	ATE (mm)
Warren and Fajen	79.0185
Wilkie and Wann	80.6222
Pham et. al.	181.9630
Flash et. al	159.1
Todorov	68.5753

Table 5.1.: Comparison results in terms of average of trajectory error (ATE).

5.5. Gaze fixations

Gaze fixation general behaviour On average, subjects performed the 95 trials of the NV condition in 11.6±1.456 s per trial and the 93 trials of the FV condition in 7.908±0.6627 s per trial. For NV the duration of the task for the first trial was greater respect to the others (Tukey-Kramer test). Fig. 5.9 shows all fixations recorded in 95 trials for NV condition (Fig. 5.9 top) and 93 trials for the FV condition (Fig. 5.9 down). The walking scenario was divided in 0.03x0.03x0.03 m volumes, as descripted in the Methods (sec. 5.3) part. In the Fig. 5.9, the dimension and the colour of the dots is proportional to the number of points in the same volume. We obtained 23437 gaze points member of 2921 fixations for 95 trials for the NV condition. This corresponded to an average of 246.705±67.911 gaze points in 29.2146±6.6527 fixations per trial. The average duration of each fixation was 8.4663±1.3385 frames (169.3±0.0268 ms). The gaze points, member of a fixation in the FV condition, were 11386 in 1653 fixations for 93 trials. This corresponded to 122.43±45.221 gaze points in 16.5335±5.2138 fixations per trial. The average duration for FV condition was 7.328±0.9837 frames (146.6±0.0197 ms). The number of points for the NV condition was greater of the number of points for the FV condition (two-way ANOVA $F(1,180)=249.16$ $p<0.001$). We also observed that the duration of the fixation was greater in the NV condition than in the FV condition (two-way ANOVA $F(1,180)=44.91$ $p<0.001$). As explained in the sec. 5.3 the first trial was always the NV condition. Multicomparison analysis shows that

the fixation number of the first trial is significantly greater than in the others trials (Tukey-Kramer test). However, the main effect showing a different fixation number between velocity conditions is still validated by considering only 9 trials per condition (two-way ANOVA (2 conditions x 9 trials) $F(1,162)=225.87$ $p<0.001$). Multicomparison analysis for fixation duration did not show difference among the trials ($p>.05$). As expected, the total duration of the trials were greater in NV condition (two-way ANOVA $F(1,180)=720.17$ $p<0.001$). Multicomparison analysis for trial duration showed that the duration of the first trial in NV condition was greater respect to the other. The effect showing a different trial duration between NV and FV conditions is still present by considering 9 trials per condition (two-way ANOVA (2 conditions x 9 trials) $F(1,162)=698.38$ $p<0.001$). Fig. 5.10 shows the averages of fixation number (Fig. 5.10 left) and the fixation duration (Fig. 5.10 right) for NV and FV over the trials.

Landmark definition The average of the self-information computed as described in the sec. 5.3, was assumed, as a threshold for each phase in each condition. Only those volumes that have more than this specific threshold of score has been considered in the landmarks. The most viewed points were chosen with respect to the defined threshold. The final landmarks have been computed by applying a hierarchical clustering method on those points. shows the landmarks obtained from one subject in the both conditions.

5.6. Landmarks and variability relation

We hypothesize that the sequence of LFPs and the sequences of MVPPs are strongly dependent. The evidence of the time relation between LFP and MVPP can be seen in Fig. 5.12, where it is showed the standard deviation of the trajectory for one subject in both conditions and the relative MVPP as green dots in local minimum. The LFPs are showed as coloured dots. Each colour corresponds to a different phase used to segment the trial as mentioned in the previous section. The first phase (in blue) ends when the subject has crossed the box and is approaching to the straight line towards the tube and the step (see sec. 5.3). The second phase ends when the subject steps down from the obstacle and turns his gaze back (in cyan). The third phase corresponds to the inflection point, before the avoiding of the obstacle (in yellow). The fourth phase compete the trial (in red). Here the most of the fixations are located to the anchor point at the end of the trial. As can be seen in the Fig. 5.12 each LFP phase corresponds to a successive decreasing of the standard deviation of the trajectory. Cross-correlation results between the LFP and MVPP are shown in Tab. 5.2 and confirm the relation between the two curves. This suggests that a LFP corresponds to a global modification of the geometry of the environment. It is clear that a LFP on the ground, where we will put the foot, predicts a MVPP. For the LFP before the obstacle this is not true, it introduces a kind of repulsion, as a

NV	FV
0.455	0.4088
0.6221	0.2917
0.5643	0.4177
0.3517	0.5716
0.3075	0.4319
0.5514	0.6587
0.5656	0.3233
0.2751	0.2605
0.4702	0.2881
0.6814	0.110

Table 5.2.:

cost in energy. It seems that for the MVPP causally related to this kind of LFP, appearing before an obstacle, the useful visual information is not given by fixation.

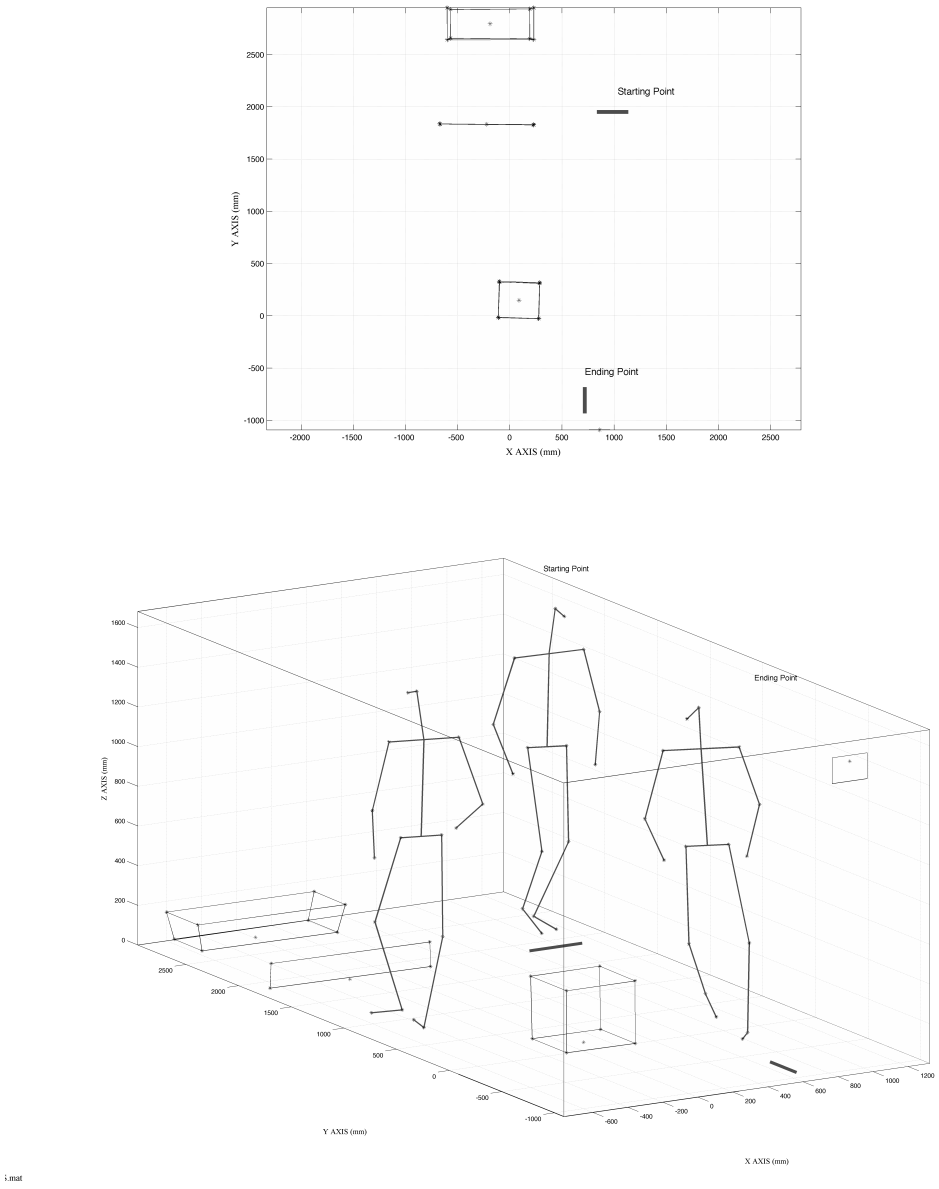

Figure 5.2.: Top. The top down view of the scenario. The red lines indicate respectively the Starting Point and the Ending Point of the trial. The red dots indicate the middle position of the obstacles. The blue line shows an example of the executed trajectory. Down. The 3D view of the scenario with three different poses of the subject markers. For the stick figure it has been used the position of specific subject markers in three different samples.

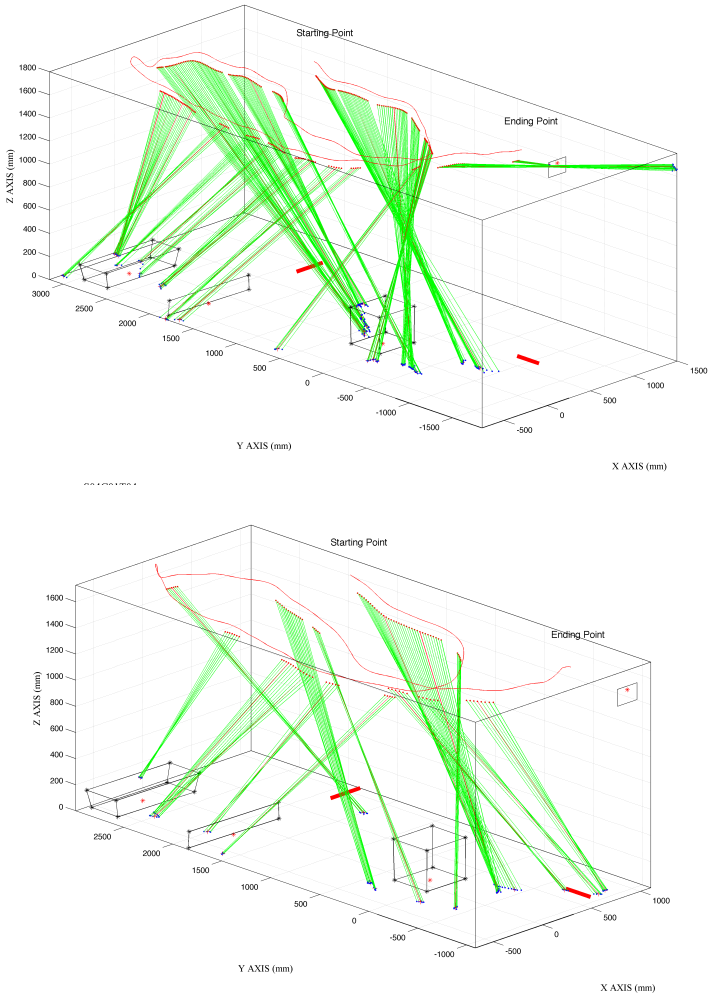

Figure 5.3.: Top. Single trial, normal velocity condition (NV). The head trajectory (red curved line) from the starting position to the ending position is shown. The green segment represents the gaze vector that connects the right eye (red dot) to the gaze point on the environment (blue dot). A red straight line representing the average of the fixation points has been showed for each fixation. Only the gaze points considered part of a fixation are shown. Down. Single trial, fast velocity condition (FV). The head trajectory (red line) from the starting position to the ending position is shown. The green segment represents the gaze vector that connects the right eye (red dot) to the gaze point on the environment (blue dot). A red straight line representing the average of the fixation points has been showed for each fixation. Only the gaze points considered part of a fixation are shown.

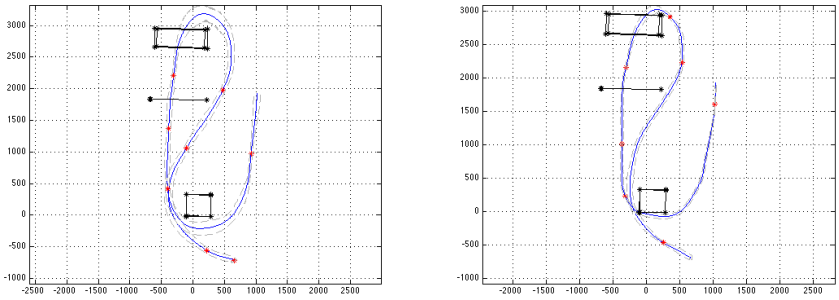

Figure 5.4.: Average (blue line) and standard deviation (grey line) of the trajectory performed by one subject in the experimental scenario. The red dots represent points where the variance of the performed trajectories reaches local minimum (MVPP). Left the NV condition and right the FV condition.

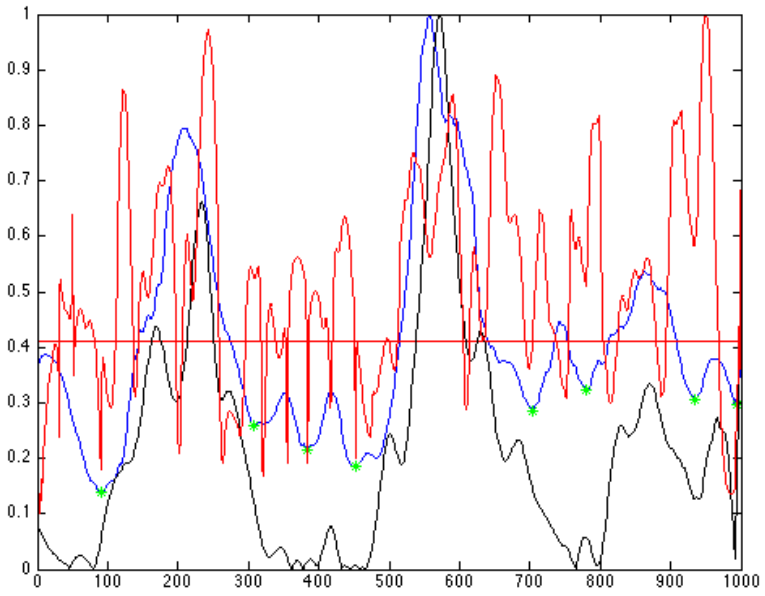

Figure 5.5.: Blue curve represents the standard deviation of ten trajectories in position. The green dots are the MVPP found. The red line is the average of the standard deviation. The black curve is the curvature of the average trajectory. The red curve is the standard deviation computed on the velocity. MVPV are computed respect to this curve.

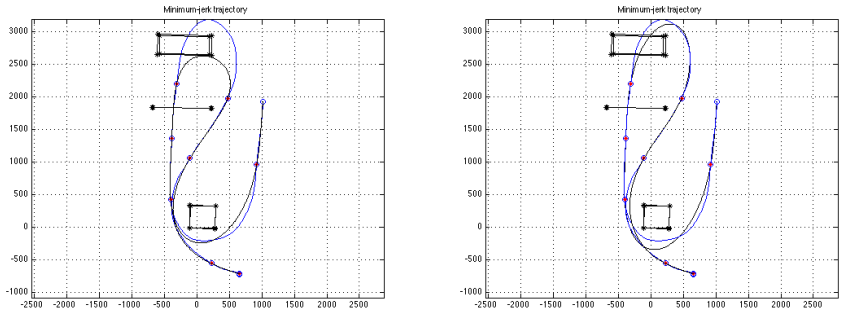

Figure 5.6.: Minimum jerk, Trial 1 without segmentation (left) and with segmentation (right).

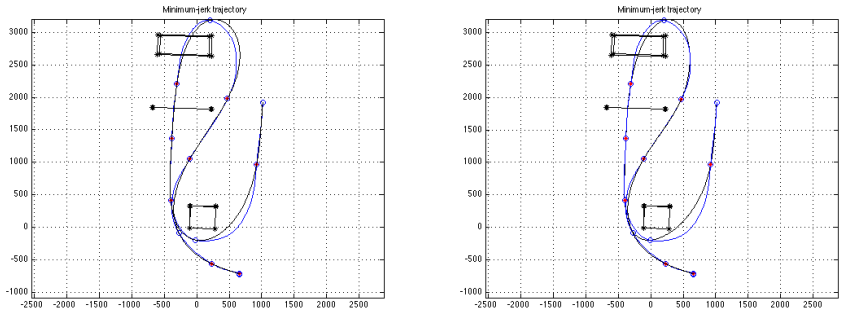

Figure 5.7.: Trial 2 with High Curvature Points (empty circles), without (left) and with segmentation (right).

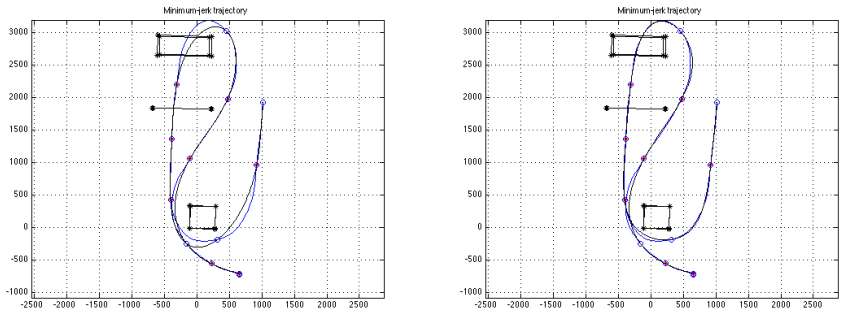

Figure 5.8.: Trial 3 with Minimum Variance Point in Velocity (empty circles), without (left) and with segmentation (right). The latter was the best result obtained.

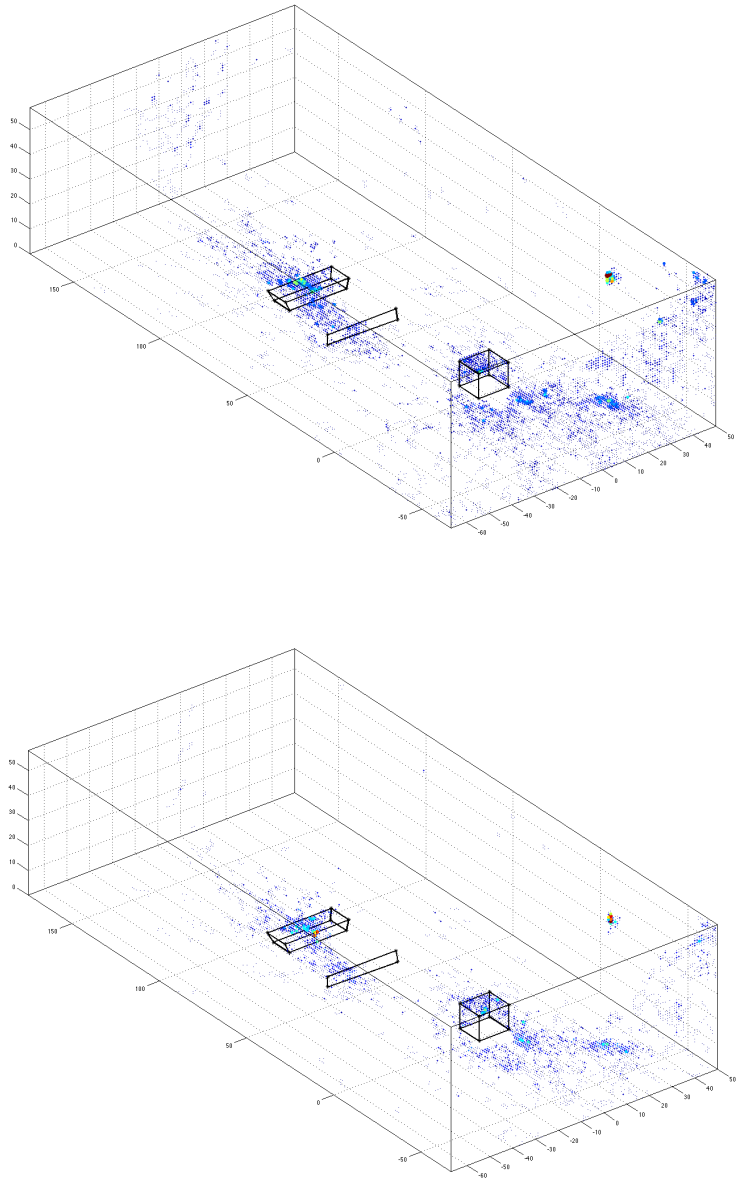

Figure 5.9.: All gaze points member of a fixation for ten subjects in 95 trials for NV condition (top) and 93 for FV condition (down). The dimension and the colour of the dots are proportional to the number of points in the same volume. A total of 24196 gaze points are sown for NV and 11677 for FV.

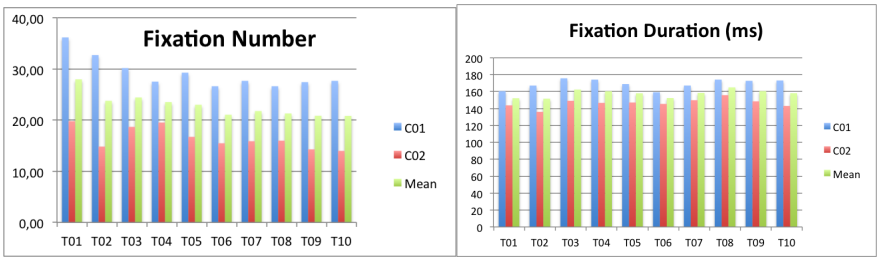

Figure 5.10.: The averages of fixation number (left) and the fixation duration (right) for NV (blue line) and FV (red line) conditions over the trials. The averages between the both conditions are also shown (green line).

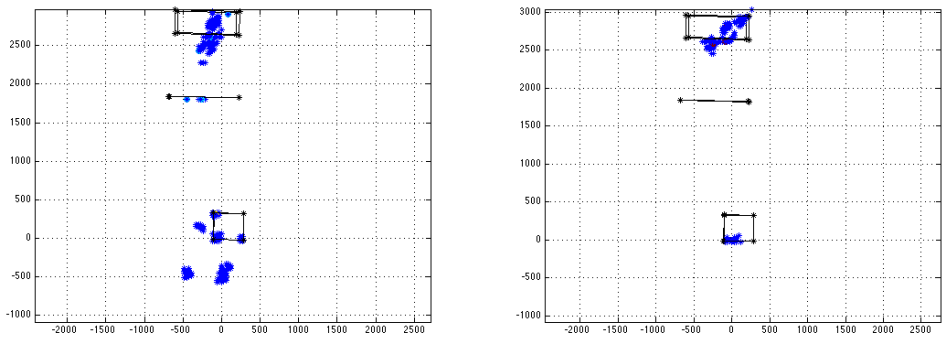

Figure 5.11.: Top down view of the Landmark Fixation Points (LFP) found for one subject in ten trials for NV condition (left) and FV condition (right).

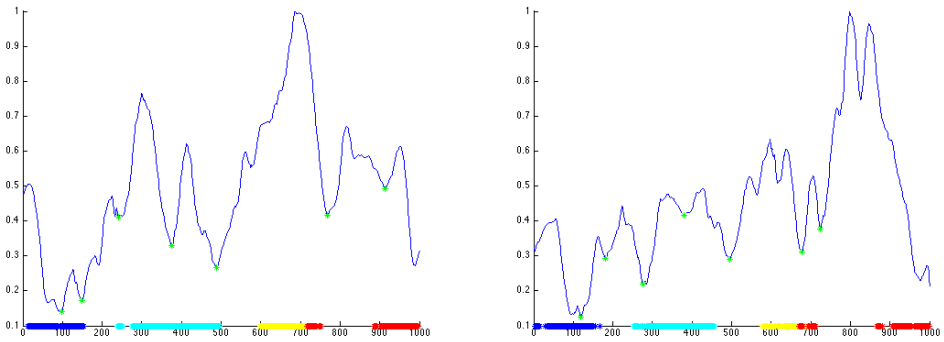

Figure 5.12.: The standard deviation of the trajectory for one subject in both conditions and the relative MVPP as green dots in local minimum. The LFP are showed as coloured dots that correspond to different phases used to segment the trial. Each LFP phase correspond to a successive decreasing of the variance.

6. Gaze guided locomotion in biped robot

6.1. Overview

In the previous section, the relation between gaze and trajectory planning has been described and analyzed. The described study is part of the European project *"RoboSoM: A Robotic Sense of Movement"*. The objective of the RoboSoM project is to investigate new neuroscience-based approaches to the design and development of humanoid robots with advanced perception and action capabilities, showing robust, adaptive, predictive and effective behaviour in the real world. The explicit aim is developing robot platforms with performance exceeding those of existing humanoid robots. These approaches to the design of humanoid robots are strongly based on the concept of human's sense of movement (Berthoz 2000). In this context the goal of the presented works is investigate the relationship between the gaze direction and body movement during locomotion to understand how the locomotor trajectory is planned and controlled during navigation tasks. In this section the first results of the robotic implementation are presented.

6.2. The RoboSoM project

The RoboSoM project aims at the study and robotic implementation of a model of the *sense of movement* (Berthoz 2000), which endows a humanoid robot with advanced perception and action capabilities in biped locomotion, based on a unified inertial reference frame and on predictive behaviour. This implementation in a very advanced humanoid robot will lead to enhanced performance in the real world, in terms of capability of accomplishing practical and helpful tasks. The objectives of the RoboSoM project include investigations on neuroscience models and robotic implementations. As final objective of the project, the SABIAN humanoid platform will be able to walk in an unconstrained environment following visual target. Hence, the proposed scenario (presented in sec. 5.3) is an example of complex locomotion task. These experiments led to the definition of one of the key models for the Sense of Movement principles: the Human trajectory planning model. As a consequence of these works, the perspective is to transfer the gained knowledge on the gaze guided locomotion into the SABIAN (Sant'Anna BIped humANoid) robotic platform. The

SABIAN humanoid platform has been assembled at the SSSA BioRobotics Institute laboratories. The robot is able to walk towards a visual target by stabilizing head movement and by predicting the structure of the visible environment.

6.3. SABIAN humanoid platform

The SABIAN (Sant'Anna BIped humANoid) platform it is a copy of WABIAN (WAseda BIped humANoid) (Kryczka et al. 2011; Ogura et al. 2006). Compared to most bipedal humanoid robots, which walk with bent knees, SABIAN is able to perform a human-like walking, with stretched knees, and to get the pelvis motion, raising the hip. SABIAN is approximately the size of the average adult Japanese women. Wabian/Sabian has the height of 1475 mm, and the weight of 64.5 kg. It has 6 DOF in each leg, 2 DOF in the waist, 2 DOF in the trunk, 1 passive DOF in each foot. Ranges of motion were defined in reference to human motion measurements. Waseda University is also partner and will make available to the project the Wabian platform and its continuously improved versions. The implementation of bio-inspired algorithm for the trajectory planning represents a good validation tool for the human models and could provide better performances for the humanoid biped robots. A recent work (Kryczka et al. 2011) proposed a novel, unified inverse kinematics method that enables the generation of the robot pattern by specifying only the task space trajectories. The head trajectory is one of the components of this control. Moreover the SABIAN trajectory can be also changed during the robot walking by using an online pattern generator recently developed (KONDO et al.). This study is part of a research for the planning of the human-like walking trajectories for the humanoid robotic platform. The head of the SABIAN platform is the head of the iCub robot (explained in sec. 2.2). In the RoboSoM project the gaze control developed for the iCub head has been used as a module of the integrated SABIAN platform (see Fig. 6.1).

6.4. Proposed trajectory planning model

In this section, a model for the trajectory planning in a complex locomotion task is presented. The conducted experiments (sec. 5.3) have been analysed in order to examine the relation between the gaze fixations and the executed task. Preliminary results show an evident role of gaze in the trajectory formation. Considering the task of walking in a complex environment and in accordance with the experimental results obtained, a model for the trajectory planning should have the following characteristics: i) it should consider the interaction with the environment; ii) such interaction should be obtained by the role of gaze as a form of anticipation; iii) the velocity constraint given by the one-third power law or a related optimality criterion, as Minimum Jerk, should be fulfilled. The overall block schema of the

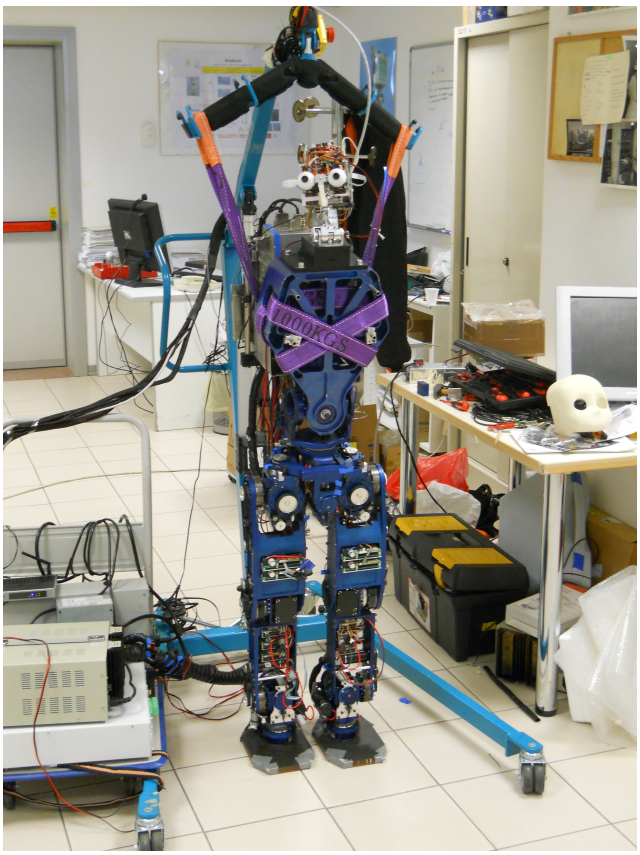

Figure 6.1.: Sabian humanoid platform.

model is shown in Fig. 6.2. The trajectory planning block generates a new trajectory consistent with the end goal position and orientation. The algorithm starts by computing the theoretical minimum jerk trajectory. Then, a first control block, "Control Loop 1" in Fig. 6.2, is used to re-plan the trajectory if an obstacle has to be avoided. It generates the closest via point following an exponential principle as used by Warren and Fajen. Then, the planning of a new trajectory is generated from the actual position to that first via point. Afterwards, enough time before the via point reaching, another trajectory is planned to steer the final goal. While the trajectory is executed, the online control loop (Control Loop 2) checks the execution accuracy. This operation should be done in accord to different perceived variables, like optic flow or vestibular information or proprioceptive information. The algorithm works as an iterative process that ensures the reaching of the target in a few steps. Fig. 6.3, two examples of this model implementation have been reported. In the first one, two obstacles are to be avoided. The original trajectory path (grey line) is too near to them so a first via point is generated and accordingly the algorithm will generate the correct path of the motion (blue line). In the second example, there is a more complex situation. A series of obstacles form a wall in front of the agent. The model continues to generate the new trajectory until it finds its way in the bottom right of

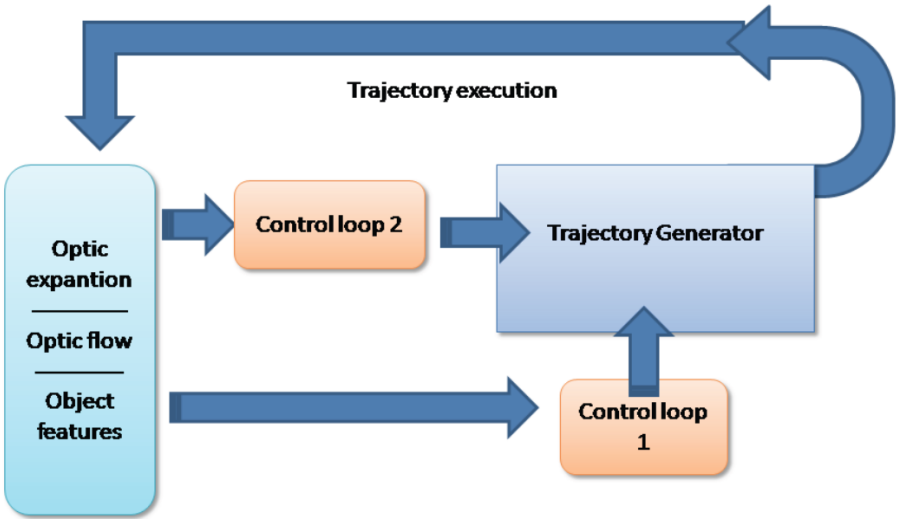

Figure 6.2.: Block diagramm of the trajectory planning model

the map. In conclusion the presented model is able to generate complex trajectories accordingly to the environment features. The online control loop can include more perceptual variables like the role of the optic flow and the vestibular sensation. At the end, the minimum jerk model produces smooth trajectory with a correct velocity profile. Moreover we suggest, that anticipation of heading by the horizontal gaze direction, and anticipation of the curvature by the vertical gaze angle, allow that the dynamic equilibrium of the body is controlled in advance. A good characterization of the model with respect to the scenario parameters and results will provide a stable and robust solution for the formation of the RoboSoM scenario task.

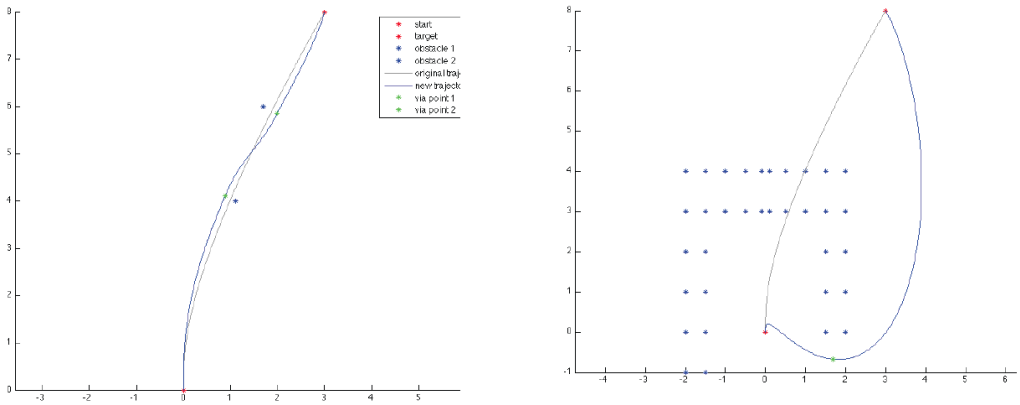

Figure 6.3.: Left. The trajectory formation for two obstacles avoidance. Right Trajectory formation for a wall of points

Acknowledgments

This work has been partially supported by the European Commission with the RoboSoM Project, FP7-ICT-248366, and by the Italian Ministry of Education and Research, in the PRIN programme. The authors would like to thank Italian Ministry of Foreign Affairs, General Directorate for Cultural Promotion and Cooperation, for its support to the establishment of the Robot-An joint laboratory.

Bibliography

Arechavaleta, G., Laumond, J.-P., Hicheur, H., and Berthoz, A. (2008). An optimality principle governing human walking. *Robotics, IEEE Transactions on*, 24(1):5–14.

Authié, C. N. and Mestre, D. (2011). Optokinetic nystagmus is elicited by curvilinear optic flow during high speed curve driving. *Vision Research*.

Baldi, P. (2009). Bayesian surprise attracts human attention. *Vision Research*.

Baldi, P. (2010). Of bits and wows: A Bayesian theory of surprise with applications to attention. *Neural Networks*.

Barborica, A. and Ferrera, V. P. (2003). Estimating invisible target speed from neuronal activity in monkey frontal eye field. *Nature Neuroscience*, 6(1):66–74.

Beira, R., Lopes, M., Praça, M., Santos-Victor, J., Bernardino, A., Metta, G., Becchi, F., and Saltaren, R. (2006). Design of the robot-cub (icub) head. *... on Robotics and ...*.

Bennequin, D., Fuchs, R., and Berthoz, A. (2009). Movement timing and invariance arise from several geometries. *PLoS Comput. Biol.*

Berthouze, L., Bakker, P., and Kuniyoshi, Y. (1996). Learning of Oculo-Motor Control: a Prelude to Robotic Imitation. *Intelligent Robots and ...*.

Berthoz, A. (2000). *The brain's sense of movement*. Harvard Univ Pr.

BROOKS, R. A. (1991). New Approaches to Robotics. *Science*, 253(5025):1227–1232.

Burbeck, C. A. and Yap, Y. L. (1990). Two mechanisms for localization? Evidence for separation-dependent and separation-independent processing of position information. *Vision Research*, 30(5):739–750.

Chou, I.-h. and Lisberger, S. G. (2004). The role of the frontal pursuit area in learning in smooth pursuit eye movements. *Journal of Neuroscience*.

Dario, P., Carrozza, M. C., Guglielmelli, E., Laschi, C., Menciassi, A., Micera, S., and Vecchi, F. (2005). Robotics as a future and emerging technology biomimetics, cybernetics, and neuro-robotics in european projects. *IEEE Robotics & Automation Magazine*, 12(2):29–45.

de Brouwer, S. and Missal, M. (2001). Role of retinal slip in the prediction of target motion during smooth and saccadic .... *Journal of neurophysiology*.

de Brouwer, S., Missal, M., and Barnes, G. (2002a). Quantitative analysis of catch-up saccades during sustained pursuit. *Journal of neurophysiology*.

de Brouwer, S., Yuksel, D., and Blohm, G. (2002b). What triggers catch-up saccades during visual tracking? *Journal of neurophysiology*.

de Xivry, O. (2007). Saccades and pursuit: two outcomes of a single sensorimotor process. *The Journal of Physiology*.

Dean, P., Porrill, J., and Stone, J. (2002). Decorrelation control by the cerebellum achieves oculomotor plant compensation .... *Proceedings of the Royal Society B: ....*

Di Fabio, R. and Greany, J. (2003). Saccade-stepping interactions revise the motor plane for obstacle avoidance . *Journal of motor behavior*.

Di Fabio, R. and Zampieri, C. (2003). Aging and saccade-stepping interactions in humans. *Neuroscience Letters*.

Dicke, P. W., Barash, S., Ilg, U. J., and Thier, P. (2004). Single-neuron evidence for a contribution of the dorsal pontine nuclei to both types of target-directed eye movements, saccades and smooth-pursuit. *The European journal of neuroscience*, 19(3):609–624.

Donelan, J. M. J. M., Shipman, D. W. D. W., Kram, R., and Kuo, A. D. (2004). Mechanical and metabolic requirements for active lateral stabilization in human walking. *Journal of biomechanics*, 37(6):827–835.

Fajen, B. and Warren, W. (2003). Behavioral dynamics of steering, obstable avoidance, and route selection. *Journal of Experimental Psychology: ....*

Fajen, B. and Warren, W. (2007). Behavioral dynamics of intercepting a moving target. *Experimental Brain Research*.

Falotico, E., Taiana, M., Zambrano, D., Bernardino, A., Santos-Victor, J., Dario, P., and Laschi, C. (2009). Predictive Tracking Across Occlusions in The iCub Robot. In *2009 9th IEEE-RAS International Conference on Humanoid Robots (Humanoids 2009)*, pages 486–491. IEEE.

Falotico, E., Zambrano, D., Muscolo, G. G., Marazzato, L., Dario, P., and Laschi, C. (2010). Implementation of a bio-inspired visual tracking model on the iCub robot. In *2010 RO-MAN: The 19th IEEE International Symposium on Robot and Human Interactive Communication*, pages 564–569. IEEE.

Fitzpatrick, P., Metta, G., and Natale, L. (2008). Towards long-lived robot genes. *Robotics and Autonomous Systems*.

Flash, T. and Hogan, N. (1985). The coordination of arm movements: an experimentally confirmed mathematical model. *The Journal of neuroscience*.

Franchak, J. M. and Adolph, K. E. (2010). Visually guided navigation: Head-mounted eye-tracking of natural locomotion in children and adults. *Vision Research*.

Franchi, E., Falotico, E., Zambrano, D., Muscolo, G. G., Marazzato, L., Dario, P., and Laschi, C. (2010). A comparison between two bio-inspired adaptive models of Vestibulo-Ocular Reflex (VOR) implemented on the iCub robot. In *2010 10th IEEE-RAS International Conference on Humanoid Robots (Humanoids 2010)*, pages 251–256. IEEE.

Fukushima, K., Yamanobe, T., Shinmei, Y., and Fukushima, J. (2002). Predictive responses of periarcuate pursuit neurons to visual target motion. *Experimental Brain Research*, 145(1):104–120.

Gibson, J. J. (1950). The perception of the visual world.

Girard, B., Cuzin, V., Guillot, A., Gurney, K. N., and Prescott, T. J. (2003). A basal ganglia inspired model of action selection evaluated in a robotic survival task. *Journal of integrative ...*.

Gomi, H. and Kawato, M. (1992). Adaptive Feedback-Control Models of the Vestibulocerebellum and Spinocerebellum. *Biological cybernetics*, 68(2):105–114.

Gottlieb, J. P., MacAvoy, M. G., and Bruce, C. J. (1994). Neural responses related to smooth-pursuit eye movements and their correspondence with electrically elicited smooth eye movements in the primate frontal eye field. *Journal of neurophysiology*, 72(4):1634–1653.

Gredebäck, G., von Hofsten, C., Karlsson, J., and Aus, K. (2005). The development of two-dimensional tracking: a longitudinal study of circular pursuit. *Experimental brain research. Experimentelle Hirnforschung. Expérimentation cérébrale*, 163(2):204–213.

Grönqvist, H., Gredebäck, G., and Hofsten, C. v. (2006). Developmental asymmetries between horizontal and vertical tracking. *Vision Research*, 46(11):1754–1761.

Gurney, K. N., Prescott, T. J., and Redgrave, P. (2001a). A computational model of action selection in the basal ganglia. I. A new functional anatomy. *Biological cybernetics*.

Gurney, K. N., Prescott, T. J., and Redgrave, P. (2001b). A computational model of action selection in the basal ganglia. II. Analysis and simulation of behaviour. *Biological cybernetics*.

Hicheur, H., Pham, Q.-C., Arechavaleta, G., Laumond, J.-P., and Berthoz, A. (2007). The formation of trajectories during goal - oriented locomotion in humans. I. A stereotyped behaviour. *European Journal of Neuroscience*, 26:2376–2390.

Hicheur, H., Vieilledent, S., and Richardson, M. (2005). Velocity and curvature in human locomotion along complex curved paths: a comparison with hand movements. *Experimental Brain Research*.

Hollands, M. A., Patla, A. E., and Vickers, J. (2002). "Look where you're going!": gaze behaviour associated with maintaining and changing the direction of locomotion. *Experimental Brain Research*.

Hollands, M. A., Ziavra, N. V., and Bronstein, A. M. (2004). A new paradigm to investigate the roles of head and eye movements in the coordination of whole-body movements. *Experimental Brain Research*, 154(2):261–266.

Humphries, M. and Gurney, K. N. (2002). The role of intra-thalamic and thalamocortical circuits in action selection. *Network: Computation in ...*.

Ilg, U. J., Schumann, S., and Thier, P. (2004). Posterior parietal cortex neurons encode target motion in world-centered coordinates. *Neuron*, 43(1):145–151.

Imai, T., Moore, S., and Raphan, T. (2001). Interaction of the body, head, and eyes during walking and turning. *Experimental Brain Research*.

Ito, M. (1984). *Cerebellum and Neural Control*. Raven Pr.

Jansen, S., Toet, A., and Werkhoven, P. J. (2011). Human locomotion through a multiple obstacle environment: strategy changes as a result of visual field limitation.

Johansson, R. S., Westling, G., and Backstrom, A. (2001). Eye-hand coordination in object manipulation. *Journal of Neuroscience*.

Kadone, H., Bernardin, D., and Bennequin, D. (2010). Gaze anticipation during human locomotion-top-down organization that may invert the concept of locomotion in humanoid robots. *RO-MAN*.

Kandel, E. R., Schwartz, J. H., and Jessell, T. M. (2000). *Principles of Neural Science*.

Kawato, M. (1990). Feedback-error-learning neural network for supervised motor learning. *Advanced neural computers*.

Kawato, M. (1999). Internal models for motor control and trajectory planning. *Current Opinion in Neurobiology*.

Kawawaki, D., Shibata, T., Goda, N., Doya, K., and Kawato, M. (2006). Anterior and superior lateral occipito-temporal cortex responsible for target motion prediction during overt and covert visual pursuit. *Neuroscience research*, 54(2):112–123.

Keller, E. L. and Missal, M. (2003). Shared brainstem pathways for saccades and smooth-pursuit eye movements. *Annals of the New York Academy of Sciences*, 1004:29–39.

Komatsu, H. and Wurtz, R. H. (1988a). Relation of cortical areas MT and MST to pursuit eye movements. I. Localization and visual properties of neurons.

Komatsu, H. and Wurtz, R. H. (1988b). Relation of cortical areas MT and MST to pursuit eye movements. III. Interaction with full-field visual stimulation.

KONDO, H., SHIMIZU, J., HASHIMOTO, K., HATTORI, K., NISHIKAWA, K., TAKEZAKI, Y., HAMA, Y., YOSHIMURA, Y., LIM, H.-O., and TAKANISHI, A. REALIZATION OF WALKING BY FFT-BASED ONLINE PATTERN GENERATION . In *Mobile Robotics - Solutions and Challenges - The Twelfth International Conference on Climbing and Walking Robots and the Support Technologies*

for Mobile Machines, pages 615–622, Singapore. World Scientific Publishing Co. Pte. Ltd.

Kowler, E. (1990). The role of visual and cognitive processes in the control of eye movement. *Reviews of oculomotor research*, 4:1–70.

Krauzlis, R. (2004). Recasting the smooth pursuit eye movement system. *Journal of neurophysiology*.

Krauzlis, R. J. (2005). The control of voluntary eye movements: new perspectives. *The Neuroscientist : a review journal bringing neurobiology, neurology and psychiatry*, 11(2):124–137.

Kryczka, P., Hashimoto, K., and Kondo, H. (2011). Stretched knee walking with novel inverse kinematics for humanoid robots. *Intelligent Robots ....*

Land, M. F. (2004). The coordination of rotations of the eyes, head and trunk in saccadic turns produced in natural situations. *Experimental Brain Research*.

Land, M. F. (2009). Vision, eye movements, and natural behavior. *Visual neuroscience*.

Land, M. F. and Lee, D. (1994). Where we look when we steer. *Nature*.

Leigh, R. J. and Kennard, C. (2004). Using saccades as a research tool in the clinical neurosciences. *Brain*, 127(Pt 3):460–477.

Levi, D. M. and Klein, S. A. (1996). Limitations on position coding imposed by undersampling and univariance. *Vision Research*.

Lewis, A., Lee, H.-K., and Patla, A. E. (2005). Foot Placement Selection Using Non-geometric Visual Properties. *The International Journal of Robotics ....*

Lisberger, S. G., Morris, E. J., and Tychsen, L. (1987). Visual motion processing and sensory-motor integration for smooth pursuit eye movements. *Annual review of neuroscience*, 10:97–129.

Ljung, L. and Soderstrom, T. (1987). Theory and Practice of Recursive Identification.

Marigold, D. (2008). Role of peripheral visual cues in online visual guidance of locomotion. *Exercise and sport sciences reviews*.

Marigold, D. and Patla, A. E. (2007). Gaze fixation patterns for negotiating complex ground terrain. *Neuroscience*.

Marigold, D. and Patla, A. E. (2008). Visual information from the lower visual field is important for walking across multi-surface terrain. *Experimental Brain Research*.

Marigold, D., Weerdesteyn, V., and Patla, A. E. (2007). Keep looking ahead? Redirection of visual fixation does not always occur during an unpredictable obstacle avoidance task. *Experimental Brain Research*.

Metta, G. and Fitzpatrick, P. (2006). Yarp: Yet another robot platform. ... *Journal on Advanced Robotics ....*

Metta, G., Natale, L., Nori, F., Sandini, G., Vernon, D., Fadiga, L., von Hofsten, C., Rosander, K., Lopes, M., Santos-Victor, J., Bernardino, A., and Montesano, L. (2010). ScienceDirect.com - Neural Networks - The iCub humanoid robot: An open-systems platform for research in cognitive development. *Neural Networks*.

Missal, M. and Keller, E. L. (2002). Common Inhibitory Mechanism for Saccades and Smooth-Pursuit Eye Movements.

Newsome, W. T., Wurtz, R. H., and Komatsu, H. (1988). Relation of cortical areas MT and MST to pursuit eye movements. II. Differentiation of retinal from extraretinal inputs.

Ogura, Y., Aikawa, H., Shimomura, K., Kondo, H., Morishima, A., ok Lim, H., and Takanishi, A. (2006). Development of a new humanoid robot WABIAN-2. In *2006 IEEE International Conference on Robotics and Automation, 2006. ICRA 2006.*, pages 76–81. IEEE.

Ono, S., Das, V. E., Economides, J. R., and Mustari, M. J. (2005). Modeling of smooth pursuit-related neuronal responses in the DLPN and NRTP of the rhesus macaque. *Journal of neurophysiology*, 93(1):108–116.

Patla, A. E. and Adkin, A. (1999). Online steering: coordination and control of body center of mass, head and body reorientation. *Experimental Brain Research*.

Patla, A. E. and Vickers, J. N. (1997). Where and when do we look as we approach and step over an obstacle in the travel path? *Neuroreport*.

Pham, Q.-C. (2009). On the open-loop and feedback processes that underlie the formation of trajectories during visual and nonvisual locomotion in humans. *Journal of neurophysiology*.

Pham, Q.-C., Hicheur, H., Arechavaleta, G., Laumond, J.-P., and Berthoz, A. (2007). The formation of trajectories during goal - oriented locomotion in humans. II. A maximum smoothness model. *European Journal of Neuroscience*, 26:2391–2403.

Porrill, J., Dean, P., and Stone, J. (2004). Recurrent cerebellar architecture solves the motor-error problem. *Proceedings of the Royal Society B: ....*

Quinn, K. J., Schmajuk, N., Baker, J. F., and Peterson, B. W. (1992). Simulation of adaptive mechanisms in the vestibulo-ocular reflex. *Biological cybernetics*, 67(2):103–112.

Rambold, H., Churchland, A., Selig, Y., Jasmin, L., and Lisberger, S. G. (2002). Partial ablations of the flocculus and ventral paraflocculus in monkeys cause linked deficits in smooth pursuit eye movements and adaptive modification of the VOR. *Journal of neurophysiology*, 87(2):912–924.

Raymond, J. L. and Lisberger, S. G. (1998). Neural learning rules for the vestibulo-ocular reflex. *The Journal of neuroscience : the official journal of the Society for Neuroscience*, 18(21):9112–9129.

Reina, G. A. and Schwartz, A. B. (2003). Eye-hand coupling during closed-loop drawing: Evidence of shared motor planning?

Robinson, D. (1965). The mechanics of human smooth pursuit eye movement. *The Journal of Physiology*.

Robinson, D., Gordon, J., and Gordon, S. (1986). Biological Cybernetics, Volume 55, Number 1 - SpringerLink. *Biological cybernetics*.

Rosander, K. and von Hofsten, C. (2004). Infants' emerging ability to represent occluded object motion. *Cognition*.

Rothkopf, C. A., Ballard, D. H., and Hayhoe, M. M. (2007). Task and context determine where you look. *Journal of Vision*, 7(14):16–16.

Roucoux, A. and Culee, C. (1983). ScienceDirect Login. *Behavioural brain research*.

Shibata, T. and Schaal, S. (2001). Biomimetic gaze stabilization based on feedback-error-learning with nonparametric regression networks. *Neural Networks*.

Shibata, T., Tabata, H., Schaal, S., and Kawato, M. (2005). A model of smooth pursuit in primates based on learning the target dynamics. *Neural Networks*.

Shibata, T., Vijayakumar, S., and Conradt, J. (2001). Biomimetic oculomotor control. *Adaptive Behavior*.

Shidara, M., Kawano, K., Gomi, H., and Kawato, M. (1993). Inverse-dynamics model eye movement control by Purkinje cells in the cerebellum. *Nature*, 365(6441):50–52.

Stone, L. S. and Lisberger, S. G. (1990a). Visual responses of Purkinje cells in the cerebellar flocculus during smooth-pursuit eye movements in monkeys. I. Simple spikes. *Journal of neurophysiology*, 63(5):1241–1261.

Stone, L. S. and Lisberger, S. G. (1990b). Visual responses of Purkinje cells in the cerebellar flocculus during smooth-pursuit eye movements in monkeys. II. Complex spikes. *Journal of neurophysiology*, 63(5):1262–1275.

Tabereau, N., Bennequin, D., Slotine, J., Berthoz, A., and Girard, B. (2007). Geometry of the superior colliculus mapping and efficient oculomotor computation. *Biological ....*

Taiana, M., Nascimento, J., Gaspar, J., and Bernardino, A. (2008). Sample-based 3D tracking of colored objects: A flexible architecture. *... of BMVC 2008*.

Taiana, M., Santos, J., Gaspar, J., Nascimento, J., Bernardino, A., and Lima, P. (2010). Tracking objects with generic calibrated sensors: An algorithm based on color and 3D shape features. *Robotics and Autonomous Systems*, 58(6):784–795.

Takagi, M., Zee, D. S., and Tamargo, R. J. (2000). Effects of Lesions of the Oculomotor Cerebellar Vermis on Eye Movements in Primate: Smooth Pursuit.

Tanaka, M. and Lisberger, S. G. (2001). Regulation of the gain of visually guided smooth-pursuit eye movements by frontal cortex. *Nature*, 409(6817):191–194.

Tanaka, M. and Lisberger, S. G. (2002). Enhancement of multiple components of pursuit eye movement by microstimulation in the arcuate frontal pursuit area in monkeys. *Journal of neurophysiology*, 87(2):802–818.

Thier, P. and Ilg, U. (2005). The neural basis of smooth-pursuit eye movements. *Current Opinion in Neurobiology*.

Tian, J. R. and Lynch, J. C. (1996). Corticocortical input to the smooth and saccadic eye movement subregions of the frontal eye field in Cebus monkeys. *Journal of neurophysiology*, 76(4):2754–2771.

Tikhanoff, V., Cangelosi, A., Fitzpatrick, P., Metta, G., Natale, L., and Nori, F. (2008a). Proceedings of the 8th Workshop on Performance Metrics for Intelligent Systems - PerMIS '08. In *the 8th Workshop*, pages 57–61, New York, New York, USA. ACM Press.

Tikhanoff, V., Fitzpatrick, P., Nori, F., and Natale, L. (2008b). The icub humanoid robot simulator. *... on Intelligent RObots ...*.

Todorov, E. (1998). Smoothness Maximization Along a Predefined Path Accurately Predicts the Speed Profiles of Complex Arm Movements. *Journal of neurophysiology*.

Todorov, E. (2002). Optimal feedback control as a theory of motor coordination. *Nature Neuroscience*.

Todorov, E. (2004). Optimality principles in sensorimotor control. *Nature Neuroscience*.

Tsagarakis, N. G., Metta, G., Sandini, G., Vernon, D., Beira, R., Becchi, F., Righetti, L., Santos-Victor, J., Ijspeert, A. J., Carrozza, M. C., and Caldwell, D. G. (2007). iCub: the design and realization of an open humanoid platform for cognitive and neuroscience research. *Advanced Robotics*, 21(10):1151–1175.

Viviani, P. and Flash, T. (1995). Minimum-jerk, two-thirds power law, and isochrony: converging approaches to movement planning. *Journal of experimental psychology Human perception and performance*, 21(1):32–53.

Viviani, P. and Terzuolo, C. (1982). Trajectory determines movement dynamics. *Neuroscience*, 7(2):431–437.

von Hofsten, C., Kochukhova, O., and Rosander, K. (2007). Predictive tracking over occlusions by 4-month-old infants. *Developmental science*, 10(5):625–640.

von Hofsten, C. and Rosander, K. (1997). ScienceDirect Login. *Vision Research*.

Wann, J. P. and Swapp, D. (2000). Why you should look where you are going. *Nature Neuroscience*.

Warren, W. (1998). Perception of heading is a brain in the neck. *Nature Neuroscience*.

Warren, W. (2006). The dynamics of perception and action. *Psychological review*.

Warren, W., Kay, B., Zosh, W., and Duchon, A. (2001). Optic flow is used to control human walking. *Nature*.

Wells, S. and Barnes, G. (1998). Fast, anticipatory smooth-pursuit eye movements appear to depend on a short-term store. *Experimental Brain Research*.

Whittaker, S. and Eaholtz, G. (1982). Learning patterns of eye motion for foveal pursuit. *Investigative ophthalmology & visual science*.

Wilkie, R. M. (2003). Eye-movements aid the control of locomotion. *Journal of Vision*.

Wilkie, R. M., Kountouriotis, G., Merat, N., and Wann, J. P. (2010). Using vision to control locomotion: looking where you want to go. *Experimental Brain Research*, pages 1–9.

Wilkie, R. M. and Wann, J. P. (2003). Controlling steering and judging heading: retinal flow, visual direction, and extraretinal information. *Journal of experimental psychology Human perception and performance*, 29(2):363–378.

Wilkie, R. M. and Wann, J. P. (2005). The role of visual and nonvisual information in the control of locomotion. *Journal of experimental psychology Human perception and performance*, 31(5):901.

Wilkie, R. M. and Wann, J. P. (2006). Judgments of path, not heading, guide locomotion. *Journal of experimental psychology Human perception and performance*, 32(1):88–96.

Wilkie, R. M. and Wann, J. P. (2011). Modeling locomotor control: The advantages of mobile gaze. *ACM Transactions on Applied ...*.

Wilkie, R. M., Wann, J. P., and Allison, R. (2008). Active gaze, visual look-ahead, and locomotor control. *Journal of experimental psychology Human perception and performance*, 34(5):1150.

Zambrano, D., Bernardin, D., Bennequin, D., Laschi, C., and Berthoz, A. (2012). A Comparison of Human Trajectory Planning Models for Implementation on Humanoid Robot. In *IEEE International Conference on Biomedical Robotics and Biomechatronics June 24-27, 2012 Roma, Italy*.

Zambrano, D., Falotico, E., Manfredi, L., and Laschi, C. (2010). A model of the smooth pursuit eye movement with prediction and learning. *Applied Bionics and Biomechanics*, 7(2):109–118.

Zhang, J. Z., Lu, Y., and Wu, Q. M. J. (2005). *Lecture Notes in Computer Science*, volume 3656 of *DavidHutchison-TakeoKanadeJosefKittlerJon M.KleinbergFriedemannMatternJohn*

C.MitchellMoniNaorOscarNierstraszC.Pandu RanganBernhardSteffenMadhuSudanDemetriTerzopoulosDoughTygarMoshe Y.VardiGerhardWeikumLecture Notes in Computer Science0302-97431611-3349. Springer Berlin Heidelberg, Berlin, Heidelberg.